ESTABLISHMENT AND UTILIZATION OF A DRUG DISCOVERY PLATFORM FOR KV11.1-3.1, A NOVEL TARGET FOR THE TREATMENT OF SCHIZOPHRENIA

by
Nicholas E. Calcaterra

A dissertation submitted to Johns Hopkins University in conformity with the requirements for the degree of Doctor of Philosophy

Baltimore, Maryland

May, 2016

ABSTRACT

The recently discovered primate brain-specific voltage-gated potassium channel, Kv11.1-3.1, was previously identified as a possible therapeutic target for the treatment of schizophrenia. While this channel has shown relevance through clinical meta-analyses, drug discovery and basic investigative efforts have been hampered due to low and inconsistent evoked currents in cell-based assays. This poor activity is hypothesized to result from deficient trafficking due to the lack of an intact channel-stabilizing Per-Ant-Sim (PAS) domain, as Kv11.1-3.1 is an N-terminally truncated isoform of the parent Kv11.1-1A or hERG (*human ether-a-go-go related gene)*. Stemming from hERG's notoriety as a drug discovery anti-target via promiscuous small molecule binding, which includes many antipsychotics, Kv11.1-3.1 has also presented itself as a possible contributor to the polypharmacology profile of conventional schizophrenia therapy. However, it has not been possible to inquire into these hypotheses. This work sought to create Kv11.1-3.1 drug discovery infrastructure by establishing robust, high throughput assays to develop tool compounds and further validate this potential target.

Initial studies characterized Kv11.1-3.1 cellular localization and revealed decreased channel expression and cell surface trafficking relative to the PAS-domain containing Kv11.1-1A. Using small molecule inhibition of proteasome degradation, cellular expression and plasma membrane trafficking were rescued. These findings implicate the importance of the unfolded-protein response and endoplasmic reticulum associated degradation pathways in the expression and regulation of this schizophrenia risk factor. Utilizing the identified rescue phenomenon, electrophysiological and high throughput assay platforms were developed. These assays were applied in screening novel compounds for structure activity relationships, along with known antipsychotics. This approach afforded a synthetic lead molecule, LI-967, which exhibits high potency, drug like properties, and selectivity for Kv11.1-3.1 relative to Kv11.1-1A. Additionally, the developed assays have revealed several antipsychotics to be Kv11.1-3.1 selective at clinical exposure levels, notably clozapine, suggesting a therapeutic contribution in specific patient populations.

This thesis is dedicated to my father, one of the many great Italian/German thinkers.

Thanks Dad.

Preface: Acknowledgments

While I am the only author listed on this work, several individuals contributed to the inspiration and content.

I would like to thank my thesis advisor, James C. Barrow, for being the best mentor and supervisor I could ask for. For a fresh-out-of-industry advisor, Jim nailed it. I could walk into Jim's office, at any time, and talk to him. Business or personal, trivial or complicated, he always made time for me. When facing tough situations, it seemed as if he unconditionally had my back. I am humbled to have had the honor as his first graduate student in what will surely be a long line of distinguished scientists, significantly more talented and intelligent than I will ever be. Although unlikely, I will always aspire to reach a fraction of Jim's professionalism, scientific knowledge, and emotional intelligence. These attributes enabled him to carve out a path for my unstoppable will, redirecting me towards productivity and achievement. For this, I owe Jim my future. Thanks Jim.

I thank the members of the Drug Discovery Division at the Lieber Institute for Brain Development. Martha has been a mother to me in the lab, bringing out the Greek-Orthodox Catholic shame whenever I needed a good lesson. As a top-notch assay development biochemist, she single-handedly facilitated my transition into graduate school. Whenever times were difficult and I needed a hug, she was there. For this and all of the above, I am most grateful. Glen, Ingrid, Francis, Mike Y, Mike P, and Pablo are all excellent chemists and have provided me with industry knowledge and veteran perspective few students have the privilege of experiencing. None of them signed up to be part-time educators to a chemical explosion liability, yet there was never hesitation to assist me with my various chemistry hardships. I thank them (and everyone else) for their patience in my slow (and incomplete) transformation into a professional scientist. I would like to thank Mike D for sharing a room with me for many years and being a model of

work ethic. Vinh was a pleasure to talk to, having common interests in video games and card games. Greg is my professional role-model. While he may not know it, I look up to him as someone who embodies the characteristics of a co-worker. I don't know how he does it, but I can tell it's one of the many reasons he will go far in life. Daniel and Anna have been a pleasure to work with. Jack is the man, making much of this work possible. Jack is a hilarious, like-minded guy who is very intelligent and whom I will miss very much as a colleague. Francis synthesized some of the early compounds in this report. Mike D, Greg, and Vinh carried out the *in vitro* and *in vivo* PK work in this report. Jack optimized the FluxOR assay.

I would like to thank all of other members of the Lieber Institute. While too numerous to individually mention in entirety, I would like to highlight a few names. Dan Hoeppner completed the work for the immunocytochemistry image acquisition and analysis during extraordinarily stressful and busy times. He was always too polite to turn me down, and for that I owe him poker lessons. Tom Hyde epitomizes comedic relief. Richard Straub's door was always open for helpful advice and pragmatic insight. I would also like to thank everyone in the Maher lab for their youthful camaraderie and enjoyable conversations, especially Matt Rannals who performed the early patch clamp work prior to my own electrophysiology training.

I would like to thank the members of my thesis committee; Jun Liu and Phil Cole provided objective critique and insight into my project. Both Jun and Phil have been excellent leaders in the Pharmacology department. Frank Bosmans is a rock star and masterful single-channel electrophysiologist. Frank proofread my papers and thesis, and was always an accessible source of advice and plasmids.

I would like to thank Min Li for his brief time on my committee, but also for the access to his lab infrastructure and team. An enormous acknowledgment must go to Kaiping Xu who had never-ending patience for my cell culture techniques while executing all of the Ionworks assays and analyses. Without her, there would be no third chapter of this thesis. I would also like to thank Beiyan, Alan, and Owen for their advice, hard work, and friendliness.

I would like to give a very special thanks to Brady J. Maher. Brady taught me to be an electrophysiologist by throwing me into a rig and seeing if I survived. I liken this treatment to the Spartans abandoning their boys in the woods so that they may learn what it takes to be a man. It wasn't until I started patching for myself did the project make any progress. Therefore, Brady made this thesis. I would like to thank Brady for always being there to talk, sharing his personal life with me, and being a friend. Brady is a passionate young investigator with big ideas and bigger dreams. He is always looking to the cutting edge and is well on his way to being a world-renown scientist; but most importantly, he is an excellent father and husband.

I would like to thank all of the friends I left in Saint Louis and gained in Baltimore over the years. Thanks for keeping me grounded and reminding me there is more to life than poor-expressing potassium channels. I would also like to thank Mike, my graduate student successor in the lab. While I have only known Mike for a brief period, I had to forgo having a fellow student in the lab for many years. With his arrival, I believe Mike has filled the last hole in our lab culture.

I couldn't have done any of this without my parents and my sisters. My dad is the one who directed me to train at Hopkins as a biochemist since I was 12 years old. However, my mom is the one who taught me how to make that possible. My parents both made countless sacrifices to send me to the best schools possible when they couldn't afford the tuition. My sister Alyssa seemingly called me every day to remind me there is a world outside my lab. This meant a lot despite my inability to express it. I am very proud of both my sisters, including Christina who is just about to begin her own foray into graduate school, or wherever the world takes her free spirit. I love all of you, and I swear that I will make up the lost time very soon.

Finally I would like to thank God for giving me the strength to overcome the plethora of obstacles I have faced in my life and for endowing me with what talents I have. I hope I can utilize them and make this world a better place through appeals to truth, morality, and free market economics.

Table of Contents

List of Figures and Schemes

List of Tables

Chapter 1

INTRODUCTION

Schizophrenia

Although vague aspects and events of psychosis have been recorded throughout human history, ranging from the Old Testament to Shakespeare, schizophrenia as a classified disorder has only existed for the last century.[1] While some diagnoses were originally referred to as "dementia praecox" to describe a heterogeneous set of symptoms, even today, what defines a schizophrenia diagnosis is controversial as patients can experience a wide variety of symptoms which are often conflated with other mental disorders.[1,2] This has led some groups to reconsider schizophrenia as a "psychosis spectrum syndrome", which they cite as more scientifically appropriate terminology.[3]

Historically, classical schizophrenia has been defined as the presentation of three distinct classes of core symptoms: positive (abnormal experiences such as sensory hallucinations, delusions, disordered thoughts and speech, etc.), negative (loss of common behavior such as apathy, anhedonia, flattened or blunted affection, alogia, asociality, etc.), and cognitive (deficits in working memory, executive function, long-term memory, learning, etc.).[2,4-6] Until recently, neurological symptoms (catatonia, posturing, mannerism, stereotypy) were included as core symptoms prior to popular dispute.[7,8] Beyond direct symptoms; substance abuse, smoking, depression, suicide, poor physical health, eating disorders, and irritable bowel syndrome have been correlated with schizophrenia.[1,9] For official diagnosis, the *Diagnostic and Statistical Manual of Mental Disorders*, has recommended the identification of two of the three core symptoms "for a significant portion of the time during a 1-month period" with some persistence

for at least 6 months. Using these criteria, reports estimate that schizophrenia occurs in approximately 0.3-0.7% of the population, and incurring an economic burden of over 80 billion dollars a year.[10,11] This burden is expanded from individual costs, as schizophrenia patients have a reduced average life expectancy (12-15 years), ongoing disability and psychotic relapses, increased rate of suicide, and are largely unemployed.[12-15]

Antipsychotics and theorized mechanisms of action

Treatment of schizophrenia includes psychotherapy, counseling, and social support; although the primary focus of conventional disease management is antipsychotic pharmacotherapy.[1] The first widely marketed antipsychotic, chlorpromazine, entered clinical use in 1952 and marked a watershed moment for psychotherapy. Over time, treatment moved from invasive procedures (psychosurgery, electroconvulsive therapy, etc.) and inevitable long-term institutional care to outpatient pharmacotherapy.[1,16,17] Since then, a wide variety of new antipsychotics have been created, representing some of the best selling drugs of all time.[18] These drugs are split into two classes, typical (chlorpromazine, haloperidol, perphenazine, etc.) and atypical (clozapine, risperidone, olanzapine, aripiprazole, etc.).[1] The difference in the two classes is atypicals are characterized by the reduced prevalence of extrapyramidal side effects (EPS) in extended use. EPS caused by antipsychotics can either be acute in early treatment, causing parkinsonism, akathisia, or dystonia; or cause tardive dyskinesia during long-term treatment. Because of their common prevalence, these neurological complications have been a major cause of burden for treatment courses and decisions.[19] Exacerbating this burden, some reports have disputed the superiority and the reduction of associated adverse effects of atypical antipsychotics compared to typicals. Various meta-analysis studies have argued that atypicals show either non-significant or no improvement in reduction of EPS events.[20-22] Furthermore, atypicals have induced other serious side effects, such as diabetes, weight gain, and agranulacytosis.[23,24] These factors have caused some physicians to reexamine first-line treatment preference for atypicals. Regardless of

this contention, both classes are only efficacious against positive symptoms. Unfortunately the basis for these treatment's antipsychotic effect, and general schizophrenia pathobiology, is still poorly understood and thus progress in characterizing pharmacotherapy limitations has been largely curtailed. However, newer tools have brought fresh insights into drug action and patient outcomes.[1]

The most prolific school of thought for schizophrenia pathology and antipsychotic efficacy is the dopamine receptor (DR) blockade hypothesis, as nearly all antipsychotics competitively block dopamine receptors to some degree.[1,25] DRs are a class of G protein-coupled receptors which contribute to many neurological pathways responsible for cognition, pleasure, motor control, learning, memory, etc.[26] There are two main families of DR's with various localizations and densities in the brain and periphery: D_1-like (D_1, D_5), coupling to $G_{s\alpha}$ which then activates adenylyl cyclase to increase intracellular cAMP; and D_2-like (D_2, D_3, D_4), coupling to $G_{i\alpha}$, which inhibits adenylyl cyclase and cAMP production.[1,27] For many years, DR's were implicated in the neurochemical and behavioral effects of antipsychotics, although it wasn't until nearly 40 years after inception that these effects were validated with *in vivo* receptor occupancy studies via neuroimaging. [28-32] These studies reported greater dopamine occupancy of D_2 receptors in the striatum of patients with schizophrenia compared to healthy individuals, which was then correlated to the presentation of positive symptoms.[33] It has also been suggested that decreased D_1 receptor occupancy in the pre-frontal cortex (PFC) may cause impairments that result in negative and cognitive symptoms, and that overall dopamine system imbalance between the subcortical mesolimbic and mesocortical PFC are critical to schizophrenia pathology.[34-36] In fact, keeping in mind all antipsychotics have no or modest selectivity for any member among the major DR's, specific D_2 receptor blockade strongly correlates to antipsychotic effect.[37] However, there are some discrepancies between various antipsychotics and the suggested required occupancy levels for efficacy, depending on the binding kinetics and ability to induce high and low affinity states of DR's.[1] While some D_1 selective antagonists have been studied, none have displayed

therapeutic benefit.[38,39] Seemingly more promising are D_1 agonists which have had mixed preliminary results.[40] Beyond selective agents, some newer/atypical antipsychotics showing minor efficacy in reversing negative and cognitive symptoms and lower EPS risk, such as clozapine, have been suggested to increase dopamine in the PFC. While not engaging the D_1 receptors directly, instead this activity is hypothesized to come from 5-HT (serotonin) receptor antagonism/partial agonism (vide infra).[33]

The wealth of research on the dopamine hypothesis has undoubtedly cemented its association with schizophrenia; however, this theory is not without limitations. In haloperidol DR occupancy and other studies, some patients do not respond to treatment despite being far above clinical threshold levels, suggesting other mechanisms than dopamine imbalance/hypersensitivity.[41] Two of the most prominent non-DR factors are 5-HT and glutamate receptors.

The link of 5-HT to schizophrenia was originally hypothesized in research comparing the disease to effects seen in lysergic acid diethylamide use, although inaccurately.[42,43] However, serotonin has been reported to play a role in many processes disrupted in schizophrenia, including cognition, memory, perception, and aggression. Conventional knowledge of 5-HT receptors in schizophrenia follows from the findings of multiple receptor subtypes, their differential impact on various neurotransmitters, and antipsychotic binding. A similar research paradigm used to elucidate the DR blockade hypothesis (clinical efficacy, occupancy neuroimaging, and symptomatic correlation) was used to interrogate the role of 5-HT receptors.[44] The vast majority of the seven 5-HT receptor families are also G protein-coupled receptors, with the exception of 5-HT_3 which are ligand-gated Na^+/K^+ channels. These receptors have various activities in both modulating cAMP levels (Increase: 5-HT_4, 5-HT_6, 5-HT_7; decrease: 5-HT_1, 5-HT_5) and increasing IP_3/DAG (5-HT_2). While nearly all of these receptors have shown antipsychotic binding, three (5-HT_{1A}, 5-HT_{2A}, 5-HT_{2C}) have been of considerable interest.[45] Antagonism of $5HT_{2A}$ receptors is a common characteristic for atypical antipsychotics, which paradoxically increases dopamine release in the PFC.[46] In fact, these drugs have higher affinity for this receptor than DR's. For

example, clozapine shows only modest occupancy of D_2 receptors at clinical levels (20-67%) while exhibiting 80% occupancy of 5-HT_{2A}.[44] 5-HT_{2C}, which activates to inhibit dopamine release in the striatum, PFC, hippocampus, nucleus accumbens, etc., is commonly antagonized by atypicals.[47] 5-HT_{1A}, a classic autoreceptor in the raphe nucleus and post synaptic receptor in other regions, has been shown to increase dopamine release in the PFC, hippocampus, and striatum upon activation.[47,48] While the partial agonist activity of many atypicals on 5-HT_{1A} fits general mechanism of action narratives for the PFC, the action in the striatum highlights the perplexing nature of the coordination of the dopaminergic and serotonin pathways.[48] Adding yet another facet to this paradox is the growing evidence of antipsychotic efficacy without DR blockade via selective serotonin antagonists and reverse agonists.[1] While the interaction of contradictory cascades resulting from 5-HT receptor blockade in the treatment of schizophrenia is still unclear, there is unquestionable clinical value in targeting these receptors.

Perhaps the most confounding evidence against the exclusive dopamine hypothesis is the potential role of glutamate receptors, specifically *N*-methyl-D-aspartate (NMDA) receptors. These receptors are a family of ionotropic glutamate receptors that are responsible for fast excitatory events in the central nervous system (CNS), with predominant actions in synaptic plasticity and memory.[49] These receptors exist as tetramers of two NR1 and two NR2(A-D) subunits, with NR3(A-B) subunits substituting for NR1 to modulate activity. The heterogeneity of these receptors contributes to differential responsiveness and general effect on local receptor populations.[50,51] Activation of these receptors requires the convergent events of ligand binding (two glycines and two glutamate molecules) and membrane depolarization, allowing for the flow of positively charged ions (such as Ca^{2+}) through the receptor-channel.[52] Initial implications of aberrant glutamatergic activity in schizophrenia arose from physiological findings of disrupted cortical pyramidal neuron connectivity, these neurons primarily using glutamate as their neurotransmitter. Further investigation through postmortem brain expression analysis and neuroimaging highlighted the extent of altered expression of NMDA receptors in schizophrenia

patients.[1] In many locations of the brain, expression analysis has yielded mixed results, partly due to brain sample heterogeneity, however some differential expression changes in the hippocampus and PFC have been reported.[1] More definitive finding have been reported using *in vivo* single photon emission computed tomography (SPECT) neuroimaging, specifically fewer receptors in the hippocampus of untreated schizophrenics, consistent with expression analysis. These techniques are unable to differentiate reductions in receptor count and activation state.[53] What may be the most important collection of evidence for the role of NMDA receptors in schizophrenia are studies examining the effects of phencyclidine (PCP) and ketamine, which are NMDA receptor antagonists. Both of these drugs simulate psychosis in healthy individuals while also worsening symptoms for patients. Positive, negative, and some cognitive symptoms have been reported in studies with ketamine.[54] These drugs have been found to increase cortical and limbic extracellular dopamine levels.[55,56]. While haloperidol and olanzapine fail to block ketamine-induced psychosis, clozapine has been found to block the exacerbation of symptoms in patients given ketamine.[54,57,58] Additionally, clozapine attenuates the reduction of NMDA receptor counts in patients by SPECT.[59] These effects are hypothesized to come from clozapine's polypharmacology, including glycine transporter blockade. Beyond isolated actions, the NMDA receptor has been found colocalized with D_1 receptors in the PFC, the interplay of both possibly contributing to cognitive deficits, especially in working memory.[60] Reports have also highlighted the effects of other schizophrenia implicated genes in NMDA activity, such as *NRG1*, *ERBB4*, *DISC1*, *DAAO*, and *SRR*, along with glutamate metabolism in glia.[61] However, like dopamine and serotonin, the role of glutamatergic signaling in schizophrenia pathogenesis is still being elucidated.

While studies of serotonin and glutamate have brought some additional insight into treating negative and cognitive symptoms, conventional medications cannot consistently alleviate these maladies. Regardless of efficacy, newer agents still cause serious adverse events. Although clozapine has repeatedly demonstrated an idiosyncratic profile across many proposed

antipsychotic targets, its proclivity towards life-threatening agranulacytosis narrows its use as a treatment of last resort. The state of schizophrenia pharmacotherapy has prompted continued research for new antipsychotics.

Modeling schizophrenia symptoms with animal behavior for drug discovery

In order to facilitate pre-clinical studies for the purpose of evaluating prospective drugs, researchers and regulators look to animal models for efficacy studies. These studies have deep limitations due to the lack of a characteristic genotype/phenotype/biomarker. Additionally, none of these models can fully simulate the positive, negative, and cognitive symptoms of human schizophrenia (e.g. inability to sense whether or not a mouse is hallucinating). Despite the poor linkage to human efficacy (failures in phase II trials), they still provide needed testing funnels to triage novel compounds.

For each animal model, a number of behavioral and cognitive tests are used to evaluate deficits and alterations reflected in human patients and simulated by the model. Schizophrenia patient sensorimotor gating deficits have been observed through prepulse inhibition tests, a common method directly utilizable in rodents.[62] Pharmacologically induced (either D_2 agonist or NMDA antagonist) hyperlocomotion in rodents has been correlated to positive symptom presentation in patients notwithstanding an apparent lack of face validity, save psychotic agitation.[63] Replicated cognitive impairments in patients have been assayed using T-maze experiments to test working memory, and the Morris water maze to study spatial learning and memory.[64,65] Novel object location tasks are used to measure spatial memory and discrimination, while novel object recognition challenges measure recognition memory.[66,67] Attentional set-shifting tests are used to evaluate attentional deficits that lead to reversal learning and discrimination impairments seen in patients.[68] Negative symptoms are typically measured through social interaction and aggression of animals with their littermates.[69,70]

Initial rodent models used for drug discovery consistently predominantly of dopaminergic

alterations. For example, prospective antagonism of apomorphine-induced emesis or pre-pulse inhibition and amphetamine-induced hyperlocomotion directly seek changes in behavior by blocking induced D_2 agonism. While these models have been somewhat useful in their predictive abilities, they do not necessarily model schizophrenia and are restricted in their validation of new agents to anti-dopaminergic efficacy.[1] More recently, models incorporating neuronal development, decreased glutamatergic activity, and transgenic animals have garnered attention.

A number of methods have been used to create disrupted neuronal development in mice and rats. Methods such as malnutrition, infection with human influenza virus/ other viruses, X-ray irradiation, and exposure to toxins have been used to inhibit corticogenesis, disrupt neural circuits and neurotransmitter systems, and diminish the activity of developed neurons.[1,71,72] The inflammatory agent polyriboinosinic-polyribocytidilic acid (PolyI:C) has been used to create dopaminergic and glutamatergic dysfunctions in mice through prenatal administration.[73] However, the validity of these models is questionable as none of these methods have any evidence associated causative factors for disease pathology, with a possible exception for influenza infection. More relevant methods of altered neuronal development are stress models and neonatal lesions.[1,74,75] Maternal and social isolation, among other stress-inducers, have been shown to create various hormonal and neurochemical changes, while also resulting in behavioral test changes, such as learning, hyperactive locomotion, and sensorimotor gating defects.[62] These changes have been successfully reversed with conventional antipsychotics, including post-development in adult mice.[76-78] Lesions created on specific regions of the rat hippocampus that project to the PFC, the ventral hippocampus and ventral subiculum which correspond to the anterior hippocampus in humans (displaying structural abnormalities in patients), have resulted in a number of schizophrenia like behavioral phenotypes and aberrant development in the PFC. Interestingly, removal of PFC neurons in rats with these lesions reverse some of the behaviors, implicating the necessity of PFC dysfunction in these schizophrenia-like characteristics.[79-81] These rats have shown glutamatergic and dopaminergic alterations, with some of the induced

behaviors being attenuated by antipsychotics.[82] Some of these findings have been reproduced in non-human primates.[83]

In order to assess drug action on glutamatergic dysfunction, NMDA antagonism using ketamine and PCP has been used as an animal model for both non-human primates and rodents. Specific altered neuronal firing patterns in the nucleus accumbens, meso-limbic, and meso-cortical areas have been shown during these treatments along with various schizophrenia-like behaviors.[84,85] This model was used to discover LY-404,039 a novel metabotropic $mGluR_{2/3}$ agonist, although the agent later failed phase II clinical trials.[86,87]

Finally, the use of transgenic animal models for drug discovery has been widely considered based on two schools of thought: 1) common disease/common allele (CD/CA) hypothesis in which pathology is driven by multiple mutations/expression deviations in low impact targets and 2) common disease/rare allele (CD/RA) in which one mutation drives disease and is overexpressed/ knocked-out.[1,88] However, the vast majority of drug discovery efforts driven by transgenic animal models consist of single gene approaches. Many schizophrenia-associated candidate genes have been used for models, including: *NRG1*, *AKT1*, *COMT*, *DISC1,* etc. In addition to targeting single genes, chromosome abnormalities (22q11.1 deletions) have be simulated in mouse models through microdeletions of mouse chromosome 16, which contains all of the respective genetic orthologs.[74,89]

The development of new transgenic animal models has been, perhaps, of greatest interest in recent years. This is likely due to the emergence of inexpensive whole genome sequencing and therefore the ability to process high-powered meta-analyses. New genes associated with schizophrenia are being discovered and their impact on development is being investigated. One import tool to measure the impact of these models is electrophysiology.[74,90]

Relating electrophysiology to schizophrenia pathology

The essential units of the brain are neurons, which are electrically excited to release

neurotransmitters through action potentials which facilitate or inhibit neuronal signaling circuits controlling various functions. The electrical signals stemming from these activities have been used to investigate differences between schizophrenia patients and healthy individuals to identify possible aberrations in schizophrenia pathology. The cognitive aspects of the disease have been especially studied in the context of electrophysiology. Working memory is a vital component of higher cognitive functions, being defined as the ability to store information for some time in order to complete tasks that may be delayed.[91] The prefrontal cortex (PFC) has been implicated to play a central role in working memory, as extracellular recordings in the PFC have shown that "a large fraction of prefrontal cortical neurons remain active after the cue and until the task is completed. Such activity can persist for several seconds without continued stimulation and has been proposed as the neural correlate of working memory."[91,92] This persistent activity is supported by a network of pyramidal neurons, the primary excitatory units of the PFC, processing various inputs and responding to glutamate and GABA (γ-aminobutyric acid) neurotransmitters.[93] It is thought that pyramidal cells achieve this activity through low-frequency, non-adapting, neuronal discharges which are regulated by combined Na^+ and K^+ currents (I_h) via conversion to high-frequency discharges.[91] This regulatory interaction causes the termination of trains of action potentials, or spike frequency adaptation. This is a common cortical firing pattern, which when synchronized within a network gives rise to electrical oscillations which can be detected via electroencephalography (EEG).[94] Specifically, it has been shown that beta, gamma, and theta oscillations are indicative of neuronal activity in working memory cognition.[95-97]

Using EEG recordings, beta and gamma oscillation abnormalities have been detected in schizophrenia patients during working memory tasks, as compared to healthy individuals.[98] In fact, changes in gamma power and synchronization have been reported in various studies using different cognitive tests. Many of these studies report contradictory data, and call into question the usefulness of the reductionist hypothesis focused on these oscillations. Reports on beta and alpha oscillations have suffered from similar issues. Theta frequency studies have been slightly

more consistent, with increased power observed in unmedicated patients, although even higher in clozapine-treated patients. It has been suggested that lower-frequency oscillations can affect gamma signals, thus perhaps a more holistic approach to EEG signals should be taken. [99]

Beyond EEG, electrophysiological recordings for the purpose of finding useful biomarkers for schizophrenia drug discovery have extended to magnetoencephalography (MEG), which can complement EEG recordings, being more sensitive to cells tangential to the brain surface. While these methods are still being developed, they are promising tools for evaluating antipsychotic intervention.[100]

Potassium channels

Potassium channels are a very large family of channels involved in a variety of physiological roles. Partitioned K^+ ions are the principally determining factor for resting membrane potentials, as cell membranes are significantly more permeable to K^+ than other cations due to the strong chemical gradient for intracellular cations to move out of the cell through K^+ leak channels (150mM intracellular K^+ vs. 5mM extracellular K^+). Potassium channels use these gradients to regulate various processes including muscle contraction, hormone secretion, and neurotransmitter release, etc. Unsurprisingly, these functions are controlled by a large family of K^+ channels with several common features. All K^+ channels are tetrameric in structure, either consisting of homologous subunits or heteromers. Each channel monomer includes a hydrophobic region, a water-filled central cavity, and a pore loop, containing a selectivity filter which allows the channel to discriminately pass K^+ ions without promiscuous transport of other ions such as Na^+ (having a 0.38 Å smaller radius).[101] The signature amino acid sequence for the selectivity filter is highly conserved in K^+ channels (TVGYG), although this is not always the case (vide infra). This selectivity filter is thought to operate by desolvating the ion by mimicking the K^+ solvation shell via aligning the selectivity filter residues' respective carbonyl oxygens to form a square anti-prism. However, this mechanism is still debated. [102] [103] There are four major families of

potassium channels: calcium activated, tandem pore domain, inwardly rectifying, and voltage gated.

Calcium activated K^+ channels are either directly activated by calcium or are structurally related. These channels are comprised of α subunits with 7 transmembrane α-helices, a pore forming loop, and a large intracellular region for calcium binding. Transmembrane regulatory subunits that interact with the α tetramers, called β subunits, can either inhibit or facilitate activation of the channel. There are three major families of human calcium activated K^+ channels: BK, IK, and SK.[104] BK channels have large conductance for K^+ and are also activated by voltage. These channels have been of interest as potential drug targets for stroke, overactive bladder, and opioid-induced respiratory depression.[105-107] IK channels are characterized by their intermediate conductance and are important for vasodilation of capillaries and neutrophil phagocytosis.[108,109] SK channels have small conductance and are voltage insensitive. These channels are thought to be involved in synaptic plasticity and are widely expressed in the central nervous system.[110]

Tandem pore domain channels are also known as "leak channels", being subject to Goldman-Hodgkin-Katz flux rectification. These channels have α subunits with only four transmembrane domains with two pore loops per unit and form functional dimers. These channels are heavily involved in maintaining resting membrane potential.[111]

Inwardly rectifying channels have two transmembrane domains and a single pore loop per α subunit and consists of seven distinct families. These channels are "inwardly-rectifying" in the sense that they conduct K^+ more efficiently into the cell rather than out of the cell. This action brings the cell back closer to resting membrane potential post-activation which is an important contribution to regulating neuronal activity. Inward rectification is distinct from the majority of potassium channels which typically facilitate passage of K^+ out of the cell, and is achieved by the presence of polyamines and magnesium that selectively block outward passage of K^+ at positive membrane potentials.[112-114] Alternatively, activation of the inward conductance is trigged by the binding of an agonist, phosphatidylinositol 4,5-bisphosphate (PIP_2).[115] These channels are

involved in prolonging the cardiac action potential, regulating nitric oxide synthase, excretion of K^+, neuronal activity, and insulin release. Logically, these channels have also been implicated in a number of different diseases.[112]

Voltage-gated K^+ (Kv) channels are similar to calcium-activated channels in that they have six transmembrane domains and a pore loop per subunit. However, each of these channels also has large intracellular N and C terminus sequences that make up various important domains for channel gating and kinetics. Some channels, such as the KCNAB, KCNE, and KCNIP families are known to have β subunits which modulate activity.[116] The Kv channels are especially important in repolarizing cells during action potentials and have been the focus of many drug discovery efforts.[117]

Voltage-gated potassium channel electrophysiology techniques for drug discovery

In order to study Kv channels, especially for the purpose of drug discovery, one must be able to monitor their activity: the conductance of K^+. The "gold standard" for observing these activities is the patch-clamp, voltage clamp method, discovered by Nobel Laureates Erwin Neher and Bert Sakmann.[118] This method consists of using a glass micropipette to record electrical cell signals, referenced by a ground in an aqueous bath mimicking extracellular conditions. Suction is applied through the pipette to create a high resistance seal, typically greater than 1 gigaohm, to filter noise and keep the membrane-pipette seal intact. Depending on the purpose of the experiment, recordings can be taken with the pipette simply on the cell (on cell), removed to examine single channels (inside-out or outside-out), or perforating the cell to monitor entire cellular activity (whole-cell).[119] The vast majority of Kv channels are monitored for drug discovery using whole-cell patch clamp technique in order to maximize signal where channels are activated/deactivated/inactivated by varying voltage inputs through automated protocols.[120] However, this also comes at a disadvantage in that the solution inside of the pipette begins to dialyze into the cell, creating artificial intracellular conditions. Therefore, the internal pipette

solution is typically formulated to mimic the intracellular solution as much as possible to limit extraneous variables.[121]

For dose-response and kinetic assays, most channels are recapitulated via recombinant channel expression in immortalized cell lines, typically Human Embryonic Kidney (HEK 293) or Chinese Hamster Ovary (CHO-K1). However, each of these cell lines may have various endogenous channels, possibly confounding recordings if not tested. [122] Expression in these cells lines have been carried out in numerous ways including transient transfections and transductions through BacMam virus, or stably transfected via plasmid/linearized DNA or lentivirus integration.[123,124]

Unfortunately, the use of voltage clamp for drug discovery, especially in early-stage hit discovery, is time-consuming and prone to variability. Efforts to automate this process, either through indirect measurements or true voltage-clamp, have yielded techniques more amenable to high throughput screening and lead optimization. Such procedures include detecting ions that pass through Kv selectivity filters (Rb^+ and Tl^+) or true voltage control through automated patch clamp (APC).[125-127] However, each of these techniques have limitations as compared to traditional manual voltage clamp so initial findings must be confirmed by traditional methods.[128]

The human ether-a-go-go related gene and Kv11.1 channels

The most notorious of all potassium channels, if not all channels in the context of drug discovery, is Kv11.1, a Kv channel encoded by the gene *KCNH2*, also known as the *human ether-à-go-go related gene* (hERG). This channel earns its acclaim for an idiosyncratic ability amongst ion channels to promiscuously bind small molecules, especially pharmaceuticals, which has caused the addition of FDA mandated black box label warnings and removal of many drugs from the market. This is due to Kv11.1's central role in a cardiac repolarization current called I_{Kr}, which results in a fatal arrhythmia called "torsades de pointes" upon channel blockade. However, Kv11.1 has been shown to play other important roles in other tissues like the brain, and has been implicated in schizophrenia pathology.[128,129]

Discovered in 1969 by William Kaplan and William Trout through mutational gene mapping in *Drosophila Melanogaster*, the name *Ether-à-go-go* was coined as a reference to dancers at the Whiskey a Go-Go, a popular nightclub on the Sunset Strip in West Hollywood, California, where many famous artists, such as Van Halen, The Doors, Metallica, Guns N' Roses, and Alice Cooper, played gigs early in their careers. When *ether-à-go-go* (EAG) mutated flies were put under the influence of ether, their legs would shake noticeably slower than other *Shaker* locus mutations, analogous to a popular dance exhibited at the Whiskey a Go-Go during the 1960's.[130] Of note, this same paper also identified the classic channel typology gene, *Shaker*.[131]

Kv11.1 channels are expressed in a number of different tissues in humans, including the hippocampus, PFC, small intestines, gallbladder, pancreas, and tumors.[128] In neurons, Kv11.1 channels have been shown to be important for spike-frequency adaptation and burst duration.[132,133] However, Kv11.1 is best known for its role in the heart, specifically in atrial and ventricular myoctyes, for its leading contribution to rapid delayed rectifier potassium currents (I_{Kr}) in cardiac repolarization. [134,135] This current controls the duration of phase 2 (or plateau) in the cardiac action potential. I_{Kr} is vital for coordinating proper heart contraction, antagonizing cardiac depolarization from premature beats i.e. rhythm, as monitored by the QT interval via electrocardiogram. Blockade of Kv11.1 channels increases risk of deadly cardiac arrhythmias, such as torsades de pointes. Kv11.1 channels also are expressed in sinoatrial and atriventricular nodes where they make a minor contribution to pacemaker activities.[136-138]

In 1994, the human ortholog of the EAG channel was identified and cloned, having sequence similarity to both Kv channels and cyclic nucleotide-gated channels.[139] Thus, the gene encoding for Kv11.1 is *KCNH2*. Spanning 33 kb, *KCNH2* is located in region q36.1 of

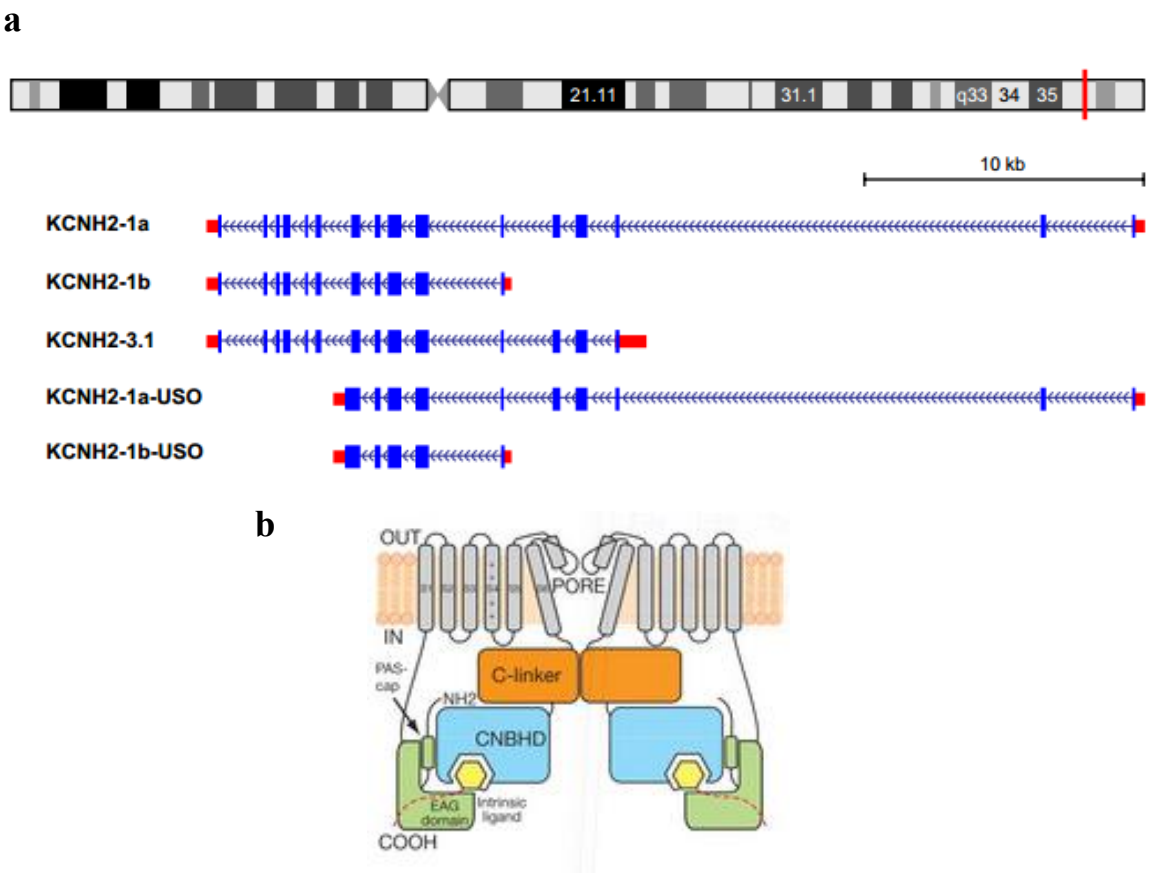

Figure 1.1 KCNH2 gene location, transcripts, and basic KCNH channel structure. ***a,*** View of chromosome 7 q36.1. *KCNH2* encodes for five unique transcripts. ***b*** General KCNH channel structure with intracellular domains.

chromosome 7 (NG_008916) and contains 15 exons, transcribing the reverse strand to yield a 3.3 kb transcript KCNH2-1a. There are two internal alternative transcription start sites, leading to two truncated transcripts, KCNH2-1b and KCNH2-3.1. Additionally, two unique premature stop transcripts have been identified (**Figure 1.1a**).[128]

Translation of KCNH2-1a results in an 1159 amino acid protein hERG or Kv11.1 or Kv11.1-1A. Kv11.1-1A is a member of the Kv superfamily of potassium channels. Like other Kv channels, Kv11.1 contains six α helical transmembrane domains (S1-S6), and a pore loop. S1-S4 create the voltage-sensing domain while S5-6 and the poor loop constitute the pore domain.[128] The voltage-sensing domain responds to changes in the transmembrane electric field and changes conformation to electromechanically influence the opening of channel at the activation gate, residing at the interface of the channel entrance and the cytoplasm.[140] The pore loop facilitates K^+ transport through the channel (vide supra), yet has a significantly different selectivity filter than typical K^+ channels, as its sequence is SVGFG (opposed to TVGYG).[141]

Additionally, Kv11.1-1A has long intracellular N and C termini that comprise the vast majority of the amino acid sequence. The N-terminal region makes up the Per-Ant-Sim (PAS) domain, and the N-terminal cap; while the C-terminal region makes up the C-linker and the cyclic nucleotide-binding homology domain (CNBHD) (**Figure 1.1b**).[128]

The PAS domain has been implicated in controlling the hallmark slow-deactivation rate kinetics of Kv11.1 channels (vide infra), but also in folding, assembly, and stabilization of the tetrameric channel structure.[142-144] While it is not necessary for normal trafficking or stabilization, when it is present, the N-terminal cap must also be intact for normal channel function and trafficking. The N-terminal cap contains an amphipathic helix that interacts with small hydrophobic region of the PAS domain to stabilize the channel and thus influences trafficking.[145] The C-linker is a structurally folded domain that connects the CNBD to the transmembrane pore areas. The CNBD

is thought to interact with the PAS domain and N-terminal cap to assist in modulating channel connects through interaction via a small hydrophobic patch on the CNBD as hypothesized from analogous channels.[146] Unsurprisingly, many mutations in these cytoplasmic regions cause altered channel characteristics and disease (vide infra).[144,147] While Kv11.1-1A has not been crystalized for structural analysis, the cytoplasmic residing domains have been the study of various crystallography and nuclear magnetic resonance (NMR) studies.[148,149]

Kv11.1-1A channels are synthesized and trafficked similarly to other K^+ channels and integral membrane proteins. mRNA is translated in the cytosol where a transmembrane signal is detected, pulling the translational machinery to the endoplasmic reticulum (ER) where the nascent peptide is strung through the ER membrane via translocation mediating proteins and lipids. Chaperone proteins bind to folding intermediates, especially the HSP40, HSP70, and HSP90 families, to prevent misfolding via binding to exposed hydrophobic regions in the intermediate channels.[128,150] Mutant channels are typically bound by chaperones for longer periods of time and eventually lead to proteasomal degradation. The regulation of trafficking versus degradation is strongly controlled and widely studied. A contemporary model of the Kv11.1-1A quality control pathway suggests that nascent channel peptides are bound by Hsp40 family members DNAJA1/2 which stimulate Hsp/Hsc70 binding via ATP hydrolysis. Various nucleotide exchange factors drive Hsp/Hsc70 binding cycles that facilitate folding along with the Hsp40's. This reaction cycle is the major checkpoint of Kv11.1-1A quality control towards either degradation or eventual trafficking to the cell surface. DNAJA1 and Hsp70 are thought to promote ER exit by recruiting Hsp90 and Hsp-organizing protein (HOP), which release Hsc70 from nascent channels allowing Hsp90 and FKBP38 to complete the folding process. Conversely, DNAJA2 is thought to promote Hsc70 and recruit CHIP, a soluble E3 ubiquitin ligase. CHIP, and possibly other E3 ligases, ubiquitinylate the misfolded channel which is then directed towards proteasome degradation.[151-154] Kv11.1-1A channels also contain a number of "RXR" motifs that signal for ER retention, although these sequences are typically hidden in well folded channels, creating another layer of folding

control.[155] Additionally, nascent channels are N-linked glycosylated at Asn598 and, possibly, Asn629 in the ER, leading to a 10 kDa addition in molecular weight (125 kDa vs 135 kDa).[156] This glycosylation event creates "core glycosylated" (CG) channels. If properly folded, the channel is trafficked to the Golgi apparatus where the nascent channel is glycosylated a second time, adding an additional 20 kDa in molecular weight. Channels that have been glycosylated twice are referred to as "fully glycosylated" (FG), which then exit the Golgi and traffic to the plasma membrane. At the plasma membrane the channels can interact with a variety of different proteins, including ubiquitin ligases which can facilitate ubiquitin –mediated lysosomal degradation (and in some cases, proteasomal) via endocytosis and retrograde translocation.[128,157]

The two most studied alternatively transcribed variants of KCNH2-1a are KCNH2-1b and KCNH2-3.1. KCNH2-3.1 will be discussed further below as it is the main channel of interest in this study. Translation of KCNH2-1b synthesizes an N-terminally truncated channel with amino acid sequence length of 819 called Kv11.1-1B.[128,158] While able to form functional homotetramers (tetramer assembly occurs in the ER) with poor activity and trafficking impairments, Kv11.1-1B is predominantly present as part of a heterotetramer with Kv11.1-1A. This poor trafficking and is due to the presence of an additional "RXR" ER retention amino acid sequence unique to the Kv11.1-1B channel, although the altered kinetics are likely due to the absence of the PAS domain and N-terminal cap. However, upon heterotetramer formation with Kv11.1-1A, this signal is shielded, promoting exit from the ER. Kv11.1 heterotetramers also display changes in channel kinetics and is thought to primarily depend on subunit stoichiometry.[155,159]

Conceptually, it is useful to think of the Kv11.1 channel existing in three states: closed, opened, and inactivated. The transition from closed to open is referred to as activation, open to inactivated as inactivation, inactivated to open as recovery from inactivation, and opened to closed as deactivation (**Figure 1.2**).

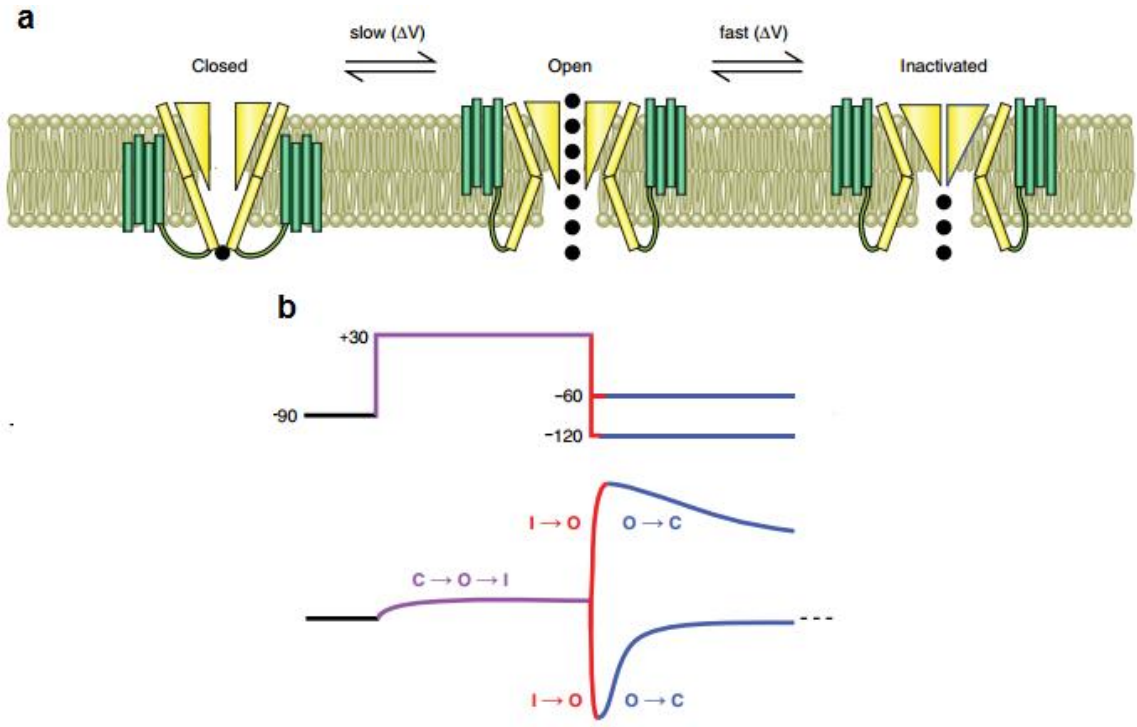

Figure 1.2. Kv11.1 channel states and gating. ***a***, Kv11.1 channels transition between closed, opened, and inactivated states. ***b***, Kv11.1 induced currents via voltage-clamp protocols. Note channel gating in response to the voltage steps and voltage-dependent current directionality of channel reactivation.

Unique from other Kv channels, Kv11.1-1A channels transition between opened and closed states slowly, needing almost an entire second to fully open/close. Transitions between opened and inactivated are much faster, on the order of milliseconds. These voltage-dependent properties are essential for normal action in cardiac repolarization (vide infra).[128]

Just as normal kinetics is important for proper channel functional, equal attention has been brought to the role of trafficking in overall contributions to cellular action. The most prolific examples of Kv11.1-1A function in the context of trafficking concerns are congenital mutations in the channel causing Long QT Syndrome, type 2 (LQTS2). It has been found that patients with LQTS2 have various mutations in *KCNH2*, causing either/or premature stop codons, misfolded or unstable channels, or altered kinetics/intrinsic activity.[128] Most of these mutations occur in the either the pore or PAS domains and have led to the discovery of their relative importance in trafficking and channel stability.[144] Effects in trafficking have been studied by exploiting the large size differences in the glycosylated states of channels by western blot. Since the ER is the major checkpoint in Kv11.1-1A trafficking, and ER retained channels are not glycosylated a second time, one can use the relative abundance of CG and FG channels to diagnose and assay changes in trafficking. This technique has led to the identification of the Kv11.1-1A quality control pathway, pharmacological agents, and other factors that affect or rescue trafficking.[128]

Kv11.1-1A channels have been found to interact with a number of other proteins that can either regulate its activity or expression. Other K^+ channels (and possibly their β subunits), such as KCNE1/2, KCNQ1, and KCR1, can associate with Kv11.1-1A and modulate its activity. Various kinases have been shown to posttranslationally phosphorylate Kv11.1-1A, influencing gating properties along with biogenesis. This includes PKA via cAMP signaling, PKB via PIP_3 signaling, and PKC through diacylglycerol signaling. Tyrosine kinase SRC has been shown to complex with Kv11.1-1A channels.[128]

As previously mentioned, Kv11.1-1A channels have been shown to promiscuously bind to small molecules. In conjunction with its vital role in cardiac repolarization, this phenomenon has

marketed Kv11.1-1A as one of the largest anti-targets in drug discovery.[160] While not the first drug to be removed from market due to effects of Kv11.1-1A blockade, the antihistamine terfenadine (Seldane®) arguably brought pharmacologically induced QT prolongation via I_{Kr} inhibition to the forefront of regulatory attention.[161] Approved in 1985, patients prescribed terfenadine were later found to be at increased risk of ventricular arrhythmias, especially those concomitantly prescribed CYP3A4 inhibiting drugs such as macrolide antibiotics. In the early 1990s it was found that terfenadine inhibited I_{Kr} currents and by 1996 it was shown that it directly inhibited Kv11.1-1A channels. Due to these studies and the introduction of less toxic antihistamines, terfenadine was withdrawn from the market in 1998.[162] Since then, a number of drugs have been withdrawn or given black box label warnings, including grepafloxacin, astemizole, cisapride, haloperidol, ziprasidone, amitriptyline, and many other CNS drugs.[163] Behind this promiscuous binding of a wide class of drugs lays two main factors: two key aromatic residues in the channel pore (Tyr652 and Phe656) and C-type channel inactivation.[128,164,165] After the channel has opened (a requirement for promiscuous molecule binding) the topology of the Kv11.1-1A channel pore allows for multiple binding modalities, although high-affinity compounds are typically anchored by interactions with either Tyr652 or Phe656 (or both.)[166] Mutagenesis screens have reported the necessity of an aromatic side chain and hydrophobic side chain at these positions, implicating π-π stacking or π-cation interactions with exogenous compounds (**Figure 1.3**).

Indeed, the generalized Kv11.1-1A pharmacophore of many high-affinity block compounds includes a basic amine or high logP-driving structures. Polar residues near the N-terminal of the pore helix have also been shown to drive compound-specific binding interactions in the pore, although these are highly conserved across multiple Kv channels. Tyr652 and Phe656 are not conserved, giving rise to the idiosyncratic binding of Kv11.1-1A.[164,166,167] Interestingly, Kv10.1 has both of these residues in analogous positions, yet does not display the same promiscuous binding. The difference in pharmacological binding between these two channels is thought to

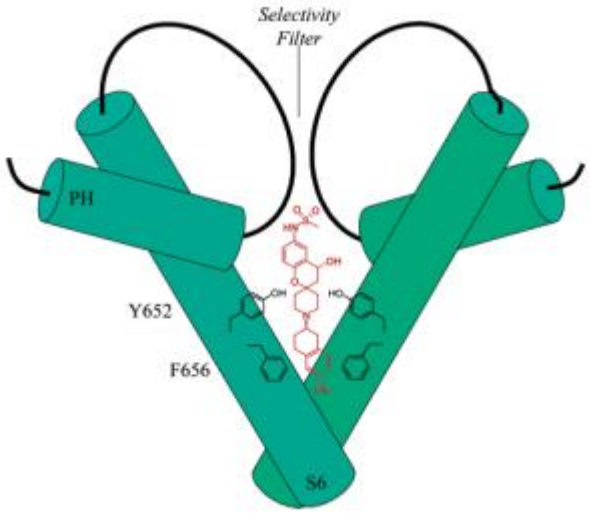

Figure 1.3. Key aromatic residues in the Kv11.1 channel pore mediate high-affinity promiscuous binding.

result from the lack of rapid C-type inactivation in Kv10.1. C-type inactivation contrasts from N-type in that, instead of closing the channel via an internal-TEA-sensitive cytoplasmic "ball and chain" inactivation particle, the channel inactivates by closing the selectivity filter and stabilizing this conformation. In fact, chimeric Kv10.1 channels, having Kv11.1-1A pore and S6 domains, exhibit high-affinity promiscuous binding.[165,168,169] However, the contributions of C-type inactivation have been quantitatively shown to be of less importance than the aromatic pore side-chains and not all drugs prefer to bind to the inactivated state.[170,171] Beyond factors that drive affinity for the Kv11.1-1A channel, their contributions are exacerbated by drug trapping inside the pore. Drug trapping artificially reduces inhibitor off rates due to the closure of the channel during repolarization.[128]

I_{Kr} blockade-induced QT prolongation is especially common among antipsychotics, but the pertinence of Kv11.1-1A to schizophrenia extends beyond adverse event risk.[172] Neuronal expression of Kv11.1-1A (and other related EAG/ERG channels) has been found in the cortex, hippocampus, substania nigra, thalamus, hypothalamus, and cerebellum. On a cellular level, Kv11.1-1A channels are expressed in the axon, dendrites, and cell body. As mentioned previously, Kv11.1-1A channels have been shown to be involved with burst firing, which regulates prolactin release in pituitary lactotropic cells. Kv11.1-1A channel inhibition in cerebellum Purkinje neurons has been reported to increase excitability and flatten spike-frequency adaptation. [133,173] However, of great interest is the role of Kv11.1-1A channels in dopaminergic neurons. These channels contribute to calcium-independent afterhyperpolarization (AHP) currents. Antipsychotic blockade of Kv11.1-1A currents in mid-brain dopaminergic neurons also significantly reduces post-stimulus inhibitory period end the end of an action potential train, increases excitability, being implicated in dopamine release.[173,174] Furthermore, these studies have suggested Kv11.1-1A channels reduce depolarization block of these neurons, the elongation of which being a common effect of antipsychotics associated with efficacy. Therefore, it has been suggested that Kv11.1-1A blockade in the CNS contributes to the therapeutic effects of certain antipsychotics and that these

channels may be novel antipsychotic drug targets.[175]

KCNH2-3.1 and Kv11.1-3.1

In 2009, a new *KCNH2* isoform was reported by Huffaker et. al.[176] Using family-based association test analyses (FBAT) for single nucleotide polymorphisms (SNPs) of gene-based haplotypes in 170 families of European descent having an offspring with schizophrenia, they found a number of closely localized schizophrenia-associated SNPs in 7q36.1, specifically the *KCNH2* and *NOS3* regions. The most statistically significant SNPs were located in the *KCNH2* gene. A selection of these SNPs were analyzed in expanded, independent family datasets and triaged for further analysis. Using a meta-analysis for all of these datasets, a number of SNPs in an intronic region of *KCNH2* were found to be significantly associated with schizophrenia. Knowing that *KCNH2* was highly expressed in brain regions important in schizophrenia pathology (dorsolateral PFC "DLPFC", hippocampus), three SNPs were found to be associated with lower IQ, slower/inefficient cognitive processing, increased cortical engagement, and decreased hippocampal structure in healthy controls via fMRI and cognitive testing studies. These phenotypes are associated with genetic risk of schizophrenia, general cognitive deficit, and impaired hippocampus/DLPFC function.[177-180]

In attempts to reduce these finding to mechanism, it was found that KCNH2-1A mRNA was reduced in the PFC and hippocampus in patients with schizophrenia, although this was not associated with specific SNP expression. However, RNA sequencing from the DLPFC of post-mortem brains obtained from schizophrenia patients was able to identify an endogenous transcript with a start site extending from exon 3 (without exons 1 or 2). This transcript corresponded to an N-terminally truncated isoform of Kv11.1-1A, missing 102 amino acids. This transcript, coined "KCNH2-3.1", was recombinantly expressed in HEK 293 cells, displaying a size difference compared to full length protein by western blot. Interestingly, western blot in human DLPFC and

rhesus monkey show bands of both sizes, suggesting comparable expression of the full length and truncated. However, KCNH2-3.1 was not found to be present in other mammals besides primates. Transcript expression of KCNH2-3.1 was subsequently shown to be brain specific, being expressed three orders of magnitude more in the hippocampus and fetal brain than in the heart. Additionally, while expression differences and developmental patterns of KCNH2-1A and KCNH2-3.1 were similar in most brain regions in postnatal samples, KCNH2-3.1 expression in fetal brain samples were found to be expressed much higher that the postnatal level. Importantly, the ratio of KCNH2-3.1 expression to KCNH2-1A expression was 2.5-fold higher in schizophrenia patients as compared to controls. Finally, increased KCNH2-3.1 expression was significantly associated with the identified risk SNP's (rs3800779 being the most prominent) in both patients and controls, suggesting a biological mechanism for schizophrenia risk.

Whereas Kv11.1 channels have been implicated in neuronal firing processes and regulation, Huffaker et. al investigated the functional role of the resulting translational product from the KCNH2-3.1 transcript, Kv11.1-3.1. Using whole-cell voltage clamp in transfected HEK 293 cells, Kv11.1-3.1 showed rapid deactivation, faster activation, and decreased hyperrepolarizing tail current amplitude as compared to Kv11.1-1A. Cells co-expressed with both channels showed intermediate phenotypes for kinetics and amplitude. Kv11.1-3.1 was transfected into primary rat cortical neurons, which presumably formed heterotetramers with endogenous Kv11.1-1A channels, and were found to exhibit similar kinetics in the pure, subtracted currents. Using current clamp protocols, Kv11.1-3.1 transfected neurons showed greater excitability via increased spike frequency. Kv11.1-1A transfected neurons showed behavior similar to transfected cells. Additionally, this excitability exhibited a non-adapting pattern, suggesting changes in spike-frequency adaptation important for PFC function and cognition.[176]

This seminal work was quickly followed by a report validating the association of SNPs in the *KCNH2* locus, including rs3800779, using an independent, Turkish male dataset.[181] Hashimoto et al. also used rs3800779 to confirm *KCNH2* association with schizophrenia in a meta-analysis of

five independent ethnic groups along with recruited Japanese subjects. In this report they used similar cognitive tests with recruited controls and patients and confirmed results found in Huffaker et al.[182] Recently, additional SNP's in the bordering locus between *KCNH2*and *NOS3* have been shown to be significantly associated with social memory, although the pertinence of these finding to schizophrenia has yet to be determined.[183] The same NIMH group examined pharmacogenetic relationships between risk SNP's and treatment outcome from a previous effort to gather genetic, clinical, and symptomatic datasets in the context of antipsychotic treatment: Clinical Antipsychotic Trials in Intervention Effectiveness (CATIE).[184,185] In the CATIE study, schizophrenia patients were randomly prescribed various antipsychotics and examined for outcomes using the PANS scale during regular intervals for 18 months.[5,185] In the follow up study seeking associations between KCNH2-3.1 risk SNP's and treatment outcomes, it was found that patients homozygous for the previously reported SNP, rs1036145, were more likely to respond to treatment for the reduction of positive symptoms with no difference for negative symptoms, but were also one-fifth as likely to discontinue olanzapine (although this result was underpowered). SNP rs3800779 did not show any significant differences between patients besides a generally more positive outcome regardless of treatment.[186]

Apart from the growing evidence of clinical significance, more studies into the cellular and mechanistic characteristics of the Kv11.1-3.1 channel were also studied. By stably expressing Kv11.1-3.1 in CHO cells, containing few endogenous K channel currents, a purer approach to determine the gating differences, as compared to Kv11.1-1A, could be taken.[122,187] Using established voltage protocols to examine Kv11.1 gating kinetics (activation rate as determined by envelope of tails, voltage-dependent steady state activation, deactivation rate, inactivation, etc.), Heide et al. confirmed the hallmark rapid deactivation rate although reported similar rates of activation and voltage-dependence of steady state activation in contrast to Huffaker et al.[128,176] However, this study also demonstrated that Kv11.1-3.1 channels have slower inactivation at depolarized membrane potentials, leading to greater current flux at these states. In the scope of

schizophrenia, these results suggest that greater populations of Kv11.1-3.1 channels leads to less current accumulation, curtailing typical Kv11.1-1A inhibition of long action potential trains, suggesting a mechanism behind the increased excitability found in Huffaker et. al.[176,187] Ke et al. were the first to formally report the trafficking defect of Kv11.1-3.1 channels, citing the absence of most of the PAS domain, yet showing this domain was not necessary for proper trafficking or activity, displaying the efficacy of a complete N-terminal truncated Kv11.1-1A mutant Δ2-135. From this report it was speculated that the N-terminus of Kv11.1-3.1 was likely not folded and would be recognized as unfolded and marked for degradation. The report also suggested that a complete PAS domain allows for proper trafficking with an N-terminal cap domain, thus intermediate residues, as found in Kv11.1-3.1, are not sufficient. Interestingly, Kv11.1-3.1 was shown to form heterotetramers with both Kv11.1-1A and Kv11.1-1B channels.[145] In a continuation of the work at the Vandenberg group, Heide et al. examined the expression of KCNH2-3.1 mRNA via *in-situ* hybridization in post-mortem DLPFC in healthy controls and schizophrenia/schizoaffective patients stratified by SNP analysis. KCNH2-3.1 mRNA was found in both large and small neurons in the DLPFC. In the combined group of schizophrenia/schizoaffective patients, a significant increase in mRNA was found as compared to healthy controls in layer III/IV small neurons only while confirming increases of fold change expression across SNP alleles.[188] In collaboration with members of the NIMH group, Heide et al. screened common antipsychotics on differential abilities to selectively inhibit Kv11.1-3.1 over Kv11.1-1A. Using the stably expressing CHO cell line, it was found that risperidone, and not its active metabolite 9-hydroxyrisperidone (paliperidone), was two-fold selective for Kv11.1-3.1, with an IC_{50}=200 nM (Kv11.1-1A IC_{50}=508 nM). Noting the difference in selectivity difference between risperidone and paliperidone, it was found that KCNH2-3.1 increasing risk SNP patients with "poor metabolizer" status (due to cytochrome P450 polymorphisms, etc.) exhibited a better treatment response to risperidone than other drugs.[189]

In order to validate Kv11.1-3.1 as a target for drug discovery for the treatment of schizophrenia,

a transgenic mouse model was developed and characterized for behavioral deficits.[190] Using a "tet-off" NSE promoter (for specific neuronal expression) transgene, a mouse model was developed that overexpressed KCNH2-3.1 in the PFC, hippocampus, striatum, and cerebellum. As adults, these mice were shown to exhibit impaired theta burst stimulation long-term potentiation (LTP), suggesting functional hippocampal impairment. Impaired basal synaptic transmission in adult mice was also observed. Primary pyramidal PFC neurons from transgenic mice were shown to have increases firing rates/increased excitability compared to wild-type mice along with the hallmark rapid deactivation rates. While the transgenic mice did exhibit characteristics of Kv11.1-3.1 expression as predicted in previously reported cellular models, these mice were also tested in t-maze working memory and object location spatial memory challenges. In the t-maze test, adult transgenic mice were found to be less accurate in 4-s delay trials, suggesting impaired working memory that requires a functional PFC. During the object location task, transgenic mice were shown to have no preference for displaced objects, suggesting impaired hippocampal memory function. While the hippocampal electrophysiological deficits were not present in juvenile mice, reduced expression in transgenic mice via doxycycline treatment (triggering the "tet-off"), reversed LTP and novel object location deficits to being statistically indistinguishable from wild-type mice. While there may be a possible developmental effect, this report also suggests that adult treatment for Kv11.1-3.1 contributing pathology may be a possibility. Most importantly, this work established a working *in-vivo* model for Kv11.1-3.1 contributions to schizophrenia-associated deficits and behaviors, a necessary tool for drug discovery.

While some basic characterization of the channel has been reported along with a promising animal model, the literature is absent of any efforts to translate the discovery of Kv11.1-3.1 into the clinic.

Scope of studies

New pharmacological agents for the treatment of schizophrenia are needed. Over the past 6 years, Kv11.1-3.1 has presented itself as a possible therapeutic target given the genetic, clinical, and transgenic mouse model findings. However, key questions remain: is it possible to get therapeutic effects in the brain without untoward effects on the heart? Does Kv11.1-3.1 apply a negative effect to the cell (requiring inhibition) or does it merely exist in the absence of a required positive (requiring activation)? The ultimate aim of this work is to create a tool compound for a drug discovery campaign that will allow us to investigate the pathology of Kv11.1-3.1 and be used as a benchmark for determining CNS efficacy and cardiovascular safety. However, the lack of high throughput screening and other assay infrastructure hinders any prospective drug development. While Kv11.1-1A channel assays have been well established in a variety of methods, including APC, Kv11.1-3.1 exhibits especially poor trafficking and low assay signal. In order to alleviate these issues and progress onto translational efforts, basic inquiries into the nature of these trafficking deficits must be taken. Upon trafficking rescue, subsequently developed assays may be used to not only drive medicinal chemistry and screening, but also to investigate a wider selection of antipsychotics with known Kv11.1-1A activity for any Kv11.1-3.1 selective behavior.

Chapter II

Kv11.1-3.1 Exhibits a Unique Trafficking Deficit that is Rescued Through Proteasome Inhibition for High Throughput Screening

Introduction

The discovery of a small molecule that could selectively modulate Kv11.1-3.1 activity presents many challenges. The most apparent issue is channel homology to Kv11.1-1A (hERG), the primary channel involved in cardiac I_{Kr} currents and frequent anti-target causing arrhythmia, Long QT Syndrome, and torsades de pointes.[128] hERG channels have also been implicated in processes such as midbrain dopaminergic bursting and epilepsy, which may present unique challenges as Kv11.1-3.1 and Kv11.1-1A channels are expressed at similar levels in the brain and have been shown to form heterotetramers in cell models.[145,174,176,191] To develop novel modulators of this channel for psychiatric indications, great care must be taken to identify molecules with selectivity over the Kv11.1-1A form of the channel to avoid cardiac and neural toxicities. Robust screening methods with consistently large signals are required to rapidly discover promising tools; however, Kv11.1-3.1 presents significant obstacles to efficient screening.[125,192] While recording from cells overexpressing Kv11.1-3.1 is possible, previous studies have shown trafficking defects and low current densities comparable to Long QT Syndrome 2 (LQTS2) Kv11.1-1A mutants, which makes high throughput screening impractical.[187] Similar to Kv11.1-3.1, many of these LQT mutants contain mutations and deletions in the PAS domain, also resulting in rapid deactivation kinetics in HEK 293 cell models.[128,144,193,194] These kinetic effects are likely due to the loss of PAS domain interactions with the amphipathic helix containing N-cap and C-terminal nucleotide binding domain (cNBD).[146,195,196] While it has been demonstrated that complete PAS

domains are not necessary for trafficking or formation of channel heterotetramers, including Kv11.1-1A and Kv11.1-3.1 heterotetramers, a partial or mutated PAS domain leads to an instable PAS structure and subsequent trafficking deficiency.[145] Molecular rescue of these defects would facilitate efforts to create such a screening platform, and many examples of possible rescue techniques have been reported and characterized.[193,197-202] Nevertheless, no successful method of rescuing Kv11.1-3.1 trafficking has been reported to date.

Efforts were taken to describe the extent of expression or trafficking defects while simultaneously applying methods to attempt rescue, compatible with HTS assay design. Here it is demonstrated that Kv11.1-3.1 shows poor steady-state expression, low channel activity, and trafficking deficits. Pharmacological agents may be used to rescue these phenotypes via blockade of proteasomal activity. Utilizing this technique, an improved channel assay signal amenable to HTS is possible.

Materials and Methods

Molecular Biology

Mammalian promoter constructs for the expression of C-terminally hemagglutinin (HA) tagged Kv11.1-3.1 or Kv11.1-1A were generated from KCNH2 and KCNH2-3.1 containing pcDNA 3.1(+) (ampicillin-resistant) mammalian expression vectors, generously donated by Jingshan Chen at the National Institute for Mental Health (See **Appendix** for all primer sequences). One Shot® TOP10 chemically competent *E. Coli* cells were thawed on ice for 15 minutes prior to inoculation with vector. Inoculated cells were incubated on ice for 30 minutes and then placed in a 42^0C water bath for heat shock transformation. Cells were incubated an additional 5 minutes on ice. Super optimal broth with catabolite repression (SOC media) was added and the cells in media were incubated at 37^0C and agitated at 300 RPM in a shaking incubator for 1 hour. Cells in SOC media were then spread on Luria-Bertani (LB) agar plates containing 100 μg/mL ampicillin and

incubated at 37^0C for 16 hours. Successfully transformed bacterial colonies were picked and grown in LB media containing 100 μg/mL ampicillin for 16 hours. Plasmid DNA was isolated and purified via Qiagen MAXI® kit per the manufacturer's instructions. DNA purity and concentration was analyzed via Nanodrop 2000®. Plasmid DNA was diluted and used as template DNA for polymerase chain reaction (PCR) in order to extend transcripts with HA tag and appropriate endonuclease restriction sites. PCR was performed using the Qiagen LR PCR® kit per the manufacturer's instructions with annealing temperatures based on the appropriate T_m calculated for each pair of primers. PCR products were analyzed and purified via agarose gel electrophoresis, visualized under UV light, and recovered using Qiagen gel purification kit per the manufacturer's instructions. Purified products and desired expression vector, PiggyBac® pHULK® IRES-Serrano RFP® (including kanamycin and puromycin resistance cassettes), were digested with appropriate restriction enzymes for 2 hours at 37^0C. Reaction mixtures were purified using the Qiagen PCR Purification® kit per the manufacturer's instructions. Purified digested expression cassettes and expression vectors were ligated using New England Biolabs® T4 ligase per the manufacturer's instructions. Ligation reaction mixture was inoculated into TOP10 cells and transformed as described. Transformed colonies were selected and analyzed for successful cloning as described. Cloning was validated via bi-directional Sanger Sequencing at the Johns Hopkins Sequencing Core. Validated clones were grown for MAXI® prep as described and the resulting purified DNA was used for transfection.

Stable cell lines expressing either Kv11.1-3.1 or Kv11.1-1A were engineered using parental Human Embryonic Kidney 293 (HEK 293) cells. Cells were thawed from frozen stocks stored in liquid nitrogen via rapid warming in a 37^0C water bath and then diluted in Glutamax® Dulbecco's modified Eagle's Medium/Ham's F-12 (DMEM/F12) supplemented with 100 U/mL Non-essential amino acids, 1x Penicillin/Streptomycin, and 10% fetal bovine serum. Media was removed by pelleting cells via centrifugation at 1000 g for 5 minutes and then aspirating the supernatant. Cells were resuspended in Glutamax media (vide supra) and plated in T75 vented

cell culture flasks. Cells were grown at 37^{0}C under 5% CO_2 to 80% confluency over a period of 1-2 days. Media was removed by aspiration and dissociated from the flask using Tryple E Express dissociation reagent and incubation for 5 minutes at 37^{0}C. Dissociated cells were resuspended in Glutamax media and the media was removed as described. Cells were plated in 6 well plates for transfection and T75 flasks for line maintenance. Cells in the 6 well dish were transfected using the engineered plasmids and Lipofectamine 3000® per the manufacturer's instructions. After 48 hours, cellular media was removed and replaced with Glutamax media containing 1 μg/mL puromycin. Single cells were selected by flow cytometry for maximum red fluorescence and plated into 96 well plates. Cells were cultured until clonal lines were established. Expression was verified by western blot and whole-cell patch clamp (vide infra). Scaled-up colonies were maintained in media containing 1μg/mL puromycin.

For stable cell line pharmacological trafficking treatments, drugs were dissolved in DMSO, and added to media (without puromycin) at DMSO final concentrations <0.2%. Cells were incubated in drug-containing media for 16-20 hours prior to assays.

Electrophysiology

HEK 293 cells stably expressing hERG channels were dissociated and plated onto PDL-coated glass coverslips in fresh puromycin-free media. Glass patch pipette electrodes were pulled using a PC-10® two-stage vertical puller. Average pipette resistance was between 2-3.5MΩ when filled with an internal solution containing: 120mM potassium gluconate, 5mM EGTA, 10mM HEPES, 20mM KCl, 1.5mM Mg-ATP, at pH 7.3 with KOH. Plated cells were immersed in a perfused extracellular solution bath containing: 1mM $MgCl_2$, 1mM $CaCl_2$, 10mM HEPES, 12.5mM Glucose, 5mM KCl, 130mM NaCl, 0.1% dimethyl sulfoxide (DMSO), at pH 7.4 with NaOH. Liquid junction potential for these solutions was calculated to be -15mV, which was not corrected for in experiments. Cells were voltage clamped in whole cell mode using an Axopatch® 200B

amplifier. Current signal was digitized at 5 kHz and filtered at 10 kHz and stored on an IBM-compatible PC interfaced with a NI USB-6221 analog-digital converter.

SDS-PAGE electrophoresis and Western Blot

Cells were washed with ice-cold PBS, harvested in ice-cold PBS via scraping, and pelleted by centrifugation at 500 g for 5 minutes. Cell pellets were resuspended with Radioimmunoprecipitation assay (RIPA) buffer supplemented with 1x protease inhibitor and rotated at 4^0C for 1 hour. Lysates were cleared by centrifugation at 16,000 g for 10 minutes and supernatants were analyzed for total protein concentration using a BCA kit per the manufacturer's instructions. 30 µg of total protein lysate was taken from each sample and fractionated on a 4-12% gradient Novex® Bis-Tris Bolt® SDS-PAGE gel via electrophoresis (185 V, 1 hour). Proteins were transferred onto 0.45 µm nitrocellulose membranes and incubated for 1hr in Odyssey® PBS blocking buffer. Membranes were probed with anti-HA (1:5,000) and anti-NaK-ATPase (1:2,500) primary antibodies in Odyssey® PBS blocking buffer overnight at 4^0C. Anti-HA and anti-NaK-ATPase signals were detected using IRdye 800 donkey anti-rabbit (1:20,000) and IRdye 680 donkey anti-mouse (1:20,000), respectively. The Li-Cor Odyssey® imaging system and software was used for antibody detection and quantification.

Co-immunoprecipitation

Dynabeads Protein G® were prepared according to the manufacturer's instructions and incubated with HA.11 anti-HA antibody for 30 minutes and then fixed with BS^3 crosslinking reagent to prevent antibody dissociation, per the manufacturer's instructions. Equal amounts of cell lysates from stably expressing Kv11.1 cell lines were prepared as before and then incubated with the prepared beads overnight at 4^0C. Beads were washed and proteins were eluted per the manufacturer's instructions and visualized via SDS-PAGE. Membranes were probed with the

antibodies described previously and anti-ubiquitin (1:1000). Antibody detection was performed as before.

Fluorescence Microscopy

Stable HEK 293 cell lines expressing either the full-length (1A) or deletion Kv11.1 (3.1) channel variant were plated onto 24 well ibiTreat® plates and grown until 80-90% confluent. For sub-cellular co-localization studies, cells were fixed with 4% paraformaldehyde in PBS for 15 minutes. Cells were simultaneously permeabilized, blocked, and quenched for background fluorescence by incubation in a PBS solution containing 0.1% Triton X-100, 10% normal goat serum, and 0.75% glycine for 15 minutes. Cells were probed with primary antibodies: anti-extracellular loop hERG (1:1000), anti-calnexin (1:1000), anti-58K Golgi protein (1:200), anti-20s proteasome β1 (1:200). For cell-surface labeling, fixation time was reduced to 10 minutes and paraformaldehyde concentration was reduced to 2% to reduce permeabilization. Cell surface labeling with anti-hERG antibody was performed as described above. Cell images were captured with the Operetta® high content imaging system and quantified with Columbus® image analysis suite.

Voltage Protocols

All voltages protocols used are illustrated on or above the relevant panel. For manual patch, to induce both steady-state and tail currents, cells were held at a potential of -80 mV, depolarized to 0 mV for 5 s and then hyperpolarized to -120 mV for 3 s. To measure rates of deactivation, cells were first depolarized to 20 mV for 500 ms to completely activate the channels. Cells were then repolarized to voltages in the range −60 to −130 mV for 5 s and traces were fitted to biexponential functions as described in Heide et al.[187]

FluxOR® Thallium Flux Assay

Stably Kv11.1 channel expressing HEK 293 cells grown to 90% confluency were then plated onto PDL coated 384 well plates and allowed to grow 16-20 hours at 37^0C with (Kv11.1-3.1) or without (Kv11.1-1A) 10 nM bortezomib. FluxOR® loading buffer supplemented with 10mM Red Dye #40 was added to each well and incubated for 45 minutes. Compounds were diluted in assay buffer containing 2.5 mM ouabain and then added and incubated for 10 minutes. Stimulation buffer was added to plates in a FDSS7000 kinetic plate reader while channel activity was monitored. Channel activity was analyzed using the Hamamatsu® FDSS software and Dotmatics®.

Data Analysis and Statistics

Electrophysisology data analysis was performed using Axograph X®. All data is presented as mean ± SEM unless specified. Unpaired T-tests, ANOVA, and subsequent Bonferroni corrections were completed using Graphpad Prism®. Microscopy data was analyzed with linear mixed models with fixed effects for the treatment variables with a random intercept by replicate/well – hERG and RFP levels were $\log_2$-transformed prior to analysis. *P* values <0.05 were accepted as significant.

Results

Kv11.1-3.1 is a poor expressing, trafficking deficient hERG channel

The HEK 293 cell overexpression model was used to determine steady-state expression levels, trafficking efficiency, and activity of Kv11.1-3.1, via electrophysiology, immunoblotting, and immunocytochemistry. With the intention of controlling for channel transcription and transfection efficiency, mRNA levels were evaluated by qPCR. Transcription levels from selected Kv11.1-1A and Kv11.1-3.1 cell lines did not vary significantly, although Kv11.1-3.1 displayed a non-

significant increase relative to Kv11.1-1A transcription (P=0.058) (**Figure 2.1b iii**). Subsequent quantified data was not normalized to transcription levels due to these findings.

Channel activity was characterized via electrophysiology using whole-cell voltage clamp to determine efficacy in downstream HTS assays. Utilizing a test pulse protocol, by holding cells at -80 mV followed by depolarization at 0 mV and hyperpolarization at -120 mV (**Figure 2.1c ii**), differences in tail current deactivation between Kv11.1-1A and Kv11.1-3.1 were evident (**Figure 2.1c i**). Consistent peak tail current expression over 1 nA was considered acceptable for drug screening. The Kv11.1-1A line was quite robust in yielding large tail currents (>4 nA) as well as exhibiting a high fidelity of expression between cells. However, the Kv11.1-3.1 cell line did not produce a robust signal response in every cell, and it was uncommon to identify cells with tail current peaks over 1 nA. Cell membrane capacitance normalized peak tail currents from Kv11.1-3.1 expressing cells (22.66 ± 6.108 pA/pF, n=8) were significantly lower (P=0.0072) than currents recorded from Kv11.1-1A expressing cells (381.6 ± 95.82 pA/pF, n=8) (**Figure 2.1c iii**). Knowing that the expression rate and magnitude are critical for HTS methods[192], it was concluded that even the best expressing Kv11.1-3.1 lines were insufficient for a drug discovery platform. Before investigating the nature of these deficits and approaches to improve channel activity, it was necessary to characterize expression and trafficking levels to better understand the cause of low channel activity.

Western blot analysis was used to quantify expression and trafficking, as reported by previous groups.[152] HEK 293 cells overexpressing Kv11.1 show distinct bands via western blot: the mature fully glycosylated (FG) band and immature core glycosylated (CG) band. The core glycosylated band for Kv11.1-1A and Kv11.1-3.1 appears at 135kD and 125kD, respectively, while the FG band for each is approximately 20 kDa higher (**Figure 2.1b i**). These bands have been used previously as a heuristic diagnostic of channel trafficking [144,152,197,199,202,203], as the lower band is representative of channel present in the ER, being subject to only one glycosylation event, while

Figure 2.1. Kv11.1-3.1 is an N-terminally truncated hERG channel with trafficking, expression, and activity deficiencies. ***a***, Illustrative examples of Kv11.1-1A (i) and Kv11.1-3.1(ii) channel structure. Full length Kv11.1 channels contain N-terminal PAS domain and amphipathic helix N-cap, suggested to interact with each other and a C-terminal cyclic nucleotide biding domain. Kv11.1-3.1, being absent of a full PAS domain, likely presents an unstably folded N-terminal motif. ***b***, Sample Western blot (i) of whole cell lysates from stably transfected HEK 293 cells expressing recombinant HA-tagged Kv11.1-1A, Kv11.1-3.1, or Kv11.1-3.1 after 20 hour incubation at 28^0C (ΔT). Lysates were probed with anti-HA and anti-NaK ATPase primary antibodies subsequently incubated with fluorescent IR dyes for quantitative detection. Ladder markers indicated with respective sizes in kDa. Arrows indicate respective FG and CG bands representative of mature fully glycosylated and immature core glycosylated channel populations. Neither 3.1 nor cold-incubated 3.1 show obvious FG band expression, suggesting the 3.1 trafficking phenotype is heat-insensitive. (ii) Summary quantification of trafficking efficiency (FG/Total hERG, n=3) and relative expression differences (Total hERG/NaK ATPase normalized to 1A expression, n=3) of 1A and 3.1 channels. 3.1 showed significant decreases in both trafficking and steady-state expression. Note that while no FG signal is visible for Kv11.1-3.1, there is a photon count present above true background. (iii) Kv11.1-3.1 expressing cells show a non-significant increase in total hERG channel transcription compared to Kv11.1-1A expressing cells via qPCR(n=3). ***c***, (i) Example whole-cell deactivation tail current voltage clamp traces from HEK 293 cells expressing 1A or 3.1 channels. (ii) Currents were recorded by holding cells at -80 mV, activating channels with a voltage step to 0 mV for 5s, followed by a hyperpolarizing step to -120 mV to induce tail currents. 3.1 displays rapid deactivation compared to 1A. (iii) Peak tail currents from 1A and 3.1 traces were normalized to cell capacitance (pA/pF, n=8) and analyzed. 3.1 shows significantly reduce average peak tail current relative to 1A. All bar graph data presented as mean ± SEM (*P=<0.05, **P=<0.01, ***P=<0.001, ****P=<0.0001).

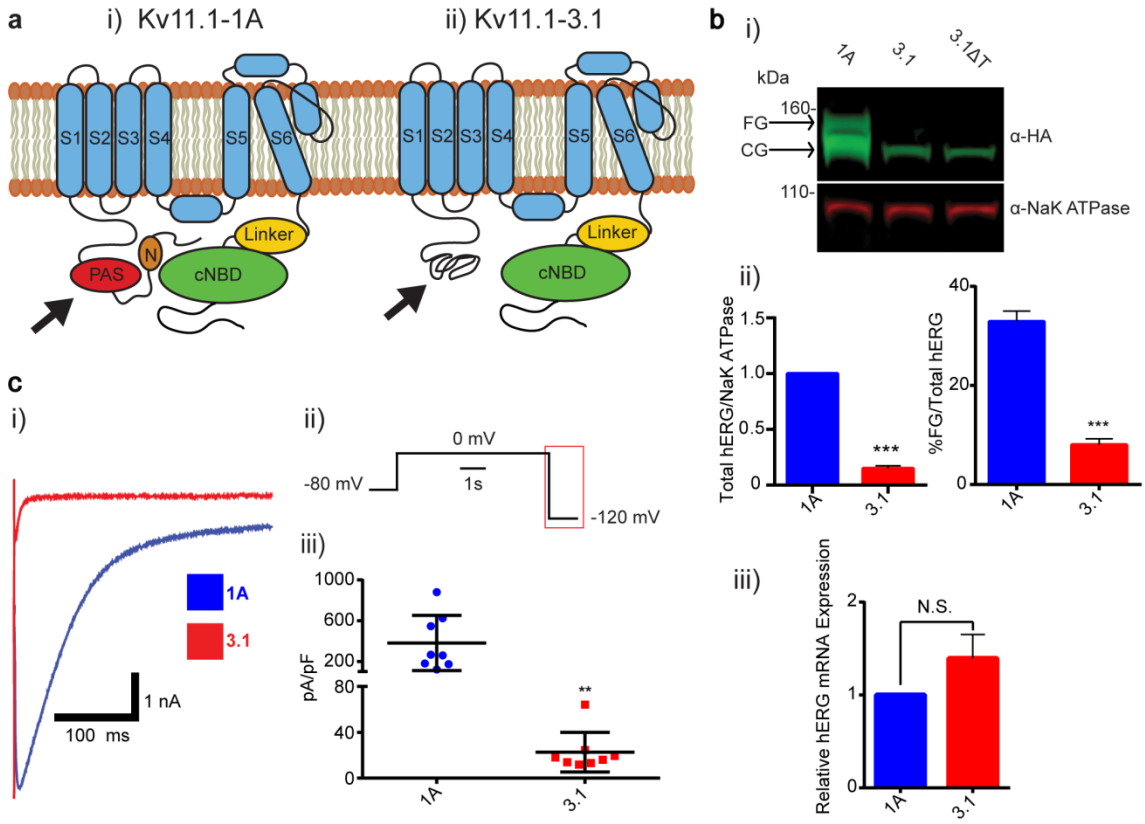
a
i) Kv11.1-1A
ii) Kv11.1-3.1
S1
S2
S3
S4
S5
S6
Linker
N
PAS
cNBD
b
i)
1A
3.1
3.1ΔT
kDa
160-
FG
CG
110-
α-HA
α-NaK ATPase
ii)
Total hERG/NaK ATPase
%FG/Total hERG
***
iii)
Relative hERG mRNA Expression
N.S.
c
i)
1A
3.1
1 nA
100 ms
ii)
0 mV
-80 mV
1s
-120 mV
iii)
pA/pF
**

the FG band is indicative of successfully trafficked channel being glycosylated again in the Golgi.[128]

The overall steady-state expression was determined by summing the total photon signal from both FG and CG bands normalized by the NaK ATPase loading control count. It was discovered that basal Kv11.1-3.1 expression was only 15±2 % (P=0.0008) of that to Kv11.1-1A levels on the same blot (**Figure 2.1b ii**). Furthermore, by calculating trafficking expression as a function of FG photon count normalized by total hERG photon count (FG+CG) it was found that Kv11.1-1A and Kv11.1-3.1 cells exhibited a significantly different (P=0.0002) trafficking efficiency of 32 ±2 % (n=3) and 8±1% (n=3) respectively (**Figure 2.1b ii**).

To establish the sub-cellular localization of Kv11.1-1A and -3.1, we performed co-localization studies using antibodies against Kv11.1 and control sub-cellular markers (**Figure 2.2**). Kv11.1 signal was measured in the nucleus and cytoplasm using DAPI as a differential counterstain for the nucleus and cytoplasm (**Figure 2.2a**). To normalize the anti-Kv11.1 antibody fluorescence in each cell, we also measured signal from the red fluorescent protein (RFP) that is expressed from an internal ribosome entry site (IRES). Characteristic fluorescence micrographs demonstrate the localization of both transgenes to the cytoplasm (**Figure 2.2b**). Total Kv11.1 fluorescence was measured in domains defined by the expression of the control organelle markers calnexin (ER), 58k (Golgi), and alpha 5 (proteasome) (**Figures 2.2c-d**). The fluorescence signal from Kv11.1-3.1 was significantly lower in all measured domains.

Kv11.1-3.1 expression and trafficking is rescued through proteasome inhibition

It has been demonstrated that many Kv11.1-1A LQT2 mutant trafficking defects are responsive to overnight low temperature incubation, while some are completely unaffected.[201] Upon incubation of Kv11.1-3.1 expressing HEK 293 cells at 28^{0}C for 16-20 hours, no FG band rescue was seen by Western (**Figure 2.1b i**). Knowing that Kv11.1-3.1 trafficking in HEK 293 cells was non-

Figure 2.2. Single cell measurements of Kv11.1-1A and Kv11.1-3.1 show reduced expression across sub-cellular compartments. ***a,*** Total Kv11.1-1A and Kv11.1-3.1 signal (RFU) was measured in each cell and normalized to the RFP signal from the same cells. Note the reduced signal in 3.1 from both nucleus and cytoplasm (n=3 unique experiments). ***b,*** Representative fluorescence micrographs show both fluorescence signal and overlay after sub-cellular image segmentation. ***c***, RFP-normalized signal from indicated sub-cellular compartments (n=3 unique experiments). ***d***, Fluorescence micrographs demonstrate localized signal from Kv11.1 and the organelle-specific masks used for sub-cellular localization. Colocalization and segmentation data used is from same experiment in **Figure 2.5**. Scale bars=100μm. All bar graph data presented as mean ± SEM (*P=<0.05).

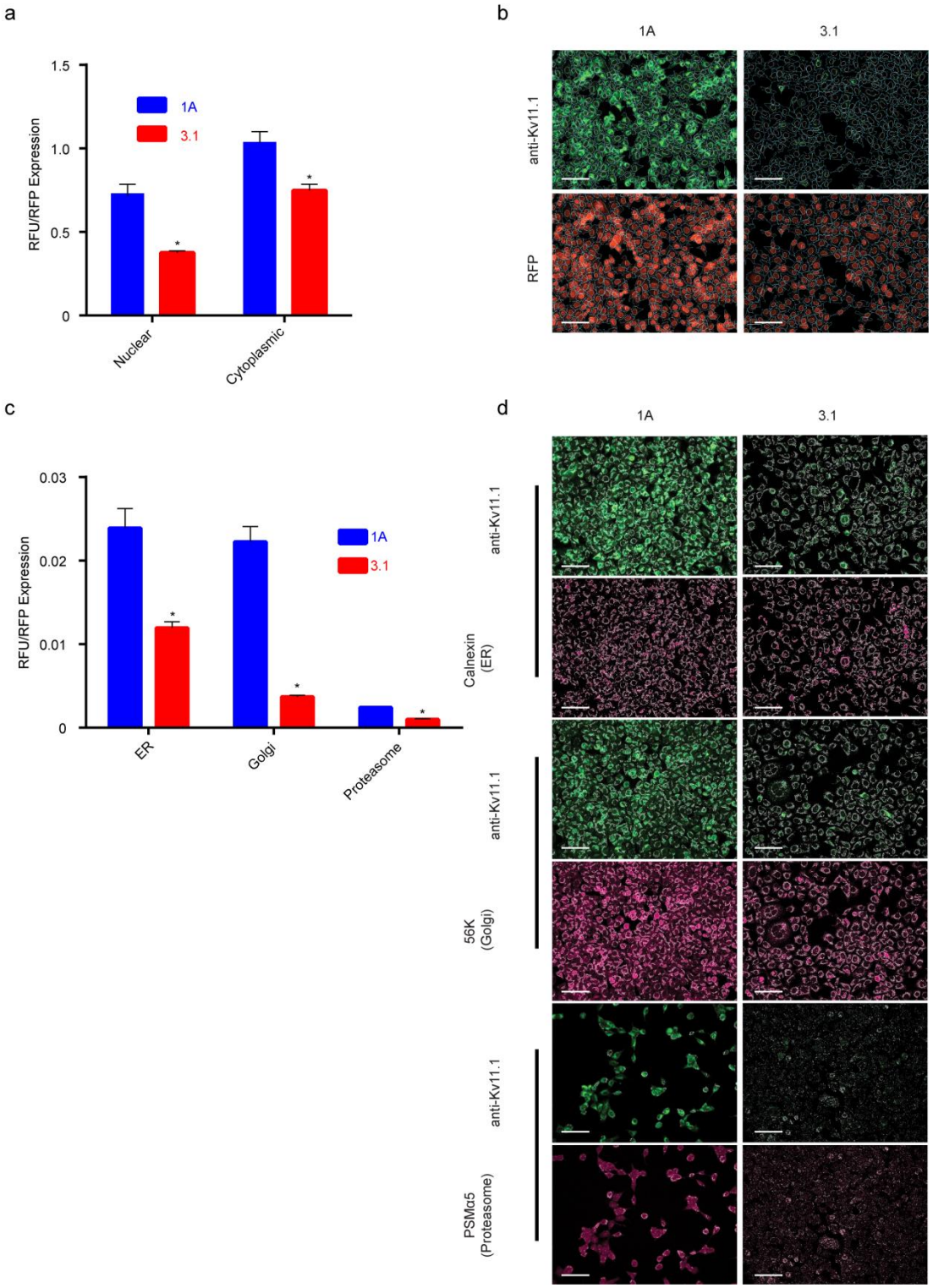
a
1.5
1.0
0.5
0
RFU/RFP Expression
1A
3.1
*
*
Nuclear
Cytoplasmic
b
1A
3.1
anti-Kv11.1
RFP
c
0.03
0.02
0.01
0
RFU/RFP Expression
1A
3.1
*
*
*
ER
Golgi
Proteasome
d
1A
3.1
anti-Kv11.1
Calnexin (ER)
anti-Kv11.1
56K (Golgi)
anti-Kv11.1
PSMα5 (Proteasome)

responsive to cold incubation, pharmacological rescue agents were then investigated using the same phenotypic Western blot screening.

A library of small molecules, that were either reported in the literature, or that were preliminarily identified for hERG activity, ERAD/UPR modulation, protease activity, or activity in other germane processes, was created[147,199,204-209]. Initially, it was found that the 26s proteasome inhibitor Mg132 [210] boosted CG expression levels, but was too cytotoxic for reproducible use (data not reported). Likewise, it was shown that the calpain/cathepsin/proteasome inhibitor N-[N-(N-acetyl-L-leucyl)-L-leucyl]-L-norlecucine (ALLN) [198,211] greatly increased Kv11.1-3.1 CG expression. (**Figure 2.3a**) Furthermore, ALLN was the only compound to show the clear presence of a Kv11.1-3.1 FG band after treatment (**Figure 2.3a**). Upon quantitative western analysis, optimal concentrations of ALLN rescued trafficking efficiency (25 ± 3%, n=3, P=0.0006) to similar levels seen in untreated Kv11.1-1A cells (**Figure 2.3b i**) and increased overall channel expression by over 4-fold (**Figure 2.3b ii**, P=0.001). Whole-cell voltage clamp test pulses evoked larger peak tail currents for ALLN treated cells expressing Kv11.1-3.1, than for untreated controls (**Figure 2.3c i**). Cell membrane capacitance normalized tail current peaks were found to be significantly greater (P=0.0472) in the ALLN treated cell groups (45.02 ± 5.079 pA/pF, n=9) compared to Kv11.1-3.1 controls (18.65 ± 4.714 pA/pF, n=8) (**Figure 2.3c ii**). To understand if this effect was selective for the Kv11.1-3.1 specific deficiencies, Kv11.1-1A expressing cells were treated with ALLN in a similar manner. Neither overall Kv11.1-1A expression nor trafficking efficiency was significantly altered with ALLN treatment (**Figure 2.3a-b**).

Although these findings supported ALLN as a good candidate for a rescue agent, ALLN contains a reactive aldehyde species and exhibits polypharmacology across multiple proteases.[200,212] Consequently it was necessary to investigate the mechanism of rescue. By comparing τ for deactivation of ALLN treated Kv11.1-3.1 expressing cells and controls (**Figure 2.4e**), it was demonstrated that no significant difference was seen in the primary Kv11.1-3.1/Kv11.1-1A-differentiating deactivation kinetics, thus rescue was not likely due to channel structure

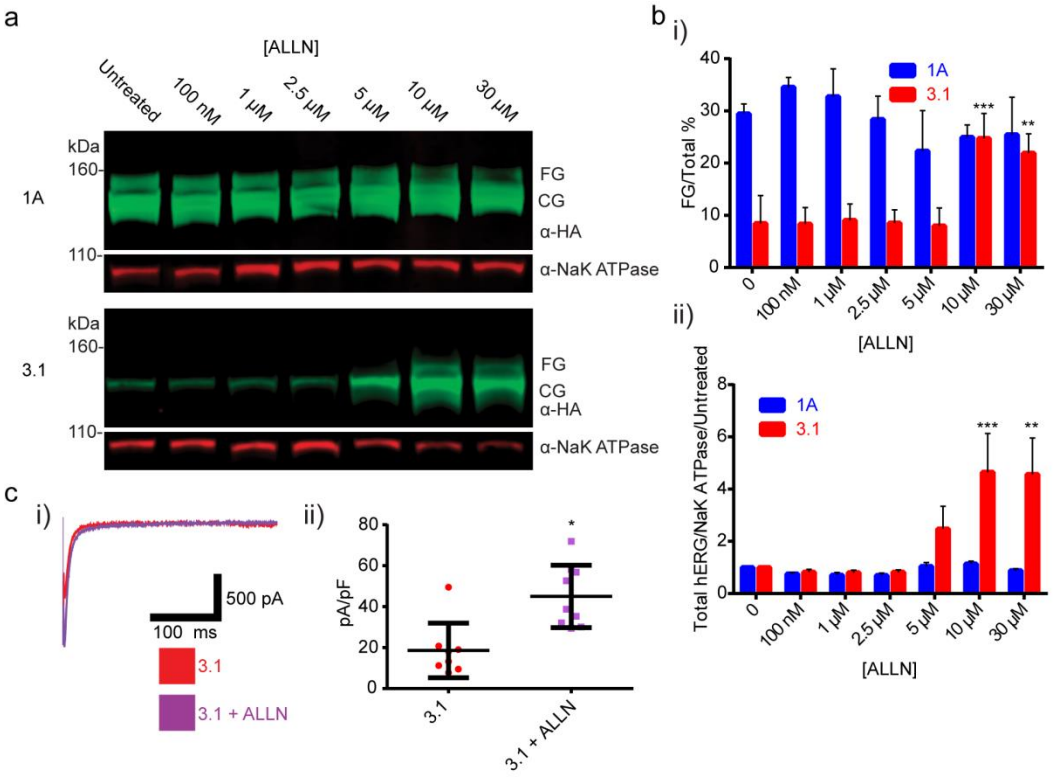

Figure 2.3. Kv11.1-3.1 expression, trafficking, and peak tail currents are significantly increased via pharmacological rescue with ALLN. ***a***, Example Western blot analysis of cells expressing 1A or 3.1 treated with the calpain/lysosomal cathepsin/proteasome inhibitor ALLN. ALLN treatment of 3.1 expressing cells resulted in presence of the FG band and increased CG band intensity while only increasing 1A CG expression. ***b,*** Quantitation summary of Western analysis shows significant increases of i) 3.1 trafficking and ii) total hERG expression upon ALLN treatment (n=3). No significant effects were seen in 1A expressing cells. ***c,*** i) Representative whole-cell voltage clamp tail current traces for ALLN treated 3.1 cells. ii) Peak tail currents were normalized to cell capacitance (n=8) and analyzed. ALLN treatment was found to significantly increase normalized peak tail currents compared to untreated cells (*P=<0.05). All bar graph data presented as mean ± SEM (*P=<0.05, **P=<0.01, ***P=<0.001).

modification. In order to deconvolute the ALLN polypharmacology for principle pharmacodynamic contributions, Kv11.1-3.1 expressing cells were treated with small molecules selective for cathepsins B,L, calpains I,II and the 26s proteasome, the multiple ALLN targets. The calpain I/II inhibitor PD 150606, the cathepsin B inhibitor CA 078, the cathepsin L inhibitor SID 26681509, and the 26s proteasome inhibitor bortezomib were chosen.[213-216] It was also anticipated that the rescue activity of ALLN might arise from the specific polypharmacological profile, so various cocktails of these inhibitors were formulated for screening. Western blot analysis from these treated cells (**Figure 2.4a**) yielded that only bortezomib was effective, hence 26s proteasome inhibition was responsible for Kv11.1-3.1 expression and trafficking increases.

Bortezomib was titrated for optimal rescue attributes and identical concentrations were tested in the Kv11.1-1A cell line (**Figure 2.4b**). At 10nM, bortezomib was found to rescue Kv11.1-3.1 channel trafficking (25 ± 2%, n=4, P=<0.0001) (**Figure 2.4c i**), increase overall Kv11.1-3.1 channel expression by an average of 6 fold (**Figure 2.4c ii**, P=<0.0001), and increase peak tail currents (**Figure 2.4d i**). The increase in cell membrane capacitance normalized peak tail currents (75.93 ± 11.84 pA/pF, n=8) was found to be greater than that of untreated Kv11.1-3.1 expressing cells (**Figure 2.4d ii**, P=<0.0001). Bortezomib treatment had no effect on Kv11.1-3.1 deactivation rate kinetics (**Figure 2.4e**).

Quantitative immunofluorescence of Kv11.1 1A and Kv11.1-3.1 supports the conclusion from electrophysiological studies that low Kv11.1-3.1 levels are a consequence of a proteasomal mechanism (**Figure 2.5**). Although modest elevation of Kv11.1 1A was detected when cultured in the presence of ALLN and bortezomib, a nearly 3-fold elevation of steady-state protein level was detected in the Kv11.1-3.1 variant when treated with ALLN or bortezomib (**Figure 2.5a**). When analyzed at subcellular segmentation and colocalization domains, both ALLN and bortezomib significantly increased Kv11.1-3.1 expression in the cytoplasm and nuclear regions along with the

Figure 2.4. Proteasome inhibition is sufficient for Kv11.1-3.1 rescue via bortezomib. ***a*****,** Example blot of 3.1 expressing cells treated with either selective calpain I/II inhibitor PD 150606, lysosomal cathepsin B/ L inhibitors CA 074/SID 26681509, 26s proteasome inhibitor bortezomib, or various cocktails in order to determine ALLN mechanism of rescue. Only samples treated with bortezomib, or a cocktail consisting thereof, resulted in the display of a FG band. ***b***, Example blot of cells expressing 1A or 3.1 treated with bortezomib. Treatment of 3.1 expressing cells with bortezomib results in presence of the FG band and increased CG band intensity while only increasing 1A CG expression. ***c,*** Quantitation summary of Western analysis shows significant increases of i) 3.1 trafficking and ii) total hERG expression upon bortezomib treatment(n=3). ***d,*** i) Representative whole-cell voltage clamp tail current traces for bortezomib treated 3.1 cells. ii) Peak tail currents were normalized to cell capacitance (n=8) and analyzed. Bortezomib treatment was found to significantly increase normalized peak tail currents compared to untreated cells (****P=<0.0001). Note data for untreated 3.1 peak tail currents is from the same experiments in **Figure 2.3c ii**. ***e,*** Pharmacological rescue conditions were tested for alterations to channel kinetics according to deactivation rate voltage protocol. i) Extrapolated τ_{deact} values for pharmacologically treated cells were not shown to be significantly different from those of controls, thus rescue compounds had no effect on Kv11.1-3.1 deactivation rates (n=3). All bar graph data presented as mean ± SEM (*P=<0.05, ***P=<0.001, ****P=<0.0001).

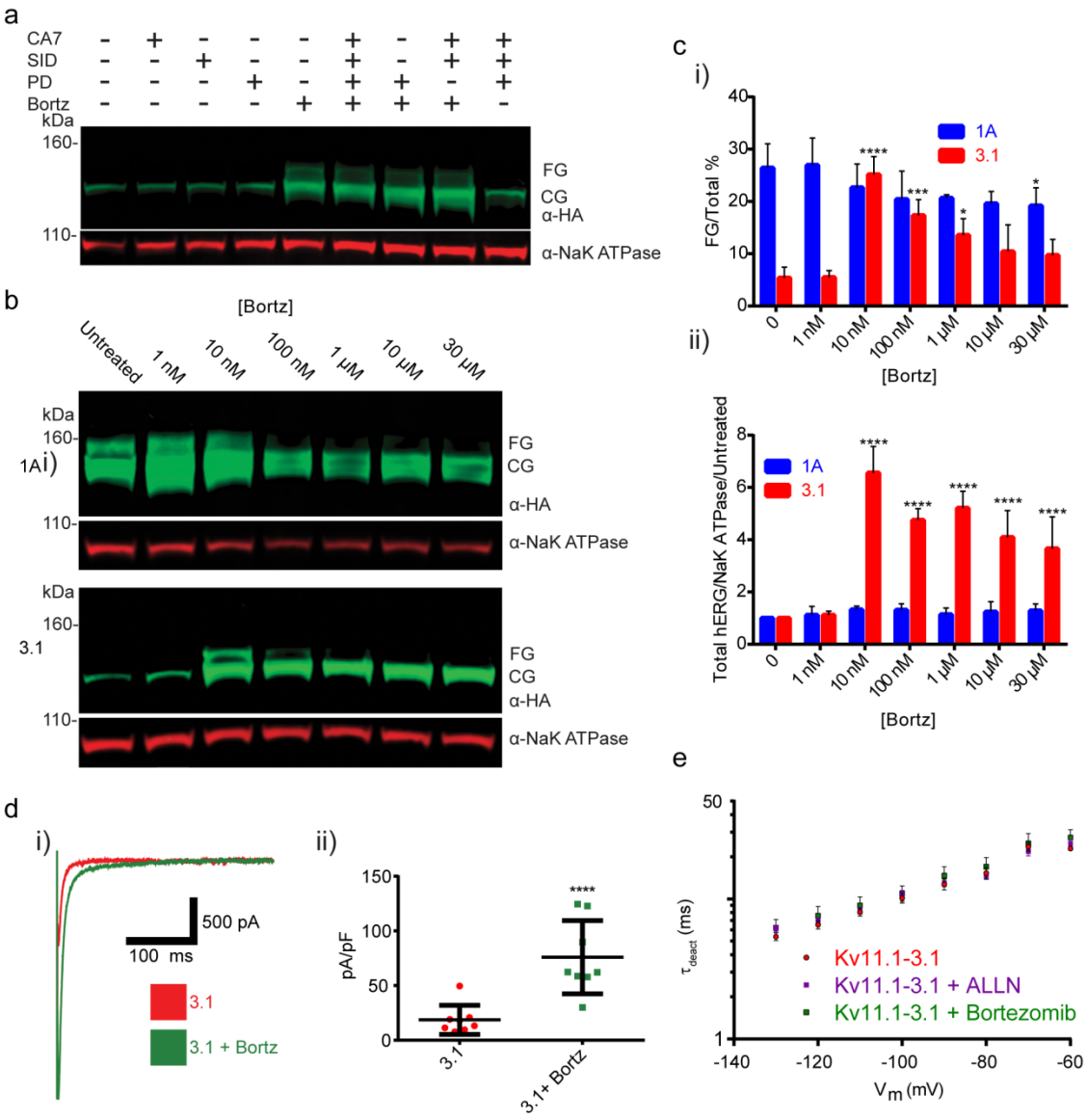
a
CA7
SID
PD
Bortz
kDa
160-
110-
FG
CG
α-HA
α-NaK ATPase
b
[Bortz]
Untreated
1 nM
10 nM
100 nM
1 μM
10 μM
30 μM
1A i)
3.1
c
i)
1A
3.1
FG/Total %
ii)
Total hERG/NaK ATPase/Untreated
d
i)
500 pA
100 ms
3.1
3.1 + Bortz
ii)
pA/pF
e
Kv11.1-3.1
Kv11.1-3.1 + ALLN
Kv11.1-3.1 + Bortezomib
τdeact (ms)
Vm (mV)

Figure 2.5. Proteasome inhibitor treated cells show Kv11.1-3.1 rescue across sub-cellular compartments and cell surface. ***a***, RFP-normalized fluorescence of Kv11.1 1A and 3.1. Note the differential elevation of 3.1 compared to 1A after the same treatments (n=3). ***b,*** Scatter plot of RFP vs surface Kv11.1 in single cells, n > 3000 measurements per condition (n=3 unique experiments). m = slope of the linear regression (solid line). The dotted lines have slope m=1 for reference. ***c***, Immunofluorescence micrographs of representative fields showing specific surface Kv11.1-3.1. Scale bars=100µm. All bar graph data presented as mean ± SEM (*P=<0.05, ****P=<0.0001).

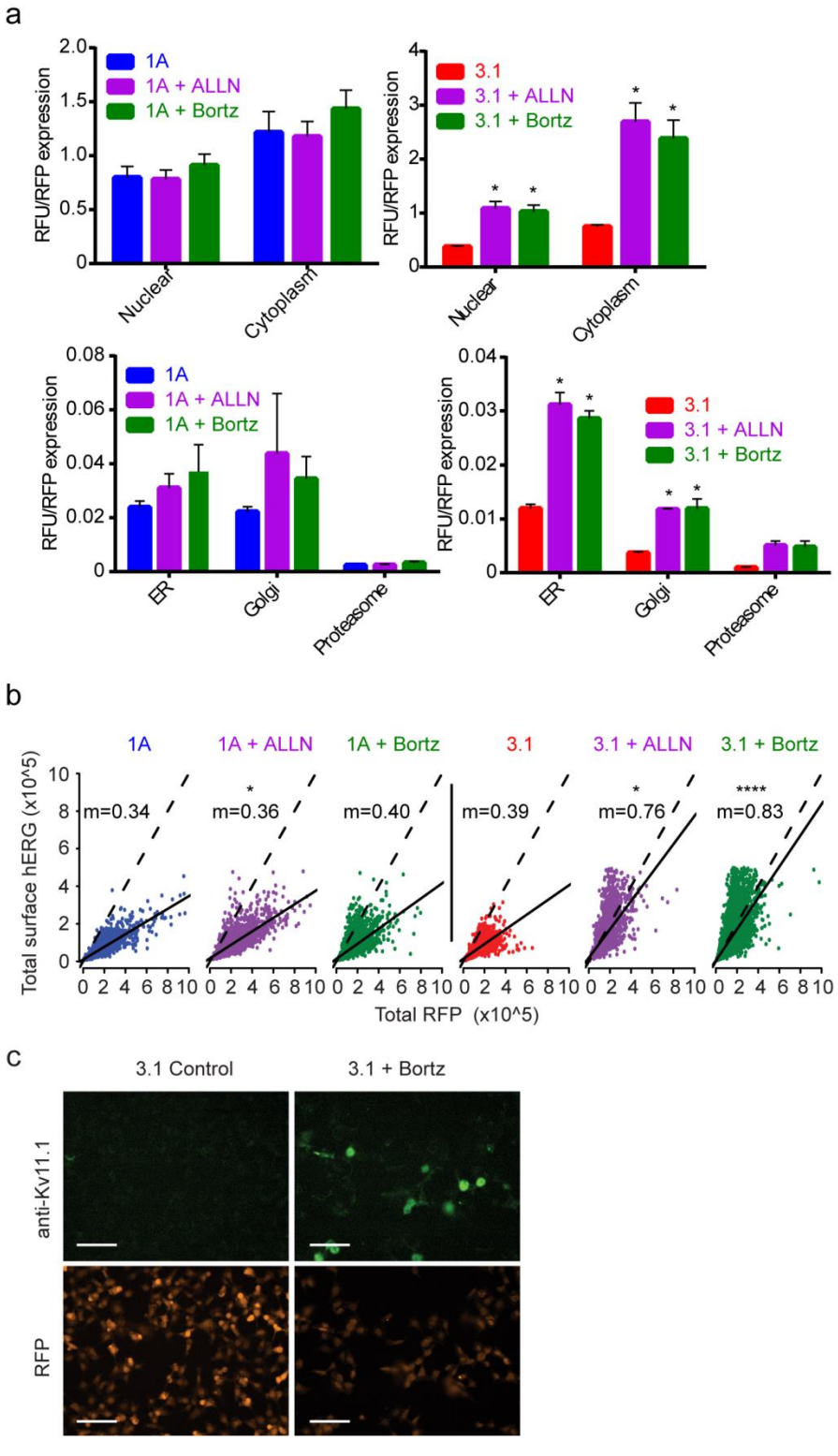
a
RFU/RFP expression
1A
1A + ALLN
1A + Bortz
3.1
3.1 + ALLN
3.1 + Bortz
Nuclear
Cytoplasm
ER
Golgi
Proteasome
b
Total surface hERG (x10^5)
Total RFP (x10^5)
m=0.34
m=0.36
m=0.40
m=0.39
m=0.76
m=0.83
c
3.1 Control
3.1 + Bortz
anti-Kv11.1
RFP

ER and Golgi. However, the increases in Kv11.1-3.1 proteasome domain expression were not found to be significant. Increased electrophysiological activity of Kv11.1-3.1 in the presence of bortezomib should involve increased localization of this channel to the cell surface. Using an antibody that recognizes an extra-cellular loop found in both Kv11.1-1A and Kv11.1-3.1, we performed immunocytochemistry with a brief fixation protocol that maintains the plasma membrane integrity (**Figure 2.5b**). To normalize the anti-Kv11.1 antibody fluorescence in each cell, we also measured signal from the red fluorescent protein (RFP) that is expressed from an internal ribosome entry site (IRES). Thus, the mRNAs for both Kv11.1 and RFP are regulated by a single common promoter, while the relative stability of each protein is a consequence of post-transcriptional mechanisms. The ratio of Kv11.1-1A/RFP (m=0.34) is minimally altered by ALLN (m=0.36, P=0.029) and bortezomib (m=.40, n.s.) as shown by the similar linear regression slopes (**Figure 2.5b**). In contrast, bortezomib and ALLN increase this ratio (b=0.39) by a factor of 2 in the Kv11.1-3.1 variant (m=0.75, P=.028 and m=0.83, P=<0.0001 respectively) (**Figure 2.5b**), demonstrating specific elevation of the Kv11.1-3.1 variant surface abundance with these small molecules. Representative fluorescence micrographs of Kv11.1 3.1 alone and in the presence of ALLN demonstrate the dramatic specific elevation of Kv11.1 3.1 (**Figure 2.5c**). Note the increase in Kv11.1 signal without change of RFP in the Kv11.1-3.1 variant only in the presence of ALLN or bortezomib. These data provide the third independent measurement of Kv11.1 3.1 demonstrating increased protein stability in the presence of proteasome inhibitors. While it is known Kv11.1-1A channels are ubiquitinylated in HEK 293 cells prior to proteasome degradation [217], no such mechanism has been shown for Kv11.1-3.1 channels, critical in exploring potential proteasome-dependent regulation of Kv11.1-3.1 channels. Immunoprecipitation of Kv11.1-1A and Kv11.1-3.1 channels was performed with and without pharmacological recue conditions with bortezomib (**Figure 2.6**). Immunoprecipitated channels lacked lysate loading control bands, and mouse IGG only samples (data not shown) did not yield signal, suggesting the IP was perfomed without residual non-specific proteins. Immunoprecipitation of the respective

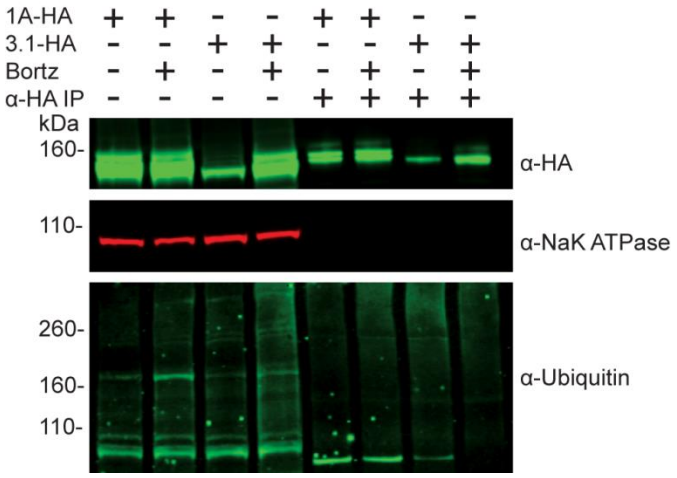

Figure 2.6. Kv11.1-1A and Kv11.1-3.1 show different channel ubiqunylation changes in response to bortezomib. HA tagged hERG channels were immunoprecipated from stably expressing hERG cell lysates that had been incubated with bortezomib or DMSO for 16 hours. Cell lysates and IP elutions were probed for HA tag, NaK ATPase, and ubiquitin. Cell lysates show increases in total ubiquitin with bortezomib treatment and both 1A and 3.1 channels show poly-ubiquitinylation. Immunoprecipitated 1A channels show increase in ubiquitnylation accumulation in bortezomib treatments. Immunoprecipitated 3.1 channels from bortezomib treated cells show less accumulation than DMSO incubated cells.

channels showed similar hERG signals as before, however the CG/FG band locates were slighty shifted up, likely due to different loading buffer conditions from the Protein A bead dissociation. Cell lysates from the respective cell lines showed increases in ubiquitin signal with bortezomib treatment. Immunoprecipitated 1A channels showed ubiquitinylation and accumulation of ubiquitin signal upon bortezomib treatment. Immunoprecipitated Kv11.1-3.1 channels showed ubiquitinylation, however, a decrease in ubiquitin signal upon bortezomib treatment.

Rescued Kv11.1-3.1 activity is suitable for High Throughput Screening

To determine if these rescue strategies could be successfully employed for a HTS assay, Kv11.1-3.1 expressing cells were treated as in the Western assays, and plated in multi-well plates in preparation for a potassium channel flux assay based on a thallium-sensitive dye.[125] ALLN and bortezomib treated cells both yielded significant signal improvement compared to untreated cells in the 384 well thallium flux assay with low variations between wells, both showing roughly 4 fold signal to background ratios (**Figure 2.7a**). Due to its lower effective concentration and repeated superiority to ALLN in assays for expression and trafficking, bortezomib was chosen as the rescue agent in subsequent HTS assays.

Using bortezomib treated Kv11.1-3.1 and untreated Kv11.1-1A cells, multiple assay plates were run in the thallium flux assay with the known Kv11.1 inhibitor E4031 and DMSO as controls. Repeated assay plates generated Z' scores of 0.811±0.07 for Kv11.1-1A cells without proteasome inhibitor and 0.797±0.02 for treated Kv11.1-3.1 cells (**Figure 2.7a**). Dose-response curves were generated (**Figure 2.7c**) for E4031 inhibition, and a known hERG activator, ML-T531.[209] Additionally, these small molecules were titrated with treated Kv11.1-3.1 and Kv11.1-1A cells in the same voltage-clamp assay used to determine capacitance normalized tail current (**Figure 2.7b**) for assay comparison. E4031 had uniformly 3-fold less potency against both channels (**Figure 2.7d**) in the thallium flux assay as compared to voltage clamp, showing no significant selectivity between channels. EC_{50} values for ML-T531 were similarly identical for Kv11.1-1A and Kv11.1-

3.1 in these assays, near 4μM. However, a higher maximum potentiation effect was seen for Kv11.1-3.1 as compared to Kv11.1-1A. EC_{50} values were also conserved across assay platforms, in contrast to E4031 IC_{50} values (**Figure 2.7d**).

Figure 2.7. Bortezomib treatment of Kv11.1-3.1 expressing cells produces sufficient currents for dose-response analysis of hERG inhibitors and activators via whole cell voltage clamp and high throughput fluorescence methods. ***a***, 3.1 expressing cells were treated with ALLN or bortezomib as before in 384 well assay plates. Plates were incubated the next day with assay loading buffer for 45 minutes, and then incubated with either E4031 or DMSO for 5 minutes prior to addition of stimulation buffer and subsequent signal detection. Comparison of pharmacologically treated 3.1 expressing cells and controls shows that both ALLN and bortezomib tremendously increase signal to background window in the thallium flux assay (n=16). Z' scores for the thallium flux assay with either 1A cells or 3.1 cells treated with bortezomib are well above the 0.5 threshold across multiple trials (n=3). ***b***, Dose-response of peak tail currents to either E4031 (n=4) or ML-T531 (1A n=3, 3.1 n=6) titration in whole-cell voltage clamp of cells expressing either 1A or 3.1 treated with bortezomib. ***c***, Dose-response of peak tail currents to either E4031 (n=4) or ML-T531 (1A n=3, 3.1 n=6) titration in thallium flux assay of cells expressing either 1A or 3.1 treated with bortezomib. ***d***, Table summary of compound potencies and activator potentiation data. E4031 potencies decrease in thallium flux assay compared to voltage-clamp by less than 3 fold. ML-T531 exhibits higher max potentiation in 3.1 channels than 1A. All graph and table data presented as mean ± SEM.

a

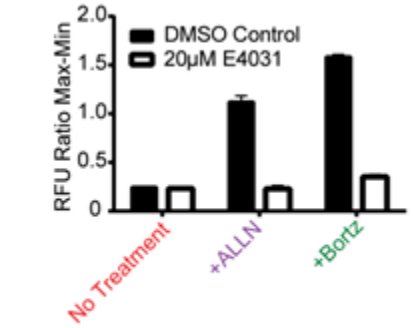

Thallium Flux Assay Z Factor	1A	3.1 + Bortz
Z'	0.811±0.07	0.797±0.02

b

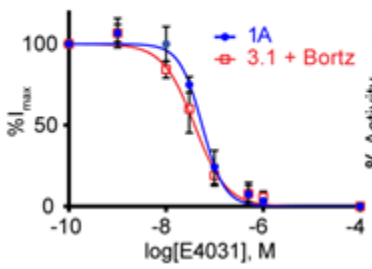

c

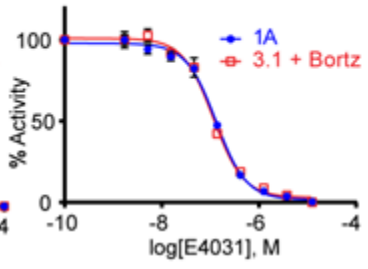

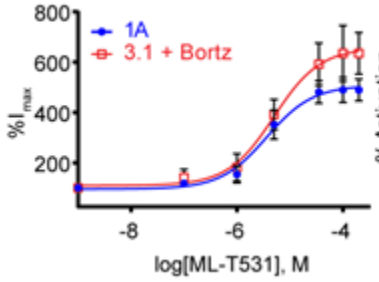

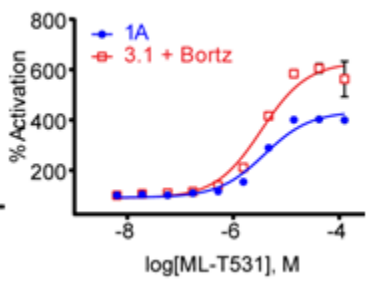

d

Channel	Assay	E4031 IC_{50}	ML-T531 EC_{50}	ML-T531 Max Potentiation
Kv11.1-1A	Manual Patch	55.1±8.5 nM	3.6±1.9 μM	509±32.1 %
	Thallium Flux	131.6±10.5 nM	3.8±1 μM	430±18.2 %
Kv11.1-3.1	Manual Patch	38.6±6.5 nM	4.9±2.4 μM	656±40.6 %
	Thallium Flux	114.6±12.9 nM	3.3± 1 μM	633±31.9 %

Discussion

In this study it was confirmed that Kv11.1-3.1 is a poorly expressed channel that displays impaired trafficking and activity (**Figure 2.1**). This data reflects general observations made concerning Kv11.1-3.1 expression in HEK cells via Western analysis [145,187]; however, this is the first time these characteristics have been quantified, analyzed, and also reflected in fluorescent microscopy (**Figure 2.2**) to our knowledge. Of particular interest are the general subcellular localization analyses; these demonstrate Kv11.1-1A is expressed over 6 fold higher in the Golgi, 2 fold higher in the ER, and 2 fold higher in the proteasome domains, as compared to Kv11.1-3.1. While 1A expression in the Golgi and ER is similar, there is a much greater ratio of Kv11.1-3.1 in the ER/Golgi, suggesting a differential kinetic distribution and thus supporting the trafficking hypothesis. Using the same methods, it was found that inhibition of proteasome activity increased steady-state expression, plasma membrane trafficking, and subsequent peak current of Kv11.1-3.1. (**Figures 2.3-2.5**) These findings were applied to the fluorescent 384 well plate thallium flux assay for potassium channel activation, and it was found that rescue via proteasome inhibition resulted in a robust response, amenable for HTS and subsequent drug discovery studies. In general, the discoveries outlined in this report suggest two principal implications: the role of ERAD and UPR in Kv11.1-3.1 regulation and a potential translational component.

Proteasome involvement is known in hERG trafficking and degradation [128,202], but is not often labeled as the key factor in these pathways. Nonspecific ALLN treatment has previously shown rescue of general hERG 1A expression when coexpressed heterogeneously with a dominant negative LQT2 mutant, although the effects on trafficking are not clear.[211] Although proteasomal inhibition via lactacystin and Mg132 treatment has been shown previously to increase hERG expression for some LQT2 mutants [202], trafficking was unable to be rescued suggesting a different limiting factor. The majority of hERG trafficking studies target LQT2 clinically relevant missense mutations and PAS truncations.[128] These cause channel retention in different compartments of the endoplasmic reticulum [147], which may vary on the mutation despite similar

CG channel expression. Related studies include the more severely truncated variant Kv11.1-1B, which results in analogous observations due to the expression of RXR retention motifs.[155] Successful rescue strategies for trafficking deficient Kv11.1-1 channels include pharmacological chaperones, incubation at reduced temperature, and expression of heterotetramers with WT Kv11.1-1A. These rescue techniques either assist in stabilizing channels or disrupt chaperone mediated quality control mechanisms. [128,155,197,199-201] In contrast, we hypothesize that Kv11.1-3-1's unstably folded N-terminal region, caused by alternative transcription, results in a unique kinetic distribution amongst ER quality control check points and possibly different chaperone interactions. Due to insensitivity to other rescue strategies (**Figure 2.1**), the robust response from bortezomib and ALLN (**Figures 2.3-2.5**), and lack of specific 3.1 ubiquitinylation upon proteasome inhibition (**Figure 2.6**), it is possible that Kv11.1-3.1 channels are more rapidly degraded by the proteasome than other defective hERG channels. Therefore, it may be improper to describe Kv11.1-3.1 as a truly trafficking deficient channel. In fact, there may be utility in comparing Kv11.1-3.1 to the previously reported Δ2-135 truncated hERG channel[145]. Despite absence of the PAS domain and N-cap, Δ2-135 has increased trafficking and similar stability compared to Kv11.1-1A. In a sense, Kv11.1-3.1 may be seen as analogous to Δ2-135 with the addition of a small misfolded region causing immediate targeting to the proteasome. It may also be worthwhile to examine LQT2 mutants, resistant to typical methods of rescue, under proteasome inhibition in HEK cells.

Continued exploration of Kv11.1-3.1's trafficking mechanisms to the proteasome in brain and other cell lines may be of interest to discover new therapeutic targets that increase Kv11.1-3.1 retention and degradation in patients with abnormally high Kv11.1-3.1 expression. Because Kv11.1-3.1 is expressed in healthy controls [176], increased Kv11.1-3.1 expression alone is not sufficient for a disease state. Considering previous work that has shown UPR to be down regulated in some groups of schizophrenia patients [218,219], it may be of value to investigate the effect of these two possible risk factors. As this study suggests ERAD and UPR play a large role

in the expression and trafficking of Kv11.1-3.1, one may imagine a feed-forward effect in a down-regulated UPR patient.

In addition to basic channel regulation, these results provided insight into the abilities of using Kv11.1-3.1 for drug discovery. Through proteasome inhibition, the Kv11.1-3.1 signal was improved and resulted in gratifying enhancement of Z' values comparable to Kv11.1-1A. The two tool compounds, E4031 and ML-T531, displayed fidelity between the voltage-clamp and fluorescent thallium flux assay (**Figure 2.5d**). Generally, IC_{50}/EC_{50} values were consistent between assays, although the thallium flux yielded 3 fold lower potencies for E4031 in both Kv11.1-1A and Kv11.1-3.1 expressing cells. Nevertheless, thallium flux data is known to correlate well (albeit not perfectly) to voltage-clamp, and these results are consistent with previous studies comparing E4031 potencies between the two assays.[125]

A principal goal of this assay is to determine selectivity of molecules for the Kv11.1-3.1 channel in order to avoid future cardiac toxicity. Neither the hERG inhibitor E4031 nor activator ML-T531 showed selectivity between Kv11.1-1A and Kv11.1-3.1. However, it was seen that ML-T531 significantly potentiated Kv11.1-3.1 current more so than Kv11.1-1A. While it is unclear as to why this is observed, it should be noted that the EC_{50} between channels was essentially identical. Therefore, the differences in potentiation increase may be attributed to intrinsic differences amongst channel fluxes and it may be considered that even nonselective compounds have a small "built-in" selectivity for Kv11.1-3.1 as compared to Kv11.1-1A.

In this study vital infrastructure has been established to interrogate Kv11.1-3.1 as a drug discovery target for new schizophrenia therapeutics through simultaneously unveiling a novel mechanism for hERG channel trafficking deficiency via rapid proteasomal degradation. While efforts to establish a pipeline for this novel cognitive target are in preliminary stages, these findings present an opportunity to discover other interacting druggable targets and create the tools necessary for identifying selective molecules.

Chapter III

Preferential activity of atypical anti-psychotics for Kv11.1-3.1

Introduction

Many antipsychotic agents have been shown to bind to Kv11.1 channels, resulting in associations with long QT risk and arrhythmic events causing sudden unexpected death and sudden cardiac death.[172] However, some reports suggest that inhibition of hERG currents may also contribute to antipsychotic efficacy as these channels have been shown to play a role in various neurological signaling processes, including dopamine regulation. Indeed, antipsychotic-induced hERG blockage reduces post-stimulus inhibitory periods in action potential trains, increasing excitability. This increase in excitability creates a time-dependent inactivation of dopamine neuron activity (depolarization block) which has been observed in animal models and is thought to correlate with clinical efficacy.[175]

Studies exhibiting the different gating kinetics of Kv11.1-1A and Kv11.1-3.1 have implicated pathological dynamics in their relative contributions to the depolarization block hypothesis. Due to rapid deactivation kinetics found in Kv11.1-3.1, less current is accumulated during repeated depolarization pulses, which may produce faster, longer lasting trains of action potentials.[187] However it is unknown whether these rapid, long lasting trains of actions potentials result in similar depolarization block or increase basal dopaminergic activity, (as current studies would suggest the latter without any trials examining the former). If Kv11.1-3.1 does apply negative function, then selective inhibition may provide a therapeutic effect.

This hypothesis has been evaluated clinically (see **Chapter 1**), with preliminary evidence showing that risperidone is 2-fold selective against Kv11.1-3.l and is correlated to improve clinical outcomes with prescribed to poor metabolizing patients with KCNH2-3.1 up-regulating

risk alleles.[189] Similar clinical effects have been reported for olanzapine, although it has shown to be non-selective between channel isoforms.[189,220]

While the study of risperidone was the first work to comparatively assay common antipsychotics on Kv11.1-3.1 activity, it was limited to only 6 agents.[189] This limitation was likely due to the burden of manual patch low throughput. If one is to compare the differential effects of agents on both channel isoforms for linking marketed antipsychotic efficacy or drug discovery, a more efficient platform is needed.

In this study, we established a high-throughput electrophysiological assay that could drastically increase screening capabilities for the evaluation of novel agents and known antipsychotics. Using a small collection of 26 antipsychotic compounds, or other agents with reported antipsychotic/CNS activity, we sought to find any other selective behaviors and confirm previous results to validate a putative high throughput assay.

Materials and Methods

Molecular biology

Bacmam virus was produced via PCR of C-terminally hemagglutinin (HA) tagged Kv11.1-1A and Kv11.1-3.1 constructs for cloning (as described in **Chapter II)** into Gateway® donor vector pENTR 1A. Donor vector was used for reaction with Virapower BacMam Gateway® vector per the manufacturer's instructions. After the completion of the Gateway recombination, DH5αBac chemically competent E.Coli cells were transformed with the Gateway product per the manufacturer's instructions, resulting in a transposition reaction of the BacMam cassette into the bacmid. Insertion was verified via bi-direction bacmid sequencing of the target site. Bacmid was used to create filtered, high titer BacMam virus ($2x10^8$ virons/mL) at Kemp Bio® via SF-9 cell

transfection for host-mediated viral replication and amplification.

FluxOR® Thallium Flux Assay

FluxOR assays were performed as described in **ChapterII**.

Electrophysiology

HEK 293 cells were grown and maintained as described in **Chapter II** using Glutamax® Dulbecco's modified Eagle's Medium (DMEM) supplemented with 100 U/mL non-essential amino acids, 1x Penicillin/Streptomycin, and 10% fetal bovine serum. Cells were dissociated and separated from media via addition of Tryple E Express® and centrifugation. Cells were resuspended in DMEM/F12 media containing 2% FBS at a concentration of 2 million cells/mL. Virus was added to cells at an MOI of 100:1 and gently rotated at room temperature in the dark for 4 hours in a centrifugal tube wrapped in aluminum foil. Virus and media was removed by centrifugation and cells were suspended in fully supplemented DMEM media containing a final concentration of 1X BacMam enhancer solution. Cells were plated onto PDL coated glass coverslips or 15 cm dishes at 15 million cells per dish and incubated at 37 ^{0}C for 4 hours. Media was removed by aspiration and replaced with fresh DMEM containing 10 nM bortezomib. Cells were manually patched using protocols as previously described in **Chapter II**. Dose response data was taken from steady-state currents. Automated patch-clamp experiments were performed using the population patch-clamp (PPC) mode of automated voltage clamp recording with IonWorks Quattro™. Briefly, compound effects on Kv11.1-1A and Kv11.1-3.1 channels were tested with a one-step voltage protocol. Cells were dispensed into a 384-well population patch-clamp mode plate. After dispensing, seal resistance of cells was measured for each well and cells were perforated by incubation with 100 μg/mL amphotericin B. Activity of

hERG was then measured with the recording protocol as follows: cells were held at −70 mV, stepped down to −80 mV for 100 ms to estimate leak currents, and depolarized to −30 mV for 100 ms to estimate non-hERG currents. Then cells were depolarized to +45 mV for 2 s followed by a hyperpolarization to −10 mV for 2 s. This series of pulses was applied to cells before and following an 8-min incubation of cells with test compounds or assay buffer. Positive (30 μM cisapride) and negative controls (external buffer with 0.02% [v/v] DMSO) were applied within each plate to evaluate the data quality. Only cells with a tail current amplitude bigger than 0.2 nA, a seal resistance >30 MOhms, and seal resistance drop rate lower than 25% were included for data analysis. The peak amplitudes of tail currents before and after compound treatment were measured. Compound effects were assessed by the percentage change in the hERG tail current. The percentage changes were calculated by dividing the difference between pre- and post-compound hERG tail currents by the respective pre-compound tail current in the same well and normalized to positive and negative controls in the same plate.

Whole-cell currents were measured in the following recording buffers: 137 mM NaCl, 4 mM KCl, 1 mM $MgCl_2$, 1.8 mM $CaCl_2$, 10 mM HEPES, and 10 mM glucose, pH 7.4 adjusted with NaOH (extracellular solution); 40 mM KCl, 100 mM K-gluconate, 1 mM $MgCl_2$, and 5 mM HEPES, pH 7.2 adjusted with KOH (intracellular solution).

Data Analysis

Manual Patch clamp and FluxOR data was analyzed similarly as in **Chapter II**. Peaky steady state currents were used for dose response measurements. The automated patch-clamp experiments were analyzed in IonWorks® 2.0.4.4. Further calculations were performed in Excel. Compound dose response curves were carried out in Origin® 7.0.

Results

Antipsychotic Screen

A small selection of CNS active compounds was acquired for assays (**Table 3.1**). Compounds screened twice using the Ionworks PPC assay (**Figure 3.1**) and in the FluxOR assay once. In order to evaluate accuracy, results were compared to literature values report for Kv11.1-1A. Due to high variance of results in the literature, the vast majority of reference values were taken from the NCI PubChem compound database or regulatory reports with preference given to values obtained via manual patch clamp in CHO-K1 or HEK 293 cells.[221]

Initial runs from Ionworks were largely inconsistent with reported values for inhibition of Kv11.1-1A. However, it is know that this platform is unable to accurately assess potent compounds, especially highly lipophilic species. Therefore, an additional screen was run on 8 selected compounds with an increased compound incubation time of 8 minutes total. Nearly all compounds showed higher potency with the increased incubation time with the exception of ziprasidone.

Many compounds were found to be selective for Kv11.1-3.1, up to 4-fold (olanzapine). No compound was found to be significantly selective for Kv11.1-1A.

Results in the FluxOR assay were closer to literature values than Ionworks for some compounds (chlorpromazine, pimozide, thioridazine, etc.), but not for others (amitriptyline, illoperidone, quetiapine, etc.). When possible to determine, selectivity for 3.1 was mostly conserved between assays.

Due to its consistent selectivity in the Ionworks and FluxOR assays (2 and 5-fold, respectively), promising clinical exposure levels, and idiosyncratic polypharmacological profile and clinical efficacy, clozapine was selected for manual patch validation Clozapine was found to be significantly two-fold selective between 1A and 3.1 (**Figure 3.2**).

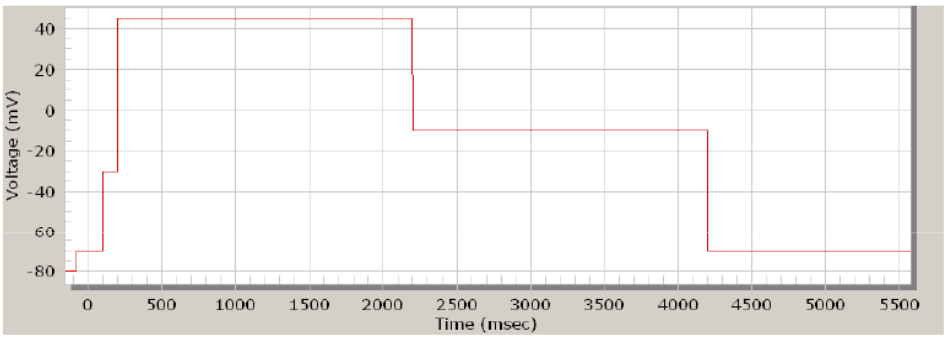

Figure 3.1. IonWorks whole-cell automated patch clamp voltage protocol.

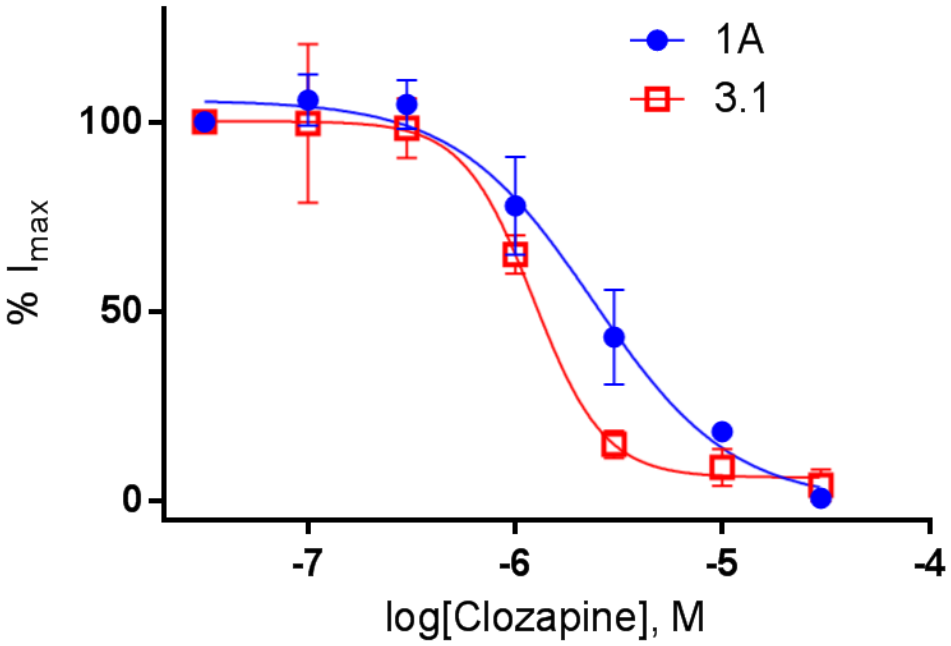

Figure 3.2. Clozapine is significantly selective for Kv11.1-3.1. BacMam transduced HEK 293 cells were patched in whole-cell voltage clamp mode and clozapine was titrated for dose-response measurements from peak steady-state currents (n=3 for each group). Clozapine had an IC_{50} of 2.4 ± 0.7 µM for Kv11.1-1A and 1.2 ± 0.3 µM for Kv11.1-3.1.

Discussion

In this study, many molecules were found to be selective in either one or both of the screening assays. Amisulpride, lurasidone, quetiapine, sertindole, and thioridazine, were found to be selective in Ionworks but were not validated in FluxOR. The FluxOR assay, in general, did not yield many unilaterally selective results (asenapine, cisapride control). No compound was found to be Kv11.1-1A selective, which may be due to the lower overall current density accumulation of Kv11.1-3.1 channels. Of concern is an artificial effect, although the pulse protocols used for both cells should not have resulted in any inherent preference for either channel.[187] There may be fewer channels on the surface for the Kv11.1-3.1 cells, although the work in **Chapter II** concerning surface and total expression argues against this theory.

Amitriptyline, a common tricyclic anti-depressant with known Kv11.1-1A activity, was selective in both assays. Although amitriptyline is known to exacerbate psychotic symptoms in patients with schizophrenia, and thus was not of interest for the purpose of examining a potential role of Kv11.1-3.1 in schizophrenia pathology, it may prove to be a useful tool in the future due to this interesting activity profile. Risperidone was validated as being selective in the Ionworks assay, although this effect was less than 2-fold in the FluxOR assay. As risperidone has been previously characterized as selective in manual patch clamp, this may suggest that the FluxOR assay may underreport compound selectivity between isoforms, perhaps leading to the fewer selective species as noted.[189] Olanzapine was found to be nearly 4-fold selective in the IonWorks assay, in contrast to a previously reported manual patch clamp report.[189] Unfortunately, olanzapine was not active in the FluxOR assay, warranting continued investigation especially considering the clinical implications in patients harboring KCNH2-3.1 inducing risk SNPs.[186]

Clozapine was the only compound followed up with manual patch validated as mentioned. The magnitude of the observed selectivity by manual patch (2-fold) was not as large as the screening assays (2.5-fold IonWorks, 5-fold FluxOR), although selectivity was consistent across all three assays in contrast to a previous report of non-selectivity by Heide et al.[189] This may be due to

differences in methods used, as Heide et all used a highly controlled perfusion system to quickly flow compounds for 20s. In this study, compound doses were applied until the current was stabilized after multiple pulse cycles, lasting up to 5 minutes in some cases. Both methods have advantages and the physiological relevance of using either is a matter of debate. While these results need verification and follow-up in more relevant systems such as neuronal cultures from KCNH2-3.1 overexpressing mice, a putative conservation of selectivity may implicate Kv11.1-3.1 action in clozapine antipsychotic efficacy. Indeed, total brain concentration of clozapine in average schizophrenia patients has been estimated in the low micromolar range, which may exist in the proposed selectivity window for Kv11.1-3.1.[221,222] Further studies comparing clinical outcomes from patients prescribed clozapine segmented by KCNH2-3.1 increasing risk SNPs are needed.

However, the implications of these screening results are restricted as this study has severe limitations. Reported Kv11.1-1A activity of the CNS-active compounds in this test was not routinely reflected in the experimentally found values (see references in **Table 3.1**). While the PubChem database represents a convenient database for Kv11.1-1A activity of various drugs, these values have been mostly taken from a handful of papers without any meta-analysis or comparison. Additionally, the primary sources used different methods to obtain activity, not only by cell type, but also voltage protocol. This lead to discrepancies, due to different modes of actions/binding preferences. This is also common in the literature for other sources of reported values Kv11.1-1A potency values. (**Table 3.1**). Additionally confounding the comparison of experimental results, each assay may display compound-specific inaccuracies due to solubility issues or assay limitations. For example, FluxOR does not reflect true electrophysiology and thus is unable to cycle through channel states, limiting the activity of some drugs that may preferentially bind to the inactivated state or those especially prone to drug-trapping. Additionally, it has been shown that FluxOR assays can underreport potency and is prone to high-variance for many compounds.[125,128] The APC platform (IonWorks Quattro™) is prone to variance from

compound specific interactions, poor seals, and batch-to-batch cell variation, (this machine has been upgraded with more accurate technology recently.)[223] Additionally, this assay is known to exhibit reduced-potency shifts similar to this report.[224] Nevertheless, the combination of these two assays in parallel with manual patch validation for specific hits has been reported as a useful strategy from Kv11.1-1A.[225]

We report that this same strategy is viable for Kv11.1-3.1 screening, and has been used to show that clozapine is a selective inhibitor, with potencies in the range of therapeutic brain concentrations. If validated, the contribution of Kv11.1-3.1 to schizophrenia pathology may partially explain the unique efficacy of clozapine in schizophrenia. Further studies and drug discovery efforts may be able to emulate these activities of clozapine in new chemical classes that are without the devastating adverse effects associated with clozapine, most notably, agranulacytosis.[24] However, it is still not known how much inhibition of Kv11.1-3.1, if any, provides a putative therapeutic effect, if at all. The synthesis of a more selective tool compound may assist in the deconvolution of Kv11.1-3.1 contribution in schizophrenia therapy.

Table 3.1. Antipsychotic and CNS active compound collection. Literature value references: **a**, Silvestre et al.[221] **b**, Tie et al.[226] **c**, Brown[227] **d**, Callier et al.[228] **e**, Yoshida et al.[229] **f**, Vigneault et al.[230] g, Spyker et al.[231] **h**, Brown et al.[232] **i**, Kongsamut et al.[233] **j**, Dosa et al.[234] * Values taken from 8 minute compound incubation screen.

Compound	Structure	Reported Voltage Clamp IC_{50} (μM)	Ion Works IC_{50} (μM)		FluxOR IC_{50} (μM)	
			1A	3.1	1A	3.1
Amisulpride	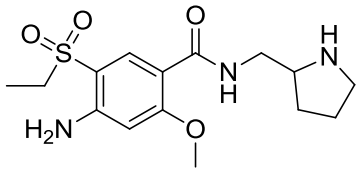	>10[a]	91	43	38	28
Amitriptyline	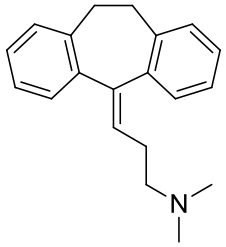	10[b]	24 14*	9.2 6.8*	58	3.4
Aripiprazole	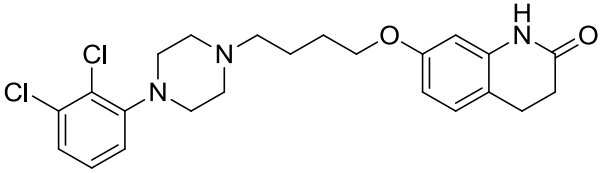	1.1[a]	9.1	7.0	2.1	1.6
Asenapine	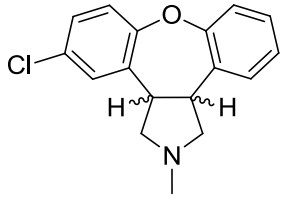	0.30[a]	6.8	4.4	19	7.9

Brexipiprazole	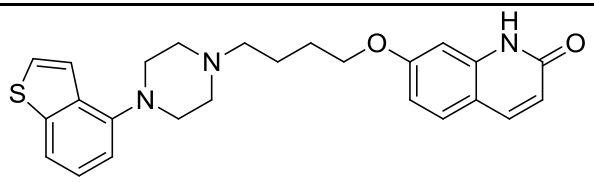	0.12[c]	3.2	3.76	2.3	2.7
Bupropion	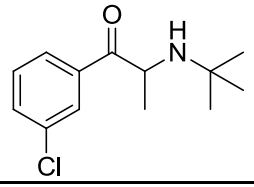	34[d]	87	55	>130	>130
Chlorpromazine	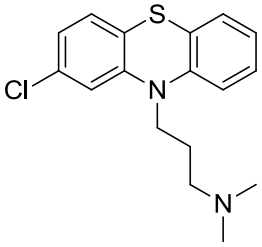	1.5[a]	6.2	6.4	2.1	1.2
Cisapride	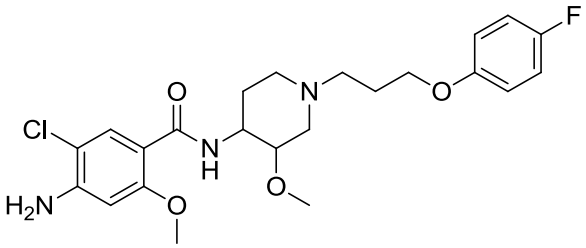	0.045[e]	0.32	0.20	0.52	0.25
Clozapine	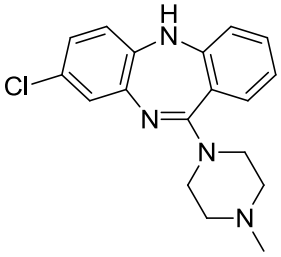	1.4[a]	22 5.1*	8.8 2.0*	66	12

Haloperidol	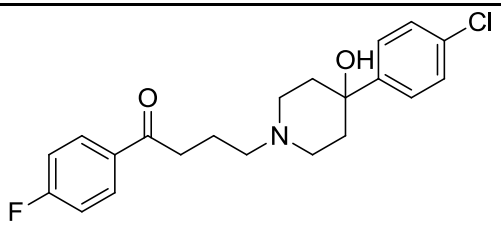	0.093[a]	0.35 0.27*	0.17 0.27*	0.29	0.33
Illoperidone	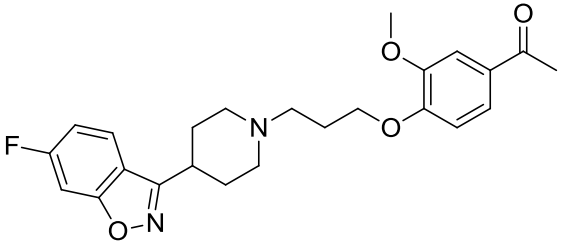	0.161[f]	0.57 0.39*	075 0.24*	1.3	1.2
Loxapine	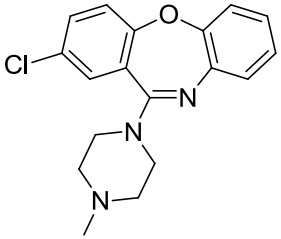	1.8[g]	12	7.4	59	31
Lurasidone	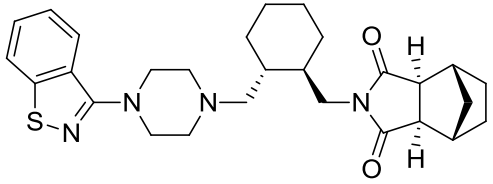	0.11[h]	7.3	2.1	4.9	3.2

Minocycline	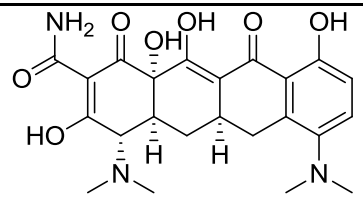	N/A	No Inhibition	No Inhibition	No Inhibition	No Inhibition
Olanzapine	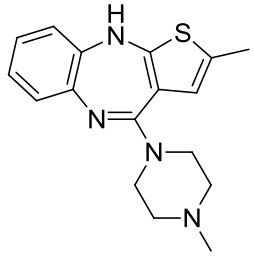	6.0[i]	39	10	>130	>130
Paliperidone	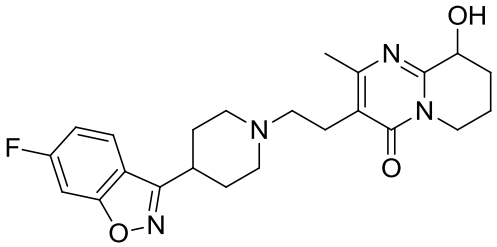	1.3[a]	1.4	0.95	18.2	20.5
Perphenazine	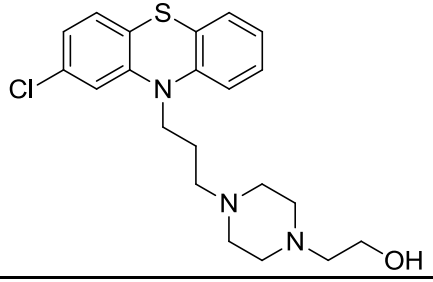	1.0[a]	5.7	3.7	1.5	1.1

Pimavanserin	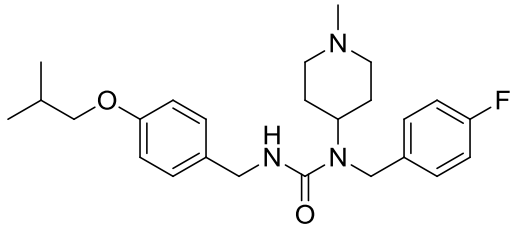	73% block @ 1 μM[j]	4.1	2.6	1.3	1.1
Pimozide	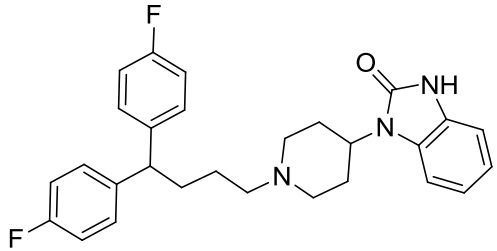	0.0064[a]	1.86 0.69*	0.5 0.39*	0.023	0.024
Quetiapine	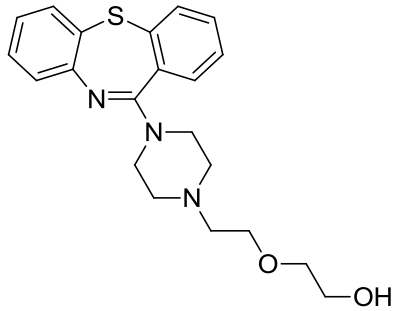	5.8[a]	25	7.8	>130	>130
Raclopride	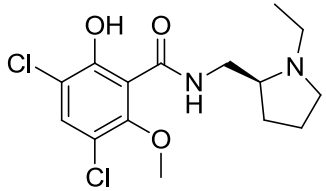	N/A	55	46	>130	>130

Risperidone	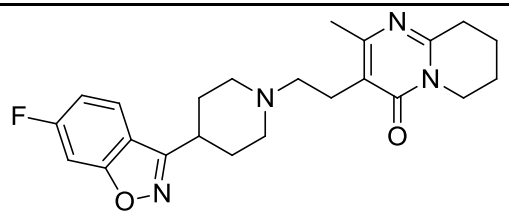	0.20[a]	1.6	0.6	11	7.29
Sertindole	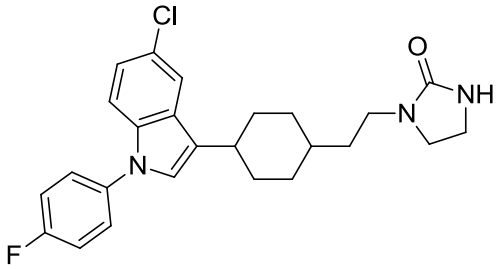	0.060[a]	1.6 0.72*	0.36 0.24*	0.28	0.21
Sulpiride	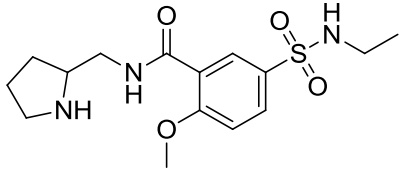	>10[a]	No Inhibition	No Inhibition	45	62
Thioridazine	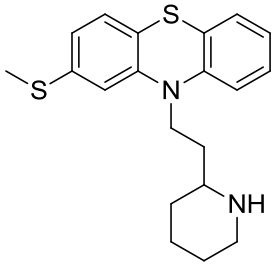	0.20[a]	7.9 3.2[j]	1.3 1.2[j]	0.18	0.13
Ziprasidone	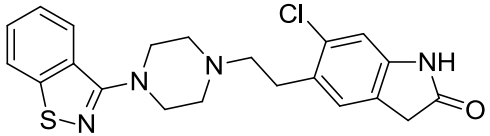	0.162[a]	0.52 1.9*	0.56 0.91*	3.1	2.0

Chapter IV

Discovery of Amino-Acetamides as selective Kv11.1-3.1 inhibitors

Introduction

While Kv11.1-3.1 is a promising target for small-molecule therapeutics, there are a number of challenges with translating these findings into the clinic. Most prominent of these issues is structural homology to Kv11.1-1A, principal contributor to cardiac I_{Kr} currents and prolific drug discovery "anti-target" due to blockade resulting in arrhythmia, long QT syndrome, and torsades de pointes.[128] Several drugs, including many antipsychotics, are known to inhibit hERG, thus it is critical to ensure selective modulation of Kv11.1-3.1 and counter-screen for I_{Kr} activity.[172] While hERG binding amongst drug-like compounds is largely promiscuous, some key factors have been identified, such as π-cation interaction and π-π stacking with key aromatic residues Y652 and F656 in the channel pore.[166] These areas are conserved in the Kv11.1-3.1 channel, and it is unknown whether this N-terminal truncation distorts relative tertiary and quaternary structures, leading to the possibility of creating selective inhibitors.[176] However, differential drug binding has been shown for homologous K channels exhibiting variable pore structure and sequences, lacking C-type inactivation, while conserving the key aromatic-side chains.[128] Residues on the interface of the selectivity filter have also been reported to affect pore-block binding, although these are highly conserved amongst Kv channels and are not thought to play a prominent role in high-affinity, promiscuous drug binding.[128]

Recognizing the difficulty in designing potent and selective molecules *de novo*, a high throughput screen of the NIH Molecular Library Program (MLP) small molecule library was performed at the National Center of Chemical Genomics utilizing a 1536 well FluxOr thallium-

flux assay (PUBCHEM AID 720544).[125,235] From these efforts a family of molecules with mid nanomolar to low micromolar potency and greater than 10-fold selectivity was identified. Most promising of these compounds was compound **1** (Figure 1) which displayed mid nanomolar potency and 50-fold selectivity for the 3.1 channel, verified using whole-cell patch clamp. From this hit led the development of this study, in which structure-activity relationships of synthesized analogs were investigated for activity against Kv11.1-1A (hERG) and Kv11.1-3.1 (3.1) using the FluxOr assay and whole-cell patch clamp.

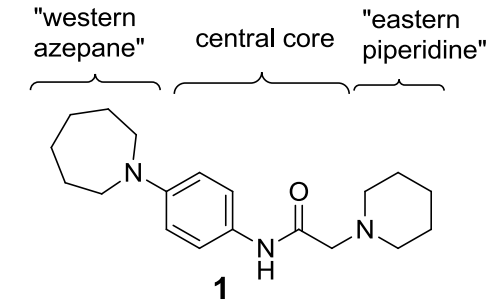

1

	FluxOR	Manual Patch
Kv11.1-3.1	210 nM	230 nM
Kv11.1-1A	11000 nM	10000 nM

Figure 4.1. Lead compound from NIH MLPCN screen via FluxOR assay.

Results

Chemistry and SAR analysis

A broad spectrum approach was taken to modify the lead via modification of 3 regions: 1) western azepane ring, 2) eastern piperidine ring, and the 3) acylated aniline core (Figure 1). Without crystal structures to guide analog synthesis, two general theoretical routes were considered in achieving the desired properties of selectivity, potency, and blood-brain penetration: 1) reduce potency on Kv11.1-1A (hERG) using transformations from the medicinal chemistry literature[166], 2) increase selectivity through discrete spatial modifications that inherently increase preferential Kv11.1-3.1 binding (empirically determined) and 3) retain chemical properties suitable for crossing the blood-brain barrier .

Optimizing compounds to reduce hERG activity has been thoroughly discussed and reported,[128] with the most general methods involving reductions of basic nitrogen pK_a and lowering of LogD. Analogs were synthesized that made variations to the three regions of interest, choosing secondary amines and heterocycles that resulted in subtle changes in size, total polar surface area/cLogD, and pK_a.[166]

Analogs containing derivatives of the azepane ring **(Table 4.1)** were constructed via synthesis **(Scheme 4.1)** of an intermediate **4** that could be readily substituted via Buchwald-Hartwig coupling[236] with various secondary amines. Surprisingly, all of the synthesized azepane ring analogs resulted in a substantial loss of potency for both forms of the channel, with only **5** maintaining activity for Kv11.1-3.1 below 10 μM. These very small changes in ring size, polarity, and basicity were not tolerated, suggesting subtle contributions from the azepane geometry or pK_a being critical for high potency. Based on these initial results, efforts were focused on modification of the core region of **1** as well as the eastern piperidine.

Modification of the eastern piperidine was accomplished through synthesis of intermediate **12** via acetylation of the 4-azepane substituted aniline **11 (Scheme 4.2)** that could be readily reacted

Scheme 4.1. Synthesis of western azepane analogs.

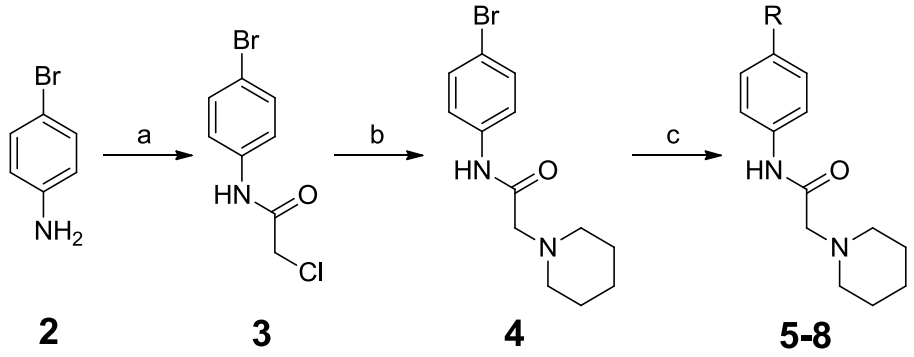

Reagents and conditions: **a)** chloroacetyl chloride, TEA, CH_2Cl_2, 0 ^{0}C **b)** piperidine, K_2CO_3, MeCN, 80 ^{0}C **c)** secondary amine, Xanphos PreCat G2, Cs_2CO_3, DMSO, 110 ^{0}C

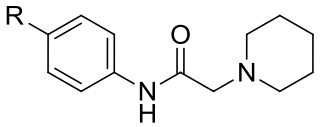

Structure	Compound	cLogD	TPSA	pKa	Kv11.1-1A IC_{50} (nM)	Kv11.1-3.1 IC_{50} (nM)	Kv11.1-3.1 selectivity
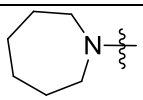	1	3.1	36	6.3	11000	210	52
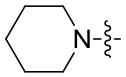	5	2.8	36	5.5	>130000	6400	>20
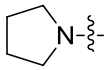	6	2.4	36	5.7	>130000	13000	>9.7
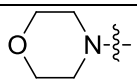	7	1.4	45	5.3	>130000	>130000	1.0
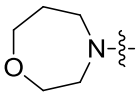	8	1.4	45	5.7	>130000	85000	>1.5

Table 4.1. Modifications to azepane ring

Scheme 4.2. Synthesis of eastern piperidine analogs.

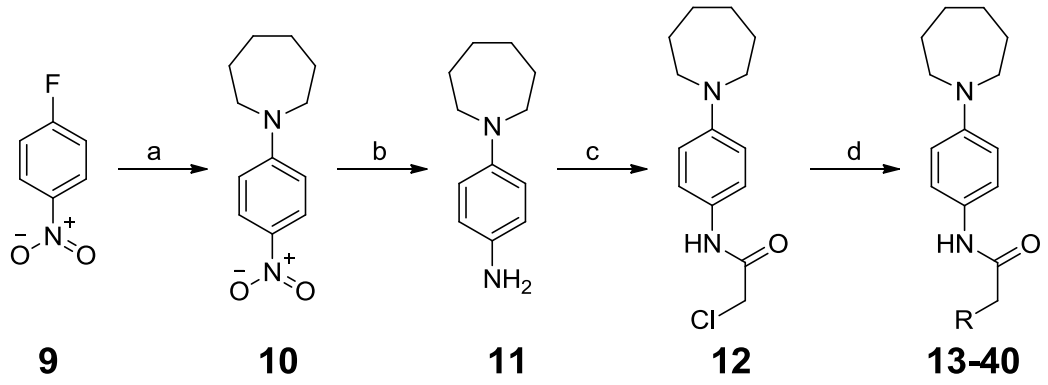

Reagents and conditions: **a)** azepane, K_2CO_3, MeCN, 80 ^{0}C **b)** 10% Pd(C), 1 atm H_2, EtOH **c)** chloroacetyl chloride, TEA, CH_2Cl_2, 0 ^{0}C **d)** secondary amine, DMF, 80 ^{0}C

with various secondary amines via nucleophilic addition to yield derivatives **13-28** in good yields. Initial modifications **(Table 4.2)** were made to attenuate the pK_a of the nitrogen in the resulting compound. Decreasing the contained nitrogen's basicity through inductive effects of oxygen in the ring or fluorine substitution reduced potency and selectivity (compounds **13-17**). Compounds with diminished pK_a but with greater reductions in cLogD via hydroxyl/H-bond donor substituents, **18-20** and **27** also displayed poor activity. The most potent of the reduced pK_a compounds was **28**, although non-selective (having similar terminal structure to haloperidol, a typical antipsychotic and potent hERG blocker[189]).

Compounds with higher or comparable basicity and slightly larger modifications were synthesized looking for positions where polarity would be tolerated in Kv11.1-3.1 but not Kv11.1-1A. While some small differences in potency and selectivity were seen with various hydroxyl-containing analogs (compounds **18-22**), all lost more potency on Kv11.1-3.1 than Kv11.1-1A compared to **1**. Carboxylic acid additions to the core which create zwitterionic species such as compounds **24** and **25** were prepared to explore this well-known mode of hERG potency reduction.[237] However, these additions eliminated activity on both forms of the channel regardless of the substitution pattern on the piperidine. Incorporation of additional polarity by addition of amines or acetamides, exemplified by compounds **26** and **27**, significantly reduced cLogD but also lost measurable activity on the channel.

Without any improvements from general modifications to physiochemical properties, more significant spatial changes were explored **(Table 4.3)**. Incremental piperidine ring reduction to compound **29** was not tolerated; however, expansion to compound **30** resulted in only a 2-fold loss of potency with conserved selectivity. In response, a compromise between the piperidine and azepane was sought through a single methyl addition to the piperidine to make analogs **31-33**.

Table 4.2. Polarity and pKa-varying modifications to piperidine ring

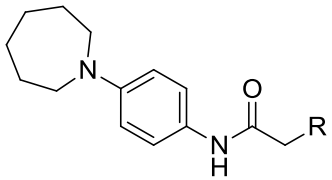

Structure	Compound	cLogD	TPSA	pKa	Kv11.1-1A IC50 (nM)	Kv11.1-3.1 IC50 (nM)	Kv11.1-3.1 selectivity
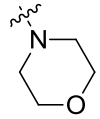	13	2.0	45	5.0	>130000	>130000	N/A
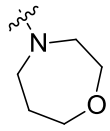	14	2.7	45	7	>130000	17000	>7.3
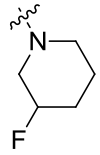	15	2.9	36	7.3	50000	4100	12.0
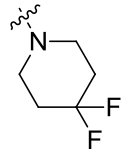	16	2.8	36	3.9	76000	24000	3.2
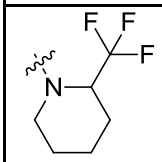	17	3.7	36	6.1	13000	4800	2.7

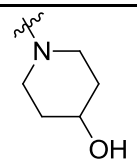	18	1.6	56	7.4	>130000	23000	>5.4
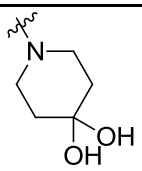	19	0.56	76	6.7	90000	40000	2.3
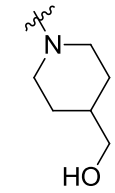	20	1.9	56	7.9	110000	49000	2.2
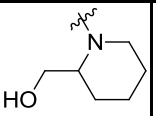	21	2.8	56	8.1	56000	15000	3.7
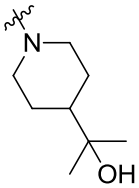	22	2.8	56	8.2	93000	42000	2.2
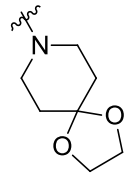	23	3.5	54	8.2	>130000	72000	>1.7
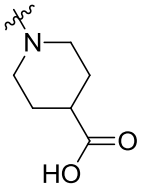	24	-0.5	73	9.0	>130000	>130000	N/A

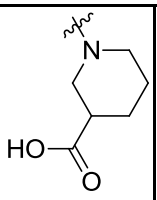	25	-0.47	73	8.5	>130000	>130000	N/A
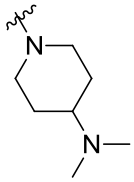	26	0.77	39	9.3	>130000	>130000	N/A
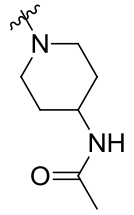	27	1.6	65	7.3	>130000	>130000	N/A
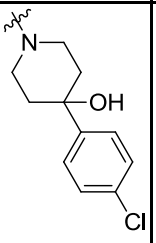	28	3.4	56	6.9	760	720	1.0

The 2-substituted methylpiperidine **31** was well tolerated, having near identical activities to **1**. While **32** and **33** had similar Kv11.1-1A activity to **1** and **31**, their 3.1 potency was between 4-5 fold lower, diminishing their selectivity in kind as anticipated by previous modifications (vide supra).

Seeking to probe additional space through larger additions, pendant phenyl groups were added in similar fashion as methyl substitutions to the piperidine. Paradoxically, 2-substituted piperidine **34** displayed higher selectivity than the 3-substituted variants **35** and **36**, but lower potency. Both **35** and **36** were highly potent on Kv11.1-3.1 with low selectivity. Combining the most selective modifications from the phenyl and methyl additions, compound **37** was unable to improve potency or conserve selectivity as a mixture of isomers. In attempts to compensate for pendant phenyl addition with piperidine ring reduction, 2-substiututed pyrrolidine **38** was not tolerated. The 3-substituted variant **39** had only modest losses in 3.1 activity, but large gains in Kv11.1-1A to the detriment of selectivity.

Increasing space, but limiting extension to that of the 2'-positions, the bicyclo compound **40** was the most potent in the series with a 3-fold increase in potency and conservation of selectivity. However, the Kv11.1-1A potency was considered suboptimal, being lower than 10 μM.

Initial modifications **(Table 4.4)** to the linker were synthesized via acylating **11** with chloroacetyl chloride analogs **(Scheme 4.2)** prior to nucleophilic substitution with piperidine. The linker was extended or methylated on the α carbon to restrict rotation, yielding compounds **41** and **42** respectively. Neither compound was tolerated, discouraging further linker analogs.

Concerns over the dianiline species being a metabolic hotspot for cytochrome P450-mediated metabolism, which may result in a potentially toxic reactive species, prompted efforts to attenuate the electron rich aromatic core.[238] To achieve this and improve ADME properties through reduced LogD, core modifications **(Table 4.5)** were prepared analogously to **Scheme 4.2**. Systematic

Table 4.3. Spatial Modifications to Piperidine Ring

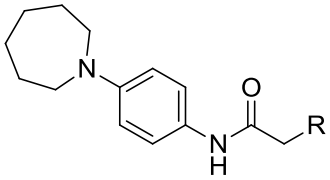

Structure	Compound	cLogD	TPA	pKa	Kv11.1-1A IC_{50} (nM)	Kv11.1-3.1 IC_{50} (nM)	Kv11.1-3.1 selectivity
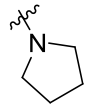	29	2.4	36	8.0	50000	17000	2.9
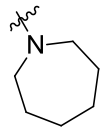	30	3.3	36	8.0	22000	470	45.9
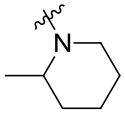	31	3.0	36	8.8	8400	230	36.5
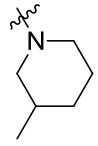	32	3.2	36	8.5	7200	800	8.8
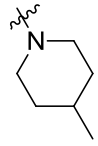	33	3.3	36	8.3	8500	900	9.2
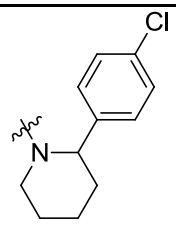	34	4.8	36	7.9	>130000	3800	>34

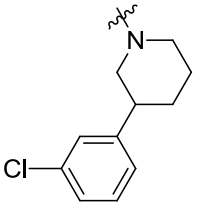	35	5	36	7.9	370	200	1.9
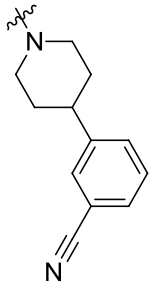	36	4	59	7.6	1200	320	3.8
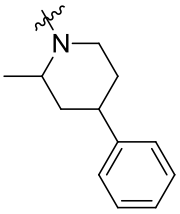	37	4.5	36	8.3	3500	1700	2.0
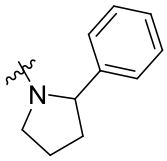	38	3.8	36	7.2	93000	42000	2.2
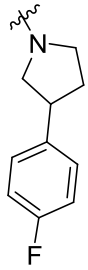	39	3.8	36	7.4	1500	690	2.1
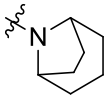	40	2.5	36	8.7	3600	73	49.3

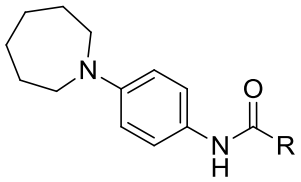

Structure	Compound	cLogD	TPA	pKa	Kv11.1-1A IC_{50} (nM)	Kv11.1-3.1 IC_{50} (nM)	Kv11.1-3.1 selectivity
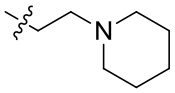	42	2.2	36	8.9	4000	12000	5.3
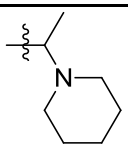	44	3.2	36	8.6	48000	7500	6.4

Table 4.4. Linker Modifications

Structure	Compound	cLogD	TPA	pKa	Kv11.1-1A IC_{50} (nM)	Kv11.1-3.1 IC_{50} (nM)	Kv11.1-3.1 selectivity
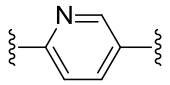	46	2.8	48	7.6	>130000	2900	>43.3
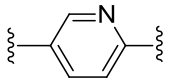	47	3.0	48	4.7	>130000	29000	4.4
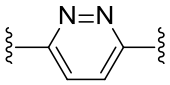	50	2.3	61	6.2	>130000	>130000	N/A
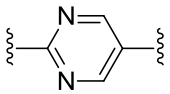	51	3.1	61	4.5	>130000	11000	11.7
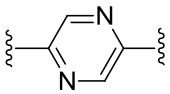	52	2.7	61	3.4	>130000	100000	1.2
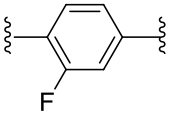	53	3.5	36	6.1	2300	140	16.5
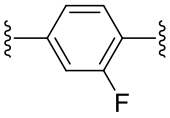	54	3.3	36	5.3	14000	4800	2.7

Table 4.5. Core Modifications

evaluation of heterocycles containing 1 and 2 nitrogen atoms at each position of the core showed substantial losses in potency with the exception of pyridine derivative **46.** Interestingly, this was the only modification that increased azepane nitrogen pK_a. Although exhibiting a 10-fold loss in potency on Kv11.1-3.1, **46** retained selectivity, greater than can be determined by the assay. The other pyridine analog **47** was not tolerated with a 100-fold loss in activity as well as pyridazine **50**. While pyrimidine **51** retained some selectivity, it lost significant Kv11.1-3.1 potency. Pyrazine **52** exhibited the lowest resulting azepane pK_a and no channel activity. Fluorine substitution produced core analogs **53** and **54** which were surprisingly different in their potency and selectivity. The calculated change in the azepane nitrogen pK_a was nearly a log unit different, suggesting that the basicity of this nitrogen may be an important factor that selectively drives Kv11.1-3.1 potency.

Seeking to balance the potency of bicyclic derivative **34** with the selectivity and improved physical properties of **46**, compound **55** was synthesized as shown in **Scheme 4.2**. Compound **55** was slightly more potent than **1** but with greatly augmented selectivity and a more desirable cLogD and TPSA for brain penetration. This activity was verified by manual patch which reported increased potencies on Kv11.1-3.1 and Kv11.1-1A, although to a slight detriment to selectivity (**Table 4.7**). Compound **55** calculated chemical properties yielded a MPO score[239] of 5.2, according to Wager et al., suggesting a greater probability of blood-brain barrier penetration.

Compounds **1**, and **46** were assayed for stability and intrinsic clearance using rat liver microsomes supplemented with NADPH, UDPGA, and alamethicin. Promising stability was observed, prompting a more complete evaluation of **55** in vivo (**Table 4.7**). Compound **55** was evaluated for mouse blood-brain barrier penetration and pharmacokinetics in rats. It was found that **55** was able to penetrate the mouse blood-brain barrier at a ratio of 16:1 total brain:plasma, at IC_{50} relevant concentrations for up to two hours. However, at eight hours there was no more compound detected, hinting at rapid clearance. This was indeed confirmed in the rat

pharmacokinetic studies which showed no detectable **55** after only 5 minutes of being dosed 10mg/kg orally. These results indicate that metabolite identification studies must be carried out to resolve the pharmacokinetic issues. A compound with a longer half-life must be synthesized, as the current compounds are not amenable to behavioral studies which require longer compound exposure.

Beyond translational aims, this work offers clues that may potentially guide new insight into unknown aspects of Kv11.1-3.1 structure and pharmacology. Despite complete transmembrane and pore sequence conservation,[176] this report, stemming from data from an initial high throughput screen, suggests that selective inhibition is indeed possible and is able to be manipulated via novel compounds. It has been previously reported that risperidone inhibits Kv11.1-3.1 with 2-fold greater potency than Kv11.1-1A, although the structural mechanism of selectivity is perplexing as most hERG blockers are thought to bind in the channel pore.[128,189] It may be possible that the lack of interactions, facilitated with the N-terminal PAS domain, has resulted in modified tertiary and quaternary channel structure. This may lead to new binding pockets within the pore. However, the possibility of binding regions outside the channel is still possible. While there is no crystal structure of Kv11.1-1A or Kv11.1-3.1[128], it may be of use to further investigate the mode of selectivity for future inhibitor design and synthesis.

Structure	Compound	cLogD	TPA	pKa	Kv11.1-1A IC_{50} (nM)	Kv11.1-3.1 IC_{50} (nM)	Kv11.1-3.1 selectivity
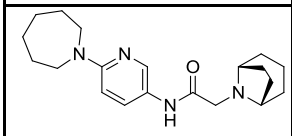	55	2.1	48	9.1	75000	170	440

Table 4.6. Compound 55 properties

Structure	Compound	Ti Flux (nM)		Patch (nM)		cLog D	RLM Stability $t_{1/2}$ (min)	Clearance (mL/min/mg)
		1A	3.1	1A	3.1			
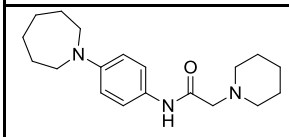	1	11000	210	10000	230	3.1	11	120
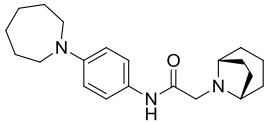	40	3600	73	N/A	N/A	2.5	24	58
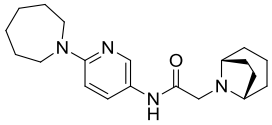	55	75000	170	9000	63	2.1	N/A	N/A

Table 4.7. Electrophysiology summary and in vitro rat liver microsome stability data

Time (hr)	Compound 55 Concentration		Brain-to-Plasma Ratio
	Brain (ng/g)	Plasma (ng/mL)	
0.5	2200 ± 1100	100 ± 52	22
1	920 ± 74	57 ± 8	16
2	290 ± 160	18 ± 3	16
8	BLQ	BLQ	N/A

Table 4.8. Compound 55 c57 mouse blood-brain barrier summary.

Materials and Methods

Synthesis

All commercially available reagents and solvents were used without further purification. Automated flash chromatography was performed on Biotage Flash Isolera using Biotage Flash cartridges with peak detection at 254 nm. Reverse phase purification was accomplished using a Gilson GX-271 liquid handler equipped with a Phenomenex Luna C18 column (50 mm X 21.2 mm i.d., 5 μm). Peak collection was triggered by UV detection at 254 nm. ^{1}H NMR spectra were recorded on a Bruker 400 instrument operating at 400 MHz with residual DMSO used as a reference. Analytical LC/MS was performed using Agilent 1260 equipped with autosampler (Agilent Poroshell 120 C18 column; 50mm X 4.6 mm i.d.; 3.5 μM); 0.05% TFA in water/acetonitrile gradient; UV detection at 254 nm) and electrospray ionization. All final compounds showed purity greater than 95% and 254 nm using this method.

N-(4-bromophenyl)-2-chloro-acetamide (3)

To a stirring 0 ^{o}C solution of 5g (29.07 mmol) **(2)** and 12.09 mL (87.2 mmol) triethylamine in 100 mL CH_2Cl_2, 2.86 mL (29.07 mmol) chloroacetyl chloride was added drop wise into the solution and allowed to warm to room temperature for 24 hours. The reaction mixture was then diluted with CH_2Cl_2, washed with 1N aqueous hydrochloric acid, washed with brine, and then dried over sodium sulfate. The mixture was filtered, concentrated and purified by flash chromatography (Biotage Isolera One, 100g silica gel, linear gradient 0-50% EtOAc:heptanes) to yield 2.92 g of **(3)** (40%). ^{1}H NMR (Chloroform-d, 400 MHz) δ: 8.24 (br s, 1H); 7.47 (d, 4H, *J*=1.8 Hz); 4.19 (s, 2H). MS [M+1]=249.9

N-(4-bromophenyl)-2-(1-piperidyl)acetamide (4)

To a stirring solution of 2.85 (11.47 mmol) **(3)** and 3.96 g (28.67 mmol) potassium carbonate in 50 mL CH_3CN, 1.53 g (12.6 mmol) piperidine hydrochloride was added. The reaction mixture was stirred at 80 ^oC for 6 hours. The solution was cooled to room temperature, filtered and concentrated. The residue was crystallized from ether/heptane to give 3.03 g of **(4)** (89%). ^1H NMR (Chloroform-d, 400 MHz) δ: 9.31 (br s, 1H); 7.47 (d, 4H, *J*=11.7 Hz); 3.06 (s, 2H); 2.56 (br s, 4H); 1.67-1.63 (m, 4H); 1.50 (m, 2H). MS [M+1]=297

2-(1-piperidyl)-N-[4-(1-piperidyl)phenyl]acetamide HCl (5)

To a stirring solution of 0.1g (0.34 mmol) **(4)**, 0.043 g (0.5 mmol) piperidine and 0.329 g (1.01 mmol) cesium carbonate in 2 mL DMSO, 0.012 g (0.02 mmol) Xanphos precat G2 [240] was added. The reaction mixture was heated to 110 ^oC for 12 hours. The solution was filtered, purified by reverse phase HPLC (C18, linear gradient 10%-95% CH_3CN/Water, 0.05% TFA additive), concentrated, then treated with 2N HCl in ether and filtered to afford 0.043 g of **(5)** (38%). ^1H NMR (DMSO-d6, 400 MHz) δ: 10.04 (br s, 1H); 7.92 (d, 2H, *J*=8.1 Hz)); 7.81 (d, 2H, *J*=9.1 Hz) 4.20 (d, 2H, *J*=4.8 Hz); 3.48 (d, 6H, *J*=8.3 Hz); 3.11 (m, 2H); 2.16-1.40 (m, 12H). MS [M+1]=302.2

2-(1-piperidyl)-N-(4-pyrrolidin-1-ylphenyl)acetamide hydrochloride (6)

To a stirring solution of 0.1 g (0.34 mmol) **(4)**, 0.035 g (0.5 mmol) pyrrolidine, and 0.329 g (1.01 mmol) cesium carbonate in 2 mL DMSO, 0.012 g (0.02 mmol) Xanphos precat G2 was added. The reaction mixture was heated to 110 ^oC for 12 hours. The solution was filtered, purified by reverse phase HPLC (C18, linear gradient 10%-95% CH_3CN/Water, 0.05% TFA additive), concentrated, then treated with 2N HCl in ether and filtered to afford 0.022 g of **(6)** (20%). ^1H NMR (DMSO-d6, 400 MHz) δ: 9.92 (br s, 1H); 7.56 (d, 2H, *J*=7.8 Hz); 7.01 (m, 2H); 4.11(m,

2H); 3.47-3.01 (m, 8H); 2.01 (m, 2H); 1.77 (m, 6H). MS [M+1]=288.2

N-(4-morpholinophenyl)-2-(1-piperidyl)acetamide hydrochloride (7)

To a stirring solution of 0.1 g (0.34 mmol) **(4)**, 0.044 g (0.5 mmol) morpholine, and 0.329 g (1.01 mmol) cesium carbonate in 2mL DMSO, 0.012 g (0.02 mmol) Xanphos precat G2 was added. The reaction mixture was heated to 110 ^{o}C for 12 hours. The solution was filtered, purified over Gilson reverse phase HPLC (C18, linear gradient 10%-95% CH_3CN/Water, 0.05% TFA additive), concentrated, then treated with 2N HCl in ether and filtered to afford 0.012 g of **(7)** (10%). ^{1}H NMR (DMSO-d6, 400 MHz) δ:9.85 (br s, 1H); 7.55 (d, 2H, *J*=8.6 Hz); 7.13 (br s, 2H); 5.19 (br s, 4H); 4.10 (d, 2H, *J*=5.1 Hz); 3.80 (br s, 4H); 3.47 (d, 2H, *J*=11.6 Hz); 3.09-3.02 (m, 2H); 1.78-1.66 (m, 6H). MS [M+1]=303.3

N-[4-(1,4-oxazepan-4-yl)phenyl]-2-(1-piperidyl)acetamide hydrochloride (8)

To a stirring solution of 0.1 g (0.34 mmol) **(4)**, 0.054 g (0.5 mmol) 1,4-oxazepane, and 0.329 g (1.01 mmol) cesium carbonate in 2mL DMSO, 0.012 g (0.02 mmol) Xanphos precat G2 was added. The reaction mixture was heated to 110 ^{o}C for 12 hours. The mixture was filtered, purified over Gilson reverse phase HPLC (C18, linear gradient 10%-95% ACN/Water, 0.05% TFA additive), and then treated with 2N HCl in ether to afford 0.026 g of **(8)** (21%). ^{1}H NMR (DMSO-d6, 400 MHz) δ: 10.81(s, 1H); 7.63 (m, 2H); 7.40 (m, 2H); 4.41 (br s, 4H); 4.13 (d, 2H, *J*=5 Hz); 3.55-3.45 (m, 4H); 3.11-3.01 (m, 4H); 1.79-1.68 (m, 6H); 1.39 (m, 2H). MS [M+1]=332.2

1-(4-nitrophenyl)azepane (10)

To a stirring solution of 5 g (35.44 mmol) **(9)** and 4.39 mL (38.98 mmol) azepane in 50 mL CH_3CN, 12.24 g (88.59 mmol) potassium carbonate was added. The reaction mixture was stirred at 70 ^{o}C for three hours. The solution was diluted with ethyl acetate, washed with water, dried

with $MgSO_4$, filtered, concentrated and purified by flash chromatography (Biotage Isolera One, 100g silica gel, linear gradient 0-10% MeOH:CH_2CL_2) to afford 7.6 g of **(10)** (97%). ^{1}H NMR (Chloroform-d, 400 MHz) δ: 8.11(d, 2H, *J*=9.4 Hz); 6.63 (d, 2H, *J*=9.3 Hz); 3.57 (t, 4H, *J*=6.1 Hz); 1.85 (m, 4H); 1.59 (m, 4H). MS [M+1]=221.1

4-(azepan-1-yl)aniline (11)

To a solution of 7.6 g (34.5 mmol) **(10)** in 100 mL ethanol, 2g (34.5 mmol)10% palladium on carbon was added. The solution was stirred under 1 atm hydrogen gas for 24 hours. The solution was filtered and concentrated to give 6.4 g of **(10)** (97%). ^{1}H NMR (Chloroform-d, 400 MHz) δ: 6.67-6.56 (m, 4H); 3.4 (m, 4H); 3.22 (m, 2H); 1.78 (br s, 4H); 1.46-1.68 (m, 4H). MS [M+1]=190.1

N-[4-(azepan-1-yl)phenyl]-2-chloro-acetamide (12)

To a solution of 0.5 g (2.62 mmol) **(11)** in 13mL CH_2Cl_2 was added 330 µL (2.4 mmol) triethyamine. The reaction mixture was stirred for 1 minute then to which was added 251 µL (3.2 mmol) chloroacetyl chloride. The reaction mixture was stirred and allowed to warm to room temperature for two hours and then diluted with 20 mL CH_2Cl_2, washed with water, dried over $MgSO_4$, filtered, and concentrated. Purification by flash chromatography (Biotage Isolera One, 24g silica gel, linear gradient 20%-60% EtOAc:heptanes) afforded 0.651 g of **(11)** (93%). 1H NMR (DMSO-d6, 400 MHz) 9.97 (s, 1H); 7.37 (d, 2H, *J*=8.6 Hz); 6.66 (br s, 2H); 4.18 (s, 2H); 3.44 (t, 4H, *J*=5.8 Hz); 1.72 (m, 4H); 1.46 (m, 4H). MS [M+1]=267.1

General procedure A

To a stirring solution of 0.030 g (0.112 mmol) **(12)** in 1 mL DMF was added 3 equivalents piperdine or other appropriate secondary amine from Tables B or C, which was then heated to 80°C for 3-18 hours. The reaction mixture was then diluted with 0.5 mL MeOH and purified by

reverse phase HPLC (C18, linear gradient 10%-95% ACN/Water, 0.05% TFA additive). Resulting purified compounds were tested as 1:1 TFA salts unless otherwise noted.

N-[4-(azepan-1-yl)phenyl]-2-morpholino-acetamide hydrochloride (13)

Prepared according to **General Procedure A** yielding 0.04 g (30%). ^{1}H NMR (DMSO-d6, 400 MHz) δ: 10.42 (s, 1H); 7.41 (br s, 2H); 6.70 (br s, 2H); 4.14 (br s, 2H); 3.94 (br s, 2H); 3.95 - 3.78 (m, 2H); 3.44 (br s, 6H); 3.27 (br s, 2H); 1.73 (br s, 4H); 1.47 (br s, 4H). MS [M+1]=318.2

N-[4-(azepan-1-yl)phenyl]-2-(1,4-oxazepan-4-yl)acetamide hydrochloride (14)

Prepared according to **General Procedure A** yielding 0.02 g (15%). ^{1}H NMR (DMSO-d6, 400 MHz) δ: 10.34 (br s, 1H); 7.52 (br s, 2H); 6.79 (br s, 2H); 4.22 (s, 2H); 3.90- 3.69 (m, 4H); 3.53-3.39 (m, 8H); 2.25-1.55 (m, 10H). MS [M+1]=332.2

N-[4-(azepan-1-yl)phenyl]-2-(3-fluoro-1-piperidyl)acetamide (15)

Prepared according to **General Procedure A** yielding 0.043 g (94%). ^{1}H NMR (DMSO-d6, 400 MHz) δ 10.23 (s, 1H); 7.36 (d, 2H, *J*=9.1 Hz); 6.67 (d, 2H, *J*=8.8 Hz); 5.15 (m, 1H); 4.13 (m, 2H); 3.8 (m, 1H); 3.43 (m, 5H); 3.22 (br s, 1H); 2.49 (m, 1H); 2.07-1.91 (m, 2H); 1.77-1.70 (m, 6H); 1.47-1.44 (m, 4H). MS [M+1]=334.2

N-[4-(azepan-1-yl)phenyl]-2-(4,4-difluoro-1-piperidyl)acetamide (16)

Prepared according to **General Procedure A** yielding 0.014 g (10%).^{1}H NMR (DMSO-d6, 400 MHz) δ: 10.62 (br s, 1H); 7.49 (br s, 2H); 6.86 (br s, 2H); 5.61 (br s, 4H); 4.24 (s, 2H); 3.65-3.39 (m, 8H); 2.00-1.53 (m, 8H). MS [M+1]=351.2

N-[4-(azepan-1-yl)phenyl]-2-[2-(trifluoromethyl)-1-piperidyl]acetamide (17)

Prepared according to **General Procedure A** yielding 0.010 (18%). ^{1}H NMR (DMSO-d6, 400 MHz) δ 9.45 (s, 1H); 7.41 (d, 2H, *J*=7.8 Hz); 6.76 (br s, 2H); 3.70 (m, 1H); 3.46-3.39 (m, 5H); 2.89-2.73 (m, 2H); 1.74-1.46 (m, 14H). MS [M+1]=384.2

N-[4-(azepan-1-yl)phenyl]-2-(4-hydroxy-1-piperidyl)acetamide (18)

Prepared according to **General Procedure A** yielding 0.038 g (76%). ^{1}H NMR (DMSO-d6, 400 MHz) δ 10.24 (s, 1H); 7.37 (m, 2H); 6.67 (d, 2H, *J*=8.8 Hz); 5.45 (br s, 1H); 4.07 (m, 2H); 3.93 (br s, 1H); 3.49 (m, 1H); 3.44 (t, 4H, *J*=6 Hz); 3.31 (m, 2H); 3.12 (m, 1H); 1.95 (m, 2H); 1.70 (br s, 6H); 1.45 (m, 4H). MS [M+1]=332.0

N-{4-(azepan-1-yl)phenyl}-2-(4,4-dihydroxyt-1-piperidl)acetamide (19)

Prepared according to **General Procedure A** yielding 0.018 g (34%). ^{1}H NMR (DMSO-d6, 400 MHz) δ 9.46 (s, 1H); 7.39 (d, 2H, *J*=8.9 Hz); 6.62 (d, 2H, *J*=9.1 Hz); 3.43 (t, 4H, *J*=6.1 Hz); 3.22 (s, 2H); 2.85 (t, 4H, *J*=6 Hz); 2.43 (t, 4H, *J*=6 Hz); 1.70 (m, 5H); 1.45 (m, 5H). MS [M+1]=348.3

N-[4-(azepan-1-yl)phenyl]-2-[4-(hydroxymethyl)-1-piperidyl]acetamide (20)

Prepared according to **General Procedure A** yielding 0.031 g (60%). ^{1}H NMR (DMSO-d6, 400 MHz) δ 10.25 (s, 1H); 7.36 (d, 2H, *J*=9.1 Hz); 6.67 (d, 2H, *J*=9 Hz); 4.02 (m, 2H); 3.53 (m, 2H); 3.43 (t, 4H, *J*=5.9 Hz); 3.27 (m, 3H); 3.05 (m, 2H); 1.84 (m, 2H); 1.70 (br s, 4H); 1.61 (m, 2H); 1.51-1.43 (m, 5H). MS [M+1]=346.3

N-[4-(azepan-1-yl)phenyl]-2-[2-(hydroxymethyl)-1-piperidyl]acetamide (21)

Prepared according to **General Procedure A** yielding 0.008 g (15%). ^{1}H NMR (DMSO-d6, 400 MHz) δ ^{1}H NMR (CD_3SO, 400 MHz) δ 10.29 (s, 1H); 7.43 (m, 5H); 7.27 (d, 1H, *J*=7.3); 6.67 (d, 1H, J=8.8 Hz) 4.07 (s, 2H); 3.55 (m, 2H); 3.44 (t, 5H, *J*=5.8 Hz); 3.32-3.17 (m, 2H); 1.94 (m, 4H);

1.70 (m, 5H); 1.45 (m, 4H). MS [M+1]=346.3

N-[4-(azepan-1-yl)phenyl]-2-[4-(1-hydroxy-1-methyl-ethyl)-1-piperidyl]acetamide (22)

Prepared according to **General Procedure A** yielding 0.019 g (35%). ^{1}H NMR (DMSO-d6, 400 MHz) δ

10.23 (s, 1H); 7.35 (d, 2H, *J*=9.1 Hz); 6.67 (d, 2H, *J*=8.8 Hz); 4.00 (d, 2H, *J*=5.1 Hz); 3.54 (m, 3H); 3.43 (t, 4H, *J*=5.8 Hz); 3.30 (m, 2H); 1.85 (m, 4H); 1.70-1.60 (m, 7H); 1.44-1.36 (m, 8H). MS [M+1]=374.3

N-[4-(azepan-1-yl)phenyl]-2-(1,4-dioxa-8-azaspiro[4.5]decan-8-yl)acetamide (23)

Prepared according to **General Procedure A** yielding 0.038 g (69%). ^{1}H NMR (DMSO-d6, 400 MHz) δ 10.26 (s, 1H); 7.37 (d, 2H, *J*=9.1 Hz); 6.68 (d, 2H, *J*=9.1 Hz); 4.13 (s, 2H); 3.94 (s, 4H); 3.56 (m, 2H); 3.44 (m, 4H); 3.22 (m, 2H); 2.09 (m, 2H); 1.86 (m, 2H); 1.71 (br s, 4H); 1.46 (m, 4H). MS [M+1]=374

1-[2-[4-(azepan-1-yl)anilino]-2-oxo-ethyl]piperidine-4-carboxylic acid (24)

Prepared according to **General Procedure A** yielding 0.016 g (35%). ^{1}H NMR (DMSO-d6, 400 MHz) δ 10.24 (s, 1H); 9.77 (br s, 1H); 7.36 (d, 2H, *J*=9.1 Hz); 6.67 (br d, 2H, *J*=9.1); 4.04 (br s, 2H); 3.55 (br d, 2H, *J*=2.7 Hz); 3.44 (m, 5H); 3.16 (m, 2H); 2.07 (m, 2H); 1.89 (m, 2H); 1.7 (m, 4H); 1.45 (m, 4H). MS [M+1]=360

1-[2-[4-(azepan-1-yl)anilino]-2-oxo-ethyl]piperidine-3-carboxylic acid (25)

Prepared according to **General Procedure A** yielding 0.019 g (43%). ^{1}H NMR (DMSO-d6, 400 MHz) δ 10.27 (s, 1H); 9.89 (br s, 1H); 7.37 (d, 2H, *J*=8.8 Hz); 6.67 (d, 2H, *J*=9.1 Hz); 4.15 (m,

2H); 3.65 (m, 1H); 3.49 (m, 1H); 3.44 (m, 4H); 2.96 (m, 2H); 2.07 (m, 1H); 1.86 (m, 2H); 1.70 (m, 5H); 1.44 (m, 5H). MS [M+1]=360

N-[4-(azepan-1-yl)phenyl]-2-[4-(dimethylamino)-1-piperidyl]acetamide (26)

Prepared according to **General Procedure A** yielding 0.032 g (48% based on 1:2 TFA salt) ^{1}H NMR (DMSO-d6, 400 MHz) δ 10.44 (s, 1H); 7.37 (d, 2H, *J*=8.8 Hz); 6.68 (d, 2H, *J*=9.1 Hz); 4.09 (br s, 2H); 3.66 (m, 2H); 3.44 (m, 6H); 3.11 (m, 1H); 2.78 (s, 6H); 2.38 (m, 2H); 2.08 (m, 2H); 1.71 (br s, 4H); 1.45 (m, 4H). MS [M+1]=359.2

2-(4-acetamido-1-piperidyl)-N-[4-(azepan-1-yl)phenyl]acetamide (27)

Prepared according to **General Procedure A** yielding 0.004 g (7%). ^{1}H NMR (DMSO-d6, 400 MHz) δ 10.23 (s, 1H); 8.02 (d, 1H, *J*=7.5 Hz); 7.37 (d, 2H, *J*=9.4 Hz); 6.68 (d, 2H, *J*=8.4 Hz); 4.04 (m, 2H); 3.5 (m, 2H); 3.45 (t, 4H, *J*=5.5 Hz) 3.17 (m, 2H); 1.97 (m, 3 H); 1.81 (s, 3H); 1.71 (m, 4H); 1.46 (m, 4H). MS [M+1]=373.2

N-[4-(azepan-1-yl)phenyl]-2-[4-(4-chlorophenyl)-4-hydroxy-1-piperidyl]acetamide (28)

Prepared according to **General Procedure A** yielding 0.030 g (71%). ^{1}H NMR (DMSO-d6, 400 MHz) δ 10.26 (s, 1H); 7.50 (m, 4H); 7.38 (d, 2H, *J*=9.1 Hz); 6.68 (d, 2H, *J*=9.1 Hz); 5.63 (br s, 1H); 4.16 (br d, 2H, *J*=4.6 Hz); 3.46 (m, 8H); 2.33 (m, 2H); 1.82 (br d, 2H, *J*=13.9 Hz); 1.71 (br s, 4H); 1.45 (m, 4H). MS [M+1]=442.2

N-[4-(azepan-1-yl)phenyl]-2-pyrrolidin-1-yl-acetamide hydrochloride (29)

Prepared according to **General Procedure A** yielding 0.068 g (53%). ^{1}H NMR (DMSO-d6, 400 MHz) δ: 10.24 (br s, 1H); 7.47 (br s, 2H); 6.76 (br s, 2H); 4.20 (d, 2H, *J*=4.0 Hz); 3.60 (d, 2H, *J*=5.6 Hz); 3.46 (m, 4H); 3.12 (d, 2H, *J*=10.9 Hz); 2.01-1.45 (m, 12H). MS [M+1]=302.2

2-(azepan-1-yl)-N-[4-(azepan-1-yl)phenyl]acetamide hydrochloride (30)

Prepared according to **General Procedure A** yielding 0.04 g (42%). ^{1}H NMR (DMSO-d6, 400 MHz) δ: 9.94 (br s, 1H); 7.47 (br s, 2H); 6.80 (br s, 2H); 4.13 (d, 2H, *J*=5.1 Hz); 3.45-3.20 (m, 8H); 1.85-1.50 (m, 16H). MS [M+1]=330.2

N-[4-(azepan-1-yl)phenyl]-2-(2-methyl-1-piperidyl)acetamide (31)

Prepared according to **General Procedure A** yielding 0.033 g (79%). ^{1}H NMR (DMSO-d6, 400 MHz) δ 10.29 (s, 1H); 7.37 (d, 2H, *J*=8.8, 2H Hz); 6.8 (d, 2H, *J*=8.8 Hz); 4.31 (dd, 1H, *J*=2,15.7 Hz); 4 (m, 1H); 3.86 (dd, 1H, *J*=6.3, 15.4 Hz); 3.54 (br d, 1H, *J*=11.6 Hz); 3.44 (t, 4 H, *J*=5.9 Hz); 3.37 (br d, 1H, *J*=6.1 Hz); 3.23 (br d, 1H, *J*=4.3 Hz); 1.85-1.63 (m, 9H); 1.47-1.44 (m, 5H); 1.31 (d, 2H, *J*=6.3 Hz); 1.24 (d, 2H, *J*=6.8 Hz). MS [M+1]=330.2

N-[4-(azepan-1-yl)phenyl]-2-(3-methyl-1-piperidyl)acetamide (32)

Prepared according to **General Procedure A** yielding 0.031 g (62%). ^{1}H NMR (DMSO-d6, 400 MHz) δ 10.24 (s, 1H); 7.37 (d, 2H, *J*=9.1); 6.68 (d, 2H, *J*=9.1); 4.02 (m, 2H); 3.43 (m, 6H); 2.94 (m, 1H); 2.70 (m, 1H); 1.96 (m, 1H); 1.80-1.71 (m, 7H); 1.46 (m, 4H); 0.90 (m, 4H). MS [M+1]=330.3

N-[4-(azepan-1-yl)phenyl]-2-(4-methyl-1-piperidyl)acetamide (33)

Prepared according to **General Procedure A** yielding 0.027 g (54%). ^{1}H NMR (DMSO-d6, 400 MHz) δ 10.20 (s, 1H); 7.36 (d, 2H, *J*=9.1 Hz); 6.66 (d, 2H, *J*=9.1 Hz); 4.01 (m, 2H); 3.49-3.40 (m, 5H); 3.25 (m, 1H); 3.04 (2H); 1.79 (m, 6H); 1.44 (m, 6H); 0.93 (m, 4H). MS [M+1]=330.3

N-[4-(azepan-1-yl)phenyl]-2-[2-(4-chlorophenyl)-1-piperidyl]acetamide (34)

Prepared according to **General Procedure A** yielding 0.024 g (59%). ^{1}H NMR (DMSO-d6, 400

MHz) δ 10.00 (s, 1H); 7.61-7.54 (m, 4H); 7.23 (d, 2H, *J*=9.1 Hz); 6.63 (d, 2H, *J*=9.1 Hz); 4.54 (br d, 1H, *J*=11.1 Hz); 3.74-3.63 (m, 3H); 3.42 (t, 4H, *J*=5.9 Hz); 3.28 (m, 1H); 2.18 (m, 1H); 2.04 (m, 1H) 1.90 (m, 3H); 1.69-1.6 (m, 5H); 1.44 (m, 4H). MS [M+1]=426.2

N-[4-(azepan-1-yl)phenyl]-2-[3-(3-chlorophenyl)-1-piperidyl]acetamide (35)

Prepared according to **General Procedure A** yielding 0.012 g (19%). ^{1}H NMR (DMSO-d6, 400 MHz) δ ^{1}H NMR (DMSO-d6, 400 MHz) δ 10.29 (s, 1H); 7.43 (m, 5H); 7.27 (d, 1H, *J*=7.3); 6.67 (d, 1H, J=8.8 Hz) 4.07 (s, 2H); 3.55 (m, 2H); 3.44 (t, 5H, *J*=5.8 Hz); 3.32-3.17 (m, 2H); 1.94 (m, 4H); 1.70 (m, 5H); 1.45 (m, 4H). MS [M+1]=426.2

N-[4-(azepan-1-yl)phenyl]-2-[4-(3-cyanophenyl)-1-piperidyl]acetamide (36)

Prepared according to **General Procedure A** yielding 0.016 g (27%). ^{1}H NMR (DMSO-d6, 400 MHz) δ 10.28 (s, 1H); 7.81 (m, 2H); 7.66 (m, 2H); 7.36 (d, 2H, *J*=7.3 Hz); 6.67 (d, 2H, *J*=7.6 Hz); 4.06 (m, 2H); 3.56 (m, 2H); 3.42-3.25 (m, 6H); 3.06 (br s, 1 H); 1.94 (m, 3H); 1.70 (br s, 5H); 1.44 (m, 4H). MS [M+1]=417.2

N-[4-(azepan-1-yl)phenyl]-2-(2-methyl-4-phenyl-1-piperidyl)acetamide (37)

Prepared according to **General Procedure A** yielding 0.045 g (77%) as a mixture of isomers. Data for major isomer: ^{1}H NMR (DMSO-d6, 400 MHz) δ 10.30 (s, 1H); 7.39-7.24 (m, 7 H); 6.69 (s, 2H, *J*=8.9 Hz); 4.37 (d, 2H, *J*=5.4 Hz); 3.67-3.64 (m, 2H); 3.44 (t, 4H, *J*=6 Hz); 3.31 (m, 1H); 2.91 (m, 1H); 2.03-1.97 (m, 4H); 1.71 (m, 4H); 1.45 (m, 4H); 1.34 (d, 3H, *J*=6.4 Hz). MS [M+1]= 406.2

N-[4-(azepan-1-yl)phenyl]-2-(2-phenylpyrrolidin-1-yl)acetamide (38)

Prepared according to **General Procedure A** yielding 0.051 g (92%). ^{1}H NMR (DMSO-d6, 400

MHz) δ 10.20 (s, 1H); 7.44-7.34 (m, 5H); 7.23 (t, 2H, *J*=8.9 Hz); 6.67 (d, 2H, *J*=8.9 Hz); 4.25 (br s, 2H); 3.80-3.68 (m, 2H); 3.5 (br s, 1H); 3.43 (t, 4H, *J*=5.9 Hz); 2.42 (m, 2H); 2.07 (m, 2H); 1.70 (br s, 4H); 1.45 (m, 4H). MS [M+1]=378.3

N-[4-(azepan-1-yl)phenyl]-2-[3-(4-fluorophenyl)pyrrolidin-1-yl]acetamide (39)

Prepared according to **General Procedure A** yielding 0.055 g (96%). ^{1}H NMR (DMSO-d6, 400 MHz) δ 10.08 (s, 1H); 7.60 (m, 1H); 7.51 (m, 3H); 7.23 (d, 2H, *J*=8.1 Hz); 6.63 (d, 2H, *J*=9.1 Hz); 4.57 (m, 1H); 4.01 (m, 2H); 3.82 (d, 1H, *J*=11.4); 3.42 (m, 5H); 2.40 (m, 1H); 2.18 (m, 3H); 1.69 (br s, 4H); 1.45 (m, 4H). MS [M+1]=396.2

2-(8-azabicyclo[3.2.1]octan-8-yl)-N-[4-(azepan-1-yl)phenyl]acetamide (40)

Prepared according to **General Procedure A** yielding 0.027 g (52%). ^{1}H NMR (DMSO-d6, 400 MHz) δ 10.14 (s, 1H); 7.35 (d, 2H, *J*=8.9 Hz); 6.67 (d, 2H, *J*=9.1 Hz); 3.97 (br s, 2H); 3.87 (d, 2H, *J*=5.5 Hz); 3.43 (t, 4H, *J*=6.1); 2.15 (m, 2H); 2.03 (m, 1H); 1.93 (m, 2H); 1.70 (m, 7H); 1.53 (m, 2H); 1.45 (m, 4H). MS [M+1]=342.2

N-[4-(azepan-1-yl)phenyl]-3-chloro-propanamide (41)

To a 4° C solution of 0.03 g (0.158 mmol) **(11)** in 1mL CH_2Cl_2 was added 20 µL (0.1435 mmol) triethyamine. The reaction mixture was stirred for 1 minute then to which was added 23 µL (0.230 mmol) 3-chloropropionyl chloride. The reaction mixture was stirred and allowed to warm to room temperature for two hours and then diluted with 20 mL CH_2Cl_2, washed with water, dried over $MgSO_4$, filtered, and concentrated which afforded 0.040 g of mixture containing **(41)** and carried on to the next step. MS [M+1]=281.2

N-[4-(azepan-1-yl)phenyl]-3-(1-piperidyl)propanamide (42)

Prepared according to **General Procedure A** yielding 0.033 g (69%). ^{1}H NMR (DMSO-d6, 400 MHz) δ 9.84 (s, 1H); 7.36 (d, 2H, *J*=8.8 Hz); 6.66 (br d, 2H, *J*=8.9 Hz); 3.45 (m, 6H); 3.34 (m, 2H); 2.92 (m, 2H); 2.77 (br t, 2H, *J*=7.2 Hz); 1.84(m, 2H); 1.71-1.58 (m, 8H); 1.45 (m, 4H). MS [M+1]=334.2

N-[4-(azepan-1-yl)phenyl]-2-chloro-propanamide (43)

To a 4° C solution of 0.03 g (0.158 mmol) **(11)** in 1mL CH_2Cl_2 was added 20 µL (0.1435 mmol) triethyamine. The reaction mixture was stirred for 1 minute then to which was added 23 µL (0.230 mmol) 3-chloropropionyl chloride. The reaction mixture was stirred and allowed to warm to room temperature for two hours and then diluted with 20 mL CH2CL2, washed with water, dried over $MgSO_4$, filtered, and concentrated in vacuo which afforded 0.040 g of mixture containing **(43)**. MS [M+1]=281.2

N-[4-(azepan-1-yl)phenyl]-2-(1-piperidyl)propanamide (44)

Prepared according to **General Procedure A** yielding 0.031 g (66%). ^{1}H NMR (DMSO-d6, 400 MHz) δ 10.36 (s, 1H); 7.40 (d, 2H, *J*=9.1 Hz); 6.70 (d, 2H, *J*=9.1 Hz); 3.98 (t, 1H, *J*=6.9 Hz); 3.55 (m, 1H); 3.45-3.35 (m, 5H); 3.07-2.89 (m, 2H); 1.80-1.71 (m, 9H); 1.53-1.45 (m, 8H) MS [M+1]=334.2

1-(5-nitro-2-pyridyl)azepane (45a)

Prepared from 0.2 g (1.4 mmol) 2-fluro-5-nitro-pyridine analogous to **(10)** yielding 0.276 g (88%). ^{1}H NMR (DMSO-d6, 400 MHz) δ 8.95 (d, 1H, *J*=2.8 Hz); 8.20 (dd, 1H, *J*=3, 9.6 Hz); 6.78 (d, 1H, *J*=9.6); 3.86 (br d, 4H, *J*=93.8 Hz); 1.73 (m, 4H); 1.49 (m, 4H). MS [M+1]=222.2

1-(6-nitro-3-pyridyl)azepane (45b)

Prepared from 0.2 g (1.4 mmol) 5-fluro-2-nitro-pyridine analogous to **(10)** yielding 0.220 g (70%).[1]H NMR (DMSO-d6, 400 MHz) δ 8.14 (d, 1H, 9.6 Hz); 8.06 (d, 1H, *J*=3.2 Hz); 7.26 (dd, 1H, *J*=3, 9.3 Hz); 3.65 (t, 4H, *J*=6.1 Hz); 1.75 (m, 4H); 1.49 (m, 4H). MS [M+1]=222.2

1-(6-chloropyridazin-3-yl)azepane (45c)

Prepared from 1 g (6.7 mmol) 3,6 dichloropyridazine analogous to **(10)** yielding 0.510 g (35%). [1]H NMR (DMSO-d6, 400 MHz) δ 7.44 (d, 1H, *J*=9.6); 7.16 (d, 1H, *J*=9.6); 3.65 (m, 4H); 1.70 (m, 4H); 1.48 (m, 4H). MS [M+1]=212.2

1-(5-nitropyrimidin-2-yl)azepane (45d)

Prepared from 0.2 g (0.98 mmol) 2-bromo-5-nitro-pyrimidine analogous to **(10)** yielding 0.148 g (67%). [1]H NMR (DMSO-d6, 400 MHz) δ 9.11 (s, 2H); 3.86, (t, 4H, *J*=6.1 Hz); 1.74 (m, 4H); 1.52 (m, 4H). MS [M+1]=223.2

1-(5-nitropyrazin-2-yl)azepane (45e)

Prepared from 0.2 g (1.2 mmol) 2-chloro-5-nitro-pyrazine analogous to **(10)** yielding 0.244 g (87%). [1]H NMR (DMSO-d6, 400 MHz) δ 9.03 (d, 1H, *J*=1 Hz); 8.12 (d, 1H, *J*=1.3 Hz); 3.82 (br d, 4H, *J*=18 Hz); 1.76 (br s, 4H); 1.50 (m, 4H). MS [M+1]=223.2

1-(2-fluoro-4-nitro-phenyl)azepane (45f)

Prepared from 0.2 g (1.2 mmol) 3,4-difluronitrobenzene analogous to **(10)** yielding 0.236 g (78%). [1]H NMR (DMSO-d6, 400 MHz) δ 7.92 (d, 2H, *J*=13.4 Hz); 6.98 (t, 1H, *J*=9.3 Hz); 3.59 (t, 4H, *J*=7 Hz); 1.76 (m, 4H); 1.52 (m, 4H). MS [M+1]=239.2

1-(3-fluoro-4-nitro-phenyl)azepane (45g)

Prepared from 0.2 g (1.2 mmol) 2,4-difluoro-1-nitrobenzene analogous to **(10)** yielding 0.252 g (84%). ^{1}H NMR (DMSO-d6, 400 MHz) δ 7.82 (dd, 1H, *J*=6.3, 9.1 Hz); 6.96 (dd, 1H, *J*=2.5, 12.6 Hz); 6.64 (m, 1H); 3.23 (t, 4H, *J*=5.5 Hz); 1.73 (br s, 4H); 1.50 (m, 4H). MS [M+1]=239.2

N-[6-(azepan-1-yl)-3-pyridyl]-2-(1-piperidyl)acetamide (46)

Prepared from **(45a)** via **Scheme 2** and analogous to **General Procedure A** yielding 0.007 g (14%). ^{1}H NMR (DMSO-d6, 400 MHz) δ 10.83 (s, 1H); 8.35 (br d, 1H *J*=2.5 Hz); 7.86 (dd, 1H, *J*=2.2, 9.6 Hz); 7.10 (br d, 1H, *J*=8.9 Hz);4.11 (s, 2H); 3.65 (t, 4H, *J*=5.9 Hz); 3.48 (m, 2H); 3.05 (br s, 2H); 1.78 (m, 10 H); 1.50 (m, 4H). MS [M+1]=317.2

N-[5-(azepan-1-yl)-2-pyridyl]-2-(1-piperidyl)acetamide (47)

Prepared from **(45b)** via **Scheme 2** and analogous to **General Procedure A** yielding 0.045 g (93%). ^{1}H NMR (DMSO-d6, 400 MHz) δ 10.75 (s, 1H); 7.84 (m, 2H); 7.18 (dd, 1H, *J*=3.4, 9.1 Hz) 4.08 (d, 2H, *J*=5.6 Hz) 3.47 (m, 6H); 3.01 (m, 2H); 1.77 (m, 10H); 1.45-1.29 (4H). MS [M+1]=317.3

tert-butyl N-[6-(azepan-1-yl)pyridazin-3-yl]carbamate (48)

To 0.20 g of **45c**, 0.92 g cesium carbonate, 0.22 g tert-butyl carbamates, and 0.074 g Brettphos precat G1[241] was added 4.7 mL deoxygenated 1,4-dioxane. The mixture was stirred and heated to 110 ^{0}C for 24 hours and then diluted with CH_2Cl_2, washed with 1N aqueous HCl and brine, dried over $MgSO_4$, filtered, and concentrated before carried over to next step.

6-(azepan-1-yl)pyridazin-3-amine (49)

To a stirring room temperature solution of 0.1 g (0.342 mmol) **(48)** crude in 4 mL CH2CL2 was added 1 mL trifluoroacetic acid. The reaction mixture was stirred for 8 hours and then diluted with CH_2Cl_2, washed with saturated sodium bicarbonate and brine, dried over $MgSO_4$, filtered and concentrated. Purification by flash chromatography (Biotage Isolera One, 24g silica gel, linear gradient 1%-20% MeOH:CH_2Cl_2) afforded 0.05 g of **(49)** (76%). ^{1}H NMR (DMSO-d6, 400 MHz) δ 7.05 (d, 1H, *J*=9.6 Hz); 6.80 (d, 1H, *J*= 9.9 Hz); 5.72 (br s, 2H) 3.54 (t, 4H, *J*=5.1 Hz); 1.67 (m, 4H); 1.45 (M, 4H). MS [M+1]=193.2

N-[6-(azepan-1-yl)pyridazin-3-yl]-2-(1-piperidyl)acetamide (50)

Prepared from **(49)** via **Scheme 2** and analogous to **General Procedure A** yielding 0.012 g (24%). ^{1}H NMR (DMSO-d6, 400 MHz) δ 9.80 (br s, 1H) 8.12 (d, 1H, *J*=10.1 Hz); 7.60 (d, 1H, *J*= 9.3 Hz); 4.18 (s, 2H); 3.70 (t, 4H, *J*=5.8 Hz); 3.49 (m, 2H); 3.05 (m, 2H); 1.78-1.69 (m, 8H); 1.51-1.43 (M, 6H). MS [M+1]=318.2

N-[2-(azepan-1-yl)pyrimidin-5-yl]-2-(1-piperidyl)acetamide (51)

Prepared from **(45d)** via **Scheme 2** and analogous to **General Procedure A** yielding 0.044 g (91%). ^{1}H NMR (DMSO-d6, 400 MHz) δ 10.44 (s, 1H); 8.48 (s, 2H); 4.08 (d, 2H, *J*=4.8); 3.71 (t, 4H, *J*=5.9); 3.48 (m, 2H); 3.02 (m, 2H); 1.78 (m, 10H); 1.49 (m, 4H). MS [M+1]=318.2

N-[5-(azepan-1-yl)pyrazin-2-yl]-2-(1-piperidyl)acetamide (52)

Prepared from **(45e)** via **Scheme 2** and analogous to **General Procedure A** yielding 0.043 g (90%). ^{1}H NMR (DMSO-d6, 400 MHz) δ 10.67 (s, 1H); 8.71 (m, 1H); 7.92 (m, 1H); 4.11 (d, 2H, *J*=4.8 Hz); 3.63 (t, 4H, *J*=5.9 Hz); 2.06 (m, 2H); 3.03 (m, 2H); 1.77 (m, 10H); 1.47(m, 4H). MS

[M+1]=318.2

N-[4-(azepan-1-yl)-3-fluoro-phenyl]-2-(1-piperidyl)acetamide (53)

Prepared from **(45f)** via **Scheme 2** and analogous to **General Procedure A** yielding 0.041 g (87%). ^{1}H NMR (DMSO-d6, 400 MHz) δ 10.48 (s, 1H); 7.46 (dd, 1H, *J*=2.6, 16 Hz); 7.14 (dd, 1H, *J*=2.5,8.8 Hz); 6.93 (m, 1H); 4.05 (d, 2H, *J*=4.8 Hz); 3.47 (m, 2H); 3.30 (t, 4H, *J*= 5.7); 3.02 (m, 2H); 1.77 (m, 10H); 1.55 (m, 4H). MS [M+1]=334.2

N-[4-(azepan-1-yl)-2-fluoro-phenyl]-2-(1-piperidyl)acetamide (54)

Prepared from **(45g)** via **Scheme 2** and analogous to **General Procedure A** yielding 0.042 g (89%). ^{1}H NMR (DMSO-d6, 400 MHz) δ 9.73 (s, 1H); 7.39 (dd, 1H, *J*=6.2, 8.5 Hz); 6.90 (dd, 1H, *J*=2.7, 11.6 Hz); 6.76 (td, 1H, *J*=2.8, 7.9 Hz); 4.12 (s, 2H); 3.48 (d, 2H, J=11.4 Hz); 3.12-3.04 (m, 6H); 1.78-1.62 (14H) MS [M+1]=334.2

2-(8-azabicyclo[3.2.1]octan-8-yl)-N-[6-(azepan-1-yl)-3-pyridyl]acetamide (55)

Prepared from **(45a)** via **Scheme 2** and analogous to **General Procedure A** yielding 0.042 g (81%). ^{1}H NMR (DMSO-d6, 400 MHz) δ 10.74 (s, 1H); 8.34 (d, 1H, *J*=2.3 Hz); 7.86 (m, 1H); 7.04 (m, 1H); 4.00 (m, 4H); 3.65 (t, 4H, *J*=5.9 Hz); 2.17 (m, 2H); 2.04 (m, 1H); 1.94 (m, 2H); 1.74 (m, 5H); 1.66 (m, 4H); 1.54 (m, 4H). MS [M+1]=343.2

FluxOr Assay

See **Chapter II** materials and methods.

Electrophysiology

See Chapter II materials and methods.

Metabolic Stability

Test compounds were incubated at a concentration of 1 and 10 μM with 0.5mg/ml pooled mixed gender human live microsomes (Xenotech, LLC) in incubation buffer (10mM Magnesium Chloride, 0.1M Potassium Phosphate, pH 7.4) in a 37°C water bath. After a 5 minute pre-incubation, reactions were initiated by addition of cofactors, β-NADPH (nicotinamide adenine dinucleotide phosphate) and UDPGA (uridine diphosphate gluronic acid, at a final concentration 1mM and 2mM, respectively. Reactions were terminated at five separate time points (0, 10, 20, 30 and 60min) by addition of three volumes of ice-cold 0.1% formic acid in acetonitrile. After mixing by vortex, the quenched reactions were centrifuged at 2650g for 30 minutes. The supernatants were then transferred and diluted with an equal volume of 0.1% formic acid in water. 5μL of each sample was injected and analyzed by LC/MS. The percent remaining at each time point was determined by comparing the internal standard response ratio to that at time 0 minute. The half-life and the intrinsic clearance were determined using Michaelis-Menton non-linear regression analysis. The samples were analyzed using an Agilent 6540 QTOF with Jet Stream Electrospray Ionization Source (ESI) and Agilent 1290 UHPLC. Solvents were 0.1% formic acid in water (A) and 0.1% formic acid in acetonitrile (B). Chromatographic separation was achieved over 2.5 minute using a Waters Acquity UPLC BEH C18 2.1 x 50mm, 1.7micron with a binary gradient starting at 5% B for 0.2minutes. The percent B was then increased to 95% from 0.2 to 1.2 minute. The gradient returned to initial conditions immediately at 1.2 minutes. The mass spec acquisition was performed using full scan MS from m/z 100 to 500 with the following source conditions: Drying and Sheath Gas temperatures at 350°C and flows at 11L/min; Nebulizer-30psig, VCap, Nozzle and Fragmenter voltages at 3000V, 600V and 125V, respectively.

Rat pharmacokinetics

Male Sprague Dawley rats were catheterized using the Instech Pinport system through jugular vein. Rats were fasted for 16 hours prior to dosing with ad libitum access to water. Three rats

were dosed 1mg/kg IV by tail vein injection and three rats were dosed 10mg/kg PO with a 1mg/mL solution of LI-967 in a solution of 0.5% 0.1M citric acid in water. 200µL of blood was collected in lithium heparin treated tubes at 5, 15, and 30minutes and at 1, 4, 8, and 24 hours via jugular vein catheter. The port was flushed with 20unit/mL lithium heparin in 50% water/glycerol solution (1:1, v/v). The blood was centrifuged at at 3200rpm for 12 minutes to collect plasma. Plasma was then collected into Thermoscientific Matrix tubes and stored at -80C until analysis.

Mouse blood-brain barrier penetration

Male C57BL/6J mice, 5 mice/timepoint, were injected IP with a 1mg/mL solution of LI-967 in a solution of 0.5% 0.1M citric acid in water. At 0.5, 1, 2 and 8 hours the mice were anaesthetized with isoflurane and the blood was drawn via cardiac puncture in the open chest cavity and collected in lithium heparin treated tubes. The brain was perfused with phosphate buffered saline (PBS) and harvested. The blood was centrifuged at 3200rpm for 12 minutes to separate the plasma. Plasma was then collected in matrix tubes and stored with the intact brains in -80C freezer until analysis. The brains lysed in a 2x volume of PBS, pH 7.4 adjusted with 1M HCl resulting in a 3x homogenate (w/w).

Analysis of Rat PK and Mouse BBB

The samples were extracted with a 3x volume (v/v) of 0.1% formic acid in acetonitrile with 1mg/mL LI-664 (internal standard) and centrifuged at 2650 rcf for 30minutes. The supernatant was mixed with 0.1% formic acid in water and analyzed using an Agilent 6540 QTOF with Jet Stream Electrospray Ionization Source (ESI) and Agilent 1290 UHPLC. Solvents were 0.1% formic acid in water (A) and 0.1% formic acid in methanol (B). Chromatographic separation was achieved over 2.5 minute using a Waters Acquity UPLC BEH C18 2.1 x 50mm, 1.7micron, column with a binary gradient starting 5% B. The gradient continued with B increasing to 95%

from 0 to 1.2 minutes with immediate drop to initial conditions at 1.21minutes. The mass spec acquisition was performed using full scan MS from m/z 100 to 1000 with the following source conditions: Drying and Sheath Gas temperatures at 350°C and flows at 11L/min; Nebulizer-30psig, VCap, Nozzle and Fragmenter voltages at 3000V, 600V and 125V, respectively.

Data Analysis

cLogD (pH 7.4), TPSA, and pKa calculated by ACD Labs Percepta. IC_{50} values calculated from mean of 4 replicate values with 4 factor variable slope fit similar to **Chapter II**.

Chapter V

Conclusion and Perspective

In this work, we have established the infrastructure necessary for Kv11.1-3.1 drug discovery while simultaneously revealing new findings concerning Kv11.1-3.1 molecular biology and anti-psychotic action. In the first chapter, we characterized the expression, trafficking, and activity deficiencies of Kv11.1-3.1. These findings lead to the development of a biochemical assay screen for pharmacological trafficking rescue which resulted in the observation that proteasome inhibition drastically rescued these deficits. Using this tool, we were able to create robust high-throughput assays, allowing us to screen molecules and proceed with the development pipeline. By focusing on maximizing expression while limiting endogenous degradation, we were able to adapt Kv11.1-3.1 onto Kv11.1-1A IonWorks Quattro™ platforms for high-throughput electrophysiology for a secondary assay. A small panel of antipsychotics was used to evaluate the accuracy of this platform. While not congruent with literature reports of manual voltage-clamp data from various cells lines for certain compounds, this assay was a seemingly better predictor of compound selectivity compared to the FluxOR assay and is a useful tool for validating that aspect. Using both of these assays, along with manual voltage-clamp in HEK 293 cells, we found clozapine to preferentially inhibit Kv11.1-3.1. Finally, we used the FluxOR assay to drive medicinal chemistry studies of a hit found in collaboration with the NCGC/NCATS. SAR of the hit led to the synthesis of compound **55** (**Chapter III**) which boasts 100-fold Kv11.1-3.1/Kv11.1-1A selectivity at mid-nanomolar potency. While this compounds displays an incredible 16:1 mouse brain to plasma ratio, it is cleared almost instantaneously in rats. Regardless, this compound has the potential for further modification to alleviate these metabolic issues and be

used as a tool compound in rodent behavioral assays.

Of specific interest in modifying **55** is further modification to the azepane ring portion of the molecule, combination of the 3.2.1 azabicyclo terminal group with the fluorinated cores, and SAR from trimming back the various rings. Modifications to the azepane core are especially desired as few existing analogs have increased the basicity of the contained nitrogen and bicyclo analogs have yet to be tested. In order to improve metabolic stability, metabolic ID studies will be used to guide the synthesis of additional analogs that will either remove the reactive hotspots identified or add substituents to lessen the degree of metabolic enzyme action. Once these new compounds are tested *in vitro* using microsomes, they will be evaluated in the same mouse blood-brain barrier and rat PK assays. Data from these studies will be used to guide dosing and timing for t-maze and novel object location cognitive tests in rodents. If any of these compounds are successful, more strenuous cardiotoxicity testing will need to be done in Kv11.1-1A binding assays, additional electrophysiology, and *in vivo* studies using guinea pigs prior to larger animals (such as dogs).[242] If a putative compound is able to pass these major hurdles, it may be appropriate to initiate investigational new drug (IND)-enabling studies in order to complete the preliminary steps prior to first-in-man phase 1 clinical trials.

However, the usefulness of such a compound in the treatment of schizophrenia is still unclear. While an aim of the same genetic studies that discovered Kv11.1-3.1 was to find novel drug targets, the evidence in the literature still traces Kv11.1-3.1 to dopamine action.[189] Granted, this is likely a biased model due to natural proclivity towards what is already known, but without knowledge of an exact contribution or effect, it is difficult to estimate the likelihood that a potential drug would attract the necessary resources for commercialization and clinical access. Studies examining the differential response of clozapine and risperidone in the risk SNP patient population may provide some statistical evidence that Kv11.1-3.1 does contribute to the disease pathology, perhaps mandating a new compound with clozapine-like pharmacology and an emphasis on Kv11.1-3.1 blockade. In order to determine the contribution of Kv11.1-3-1

overexpression in schizophrenia, it may be of use to examine neuronal firing in more humanized systems, such as stem cells or brain organoids.[243]

What may be a potentially faster route to relevance is in the continued examination of *KCNH2* risk SNPs in the context of other schizophrenia-associated genes. *KCNH2* is not among the significant loci reported in any iteration of the PGC consortium studies, yet we have strong evidence that it is indeed associated with schizophrenia in certain contexts. One possible reason for this disconnect is the limitations of the PGC GWAS studies to detect epistatic effects and the possible strong regulation of Kv11.1-3.1 expression by ERAD and the proteasome. As mentioned previously in **Chapter II**, the ubiquitin-proteasome system (UPS) and ERAD proteins have been implicated in schizophrenia, especially via downregulation. While these reports attempt to model deficient UPS to increased lysosome activity which targets neurotransmitter receptors, myelin, BDNF, etc., Kv11.1-3.1 presents a straightforward exacerbation of risk.[218,219,244] In addition to these highly contextual studies, a 20S subunit member *PSMA4* has been recently found to be significantly associated with schizophrenia in the PGC GWAS which may be a powerful tool for KCNH2 epistatic computational studies, or as a member of a general "UPS score" that would recapitulate total UPS activity. It has also been recently discovered in our lab that *AS3MT*, a top PGC GWAS hit, interacts with multiple members of the UPS and thus may be another "effector" in a conjectured "UPS-mediated schizophrenia" subtype.[90] The global down-regulation of UPS-effector relationship in this hypothesis also resists the plague of cellular mosacism to a certain extent, as a variety of targets play highly exchangeable or interactive roles in UPS and the degree to which proteins can assume effector roles is seemingly limitless. Clearly this is difficult to approach for the purpose of designing new therapeutics beyond gene-editing, although Kv11.1-3.1 may be a fortunate and druggable discovery in this paradigm.

References

1. Weinberger, D.R.H., P. J. *Schizophrenia*, (Wiley-Blackwell, Hoboken, NJ, 2011).
2. Association, A.P. *Diagnostic and Statistical Manual of Mental Disorders*, (American Psychiatric Publishing, Washington, DC, 2013).
3. Os, J.v. "Schizophrenia" does not exist. *BMJ* **352**(2016).
4. Berrios, G.E. Positive and Negative Symptoms and Jackson - a Conceptual History. *Arch. Gen. Psychiatry* **42**, 95-97 (1985).
5. Good, K.P.*, et al.* The relationship of neuropsychological test performance with the PANSS in antipsychotic naive, first-episode psychosis patients. *Schizophr. Res.* **68**, 11-19 (2004).
6. Minzenberg, M.J., Laird, A.R., Thelen, S., Carter, C.S. & Glahn, D.C. Meta-analysis of 41 Functional Neuroimaging Studies of Executive Function in Schizophrenia. *Arch. Gen. Psychiatry* **66**, 811-822 (2009).
7. Heckers, S., Tandon, R. & Bustillo, J. Catatonia in the DSM-Shall We Move or Not? *Schizophr. Bull.* **36**, 205-207 (2010).
8. Taylor, M.A. & Fink, M. Catatonia in psychiatric classification: A home of its own. *Am. J. Psychiatry* **160**, 1233-1241 (2003).
9. Fadgyas-Stanculete, M., Buga, A.-M., Popa-Wagner, A. & Dumitrascu, D.L. The relationship between irritable bowel syndrome and psychiatric disorders: from molecular changes to clinical manifestations. *Journal of Molecular Psychiatry* **2**, 4 (2014).
10. Simeone, J.C., Ward, A.J., Rotella, P., Collins, J. & Windisch, R. An evaluation of variation in published estimates of schizophrenia prevalence from 1990-2013: a systematic literature review. *BMC Psychiatry* **15**(2015).

11. Chong, H.Y.*, et al.* Global economic burden of schizophrenia: a systematic review. *Neuropsychiatr. Dis. Treat.* **12**, 357-373 (2016).

12. van Os, J. & Kapur, S. Schizophrenia. *Lancet* **374**, 635-645 (2009).

13. Palmer, B.A., Pankratz, V.S. & Bostwick, J.M. The lifetime risk of suicide in schizophrenia - A reexamination. *Arch. Gen. Psychiatry* **62**, 247-253 (2005).

14. Smith, T., Weston, C. & Lieberman, J. Schizophrenia (Maintenance Treatment). *Am. Fam. Physician* **82**, 338-339 (2010).

15. Rosenheck, R.*, et al.* Barriers to employment for people with schizophrenia. *Am. J. Psychiatry* **163**, 411-417 (2006).

16. Stolt, C.M. *Moniz, lobotomy, and the 1949 Nobel Prize.*, (Universal Academy Press, Tokyo, 2002).

17. Ban, T.A. Fifty years chlorpromazine: a historical perspective. *Neuropsychiatr. Dis. Treat.* **3**, 495-500 (2007).

18. Lindsley, C.W. 2014 Prescription Medications in the United States: Tremendous Growth, Specialty/Orphan Drug Expansion, and Dispensed Prescriptions Continue to Increase. *ACS Chem. Neurosci.* **6**, 811-812 (2015).

19. Casey, D.E. Neuroleptic Drug-Induced Extrapyramidal Syndromes and Tardive-Dyskinesia. *Schizophr. Res.* **4**, 109-120 (1991).

20. Leucht, S.*, et al.* Comparative efficacy and tolerability of 15 antipsychotic drugs in schizophrenia: a multiple-treatments meta-analysis. *Lancet* **382**, 951-962 (2013).

21. Hartling, L.*, et al.* Antipsychotics in Adults With Schizophrenia: Comparative Effectiveness of First-Generation Versus Second-Generation Medications A Systematic Review and Meta-analysis. *Ann. Intern. Med.* **157**, 498-U100 (2012).

22. Tiihonen, J.*, et al.* Effectiveness of antipsychotic treatments in a nationwide cohort of patients in community care after first hospitalisation due to schizophrenia and schizoaffective disorder: observational follow-up study. *Br. Med. J.* **333**, 224-227 (2006).

23. Newcomer, J.W. Antipsychotic medications: Metabolic and cardiovascular risk. *J. Clin. Psychiatry* **68**, 8-13 (2007).

24. Wenthur, C.J. & Lindsley, C.W. Classics in Chemical Neuroscience: Clozapine. *ACS Chem. Neurosci.* **4**, 1018-1025 (2013).

25. Seeman, P. & Kapur, S. Schizophrenia: More dopamine, more D-2 receptors. *Proc. Natl. Acad. Sci. U. S. A.* **97**, 7673-7675 (2000).

26. Girault, J.A. & Greengard, P. The neurobiology of dopamine signaling. *Arch. Neurol.* **61**, 641-644 (2004).

27. Neves, S.R., Ram, P.T. & Iyengar, R. G protein pathways. *Science* **296**, 1636-1639 (2002).

28. Seeman, P., Chauwong, M., Tedesco, J. & Wong, K. Brain Receptors for Antipsychotic-Drugs and Dopamine - Direct Binding Assays. *Proc. Natl. Acad. Sci. U. S. A.* **72**, 4376-4380 (1975).

29. Niemegeers, C.J.E. & Janssen, P.A.J. Systematic Study of the Pharmacological Activities of Dopamine Antagonists. *Life Sci.* **24**, 2201-2216 (1979).

30. Carlsson, A. & Lindqvist, M. Effect of Chlorpromazine or Haloperidol on Formation of 3-Methoxytyramine and Normetanephrine in Mouse Brain. *Acta Pharmacol. Toxicol. (Copenh.)* **20**, 140-& (1963).

31. Burt, D.R., Creese, I. & Snyder, S.H. Properties of [Haloperidol-H-3] and [Dopamine-H-3] Binding Associated with Dopamine Receptors in Calf Brain Membranes. *Mol. Pharmacol.* **12**, 800-812 (1976).

32. Abi-Dargham, A.*, et al.* Increased baseline occupancy of D-2 receptors by dopamine in schizophrenia. *Proc. Natl. Acad. Sci. U. S. A.* **97**, 8104-8109 (2000).

33. Guillin, O., Abi-Dargham, A. & Laruelle, M. Neurobiology of dopamine in schizophrenia. *Integrating the Neurobiology of Schizophrenia* **78**, 1-+ (2007).

34. Knable, M.B. & Weinberger, D.R. Dopamine, the prefrontal cortex and schizophrenia. *J Psychopharmacol* **11**, 123-131 (1997).

35. Seamans, J.K. & Yang, C.R. The principal features and mechanisms of dopamine modulation in the prefrontal cortex. *Prog. Neurobiol.* **74**, 1-57 (2004).

36. Tzschentke, T.M. Pharmacology and behavioral pharmacology of the mesocortical dopamine system. *Prog. Neurobiol.* **63**, 241-320 (2001).

37. Seeman, P. Dopamine Receptor Sequences - Therapeutic Levels of Neuroleptics Occupy D2-Receptors, Clozapine Occupies D4. *Neuropsychopharmacology* **7**, 261-284 (1992).

38. Denboer, J.A.*, et al.* Differential-Effects of the D1-Da Receptor Antagonist Sch139166 on Positive and Negative Symptoms of Schizophrenia. *Psychopharmacology (Berl.)* **121**, 317-322 (1995).

39. Karle, J.*, et al.* Nnc-01-0687, a Selective Dopamine D1 Receptor Antagonist, in the Treatment of Schizophrenia. *Psychopharmacology (Berl.)* **121**, 328-329 (1995).

40. Girgis, R.R.*, et al.* A proof-of-concept, randomized controlled trial of DAR-0100A, a dopamine-1 receptor agonist, for cognitive enhancement in schizophrenia. *J Psychopharmacol* (2016).

41. Kapur, S., Zipursky, R., Jones, C., Remington, G. & Houle, S. Relationship between dopamine D-2 occupancy, clinical response, and side effects: A double-blind PET study of first-episode schizophrenia. *Am. J. Psychiatry* **157**, 514-520 (2000).

42. Woolley, D.W. & Shaw, E. A Biochemical and Pharmacological Suggestion About Certain Mental Disorders. *Proc. Natl. Acad. Sci. U. S. A.* **40**, 228-231 (1954).

43. Snyder, S.H., Banerjee, S.P., Yamamura, H.I. & Greenber.D. Drugs, Neurotransmitters, and Schizophrenia. *Science* **184**, 1243-1253 (1974).

44. Meltzer, H.Y. The Role of Serotonin in Schizophrenia and the Place of Serotonin-Dopamine Antagonist Antipsychotics. *J. Clin. Psychopharmacol.* **15**, S2-S3 (1995).

45. Malenka, R.C.N., E.J.; Hyman, S.E. *Molecular Neuropharmacology: A Foundation for Clinical Neuroscience*, (McGraw-Hill Medical, New York 2002).

46. Lawrence, A.J. Optimisation of anti-psychotic therapeutics: a balancing act? *Br. J. Pharmacol.* **151**, 161-162 (2007).

47. Masana, M., Santana, N., Artigas, F. & Bortolozzi, A. Dopamine Neurotransmission and Atypical Antipsychotics in Prefrontal Cortex: A Critical Review. *Curr. Top. Med. Chem.* **12**, 2357-2374 (2012).

48. Bantick, R.A., De Vries, M.H. & Grasby, P.M. The effect of a 5-HT1A receptor agonist on striatal dopamine release. *Synapse* **57**, 67-75 (2005).

49. Li, F. & Tsien, J.Z. Memory and the NMDA Receptors. *N. Engl. J. Med.* **361**, 302-303 (2009).

50. Cheffings, C.M. & Colquhoun, D. Single channel analysis of a novel NMDA channel from Xenopus oocytes expressing recombinant NR1a, NR2A and NR2D subunits. *J Physiol-London* **526**, 481-491 (2000).

51. Fukaya, M., Hayashi, Y. & Watanabe, M. NR2 to NR3B subunit switchover of NMDA receptors in early postnatal motoneurons. *Eur. J. Neurosci.* **21**, 1432-1436 (2005).

52. Kew, J.N.C. & Kemp, J.A. Ionotropic and metabotropic glutamate receptor structure and pharmacology. *Psychopharmacology (Berl.)* **179**, 4-29 (2005).

53. Pilowsky, L.S*., et al.* First in vivo evidence of an NMDA receptor deficit in medication-free schizophrenic patients. *Mol. Psychiatry* **11**, 118-119 (2006).

54. Krystal, J.H*., et al.* Interactive effects of subanesthetic ketamine and haloperidol in healthy humans. *Psychopharmacology (Berl.)* **145**, 193-204 (1999).

55. Moghaddam, B., Adams, B., Verma, A. & Daly, D. Activation of glutamatergic neurotransmission by ketamine: A novel step in the pathway from NMDA receptor blockade to dopaminergic and cognitive disruptions associated with the prefrontal cortex. *J. Neurosci.* **17**, 2921-2927 (1997).

56. Takahata, Y. & Moghaddam, B. Glutamatergic regulation of basal and stimulus-activated dopamine release in the prefrontal cortex. *J. Neurochem.* **71**, 1443-1449 (1998).

57. Lahti, A.C*., et al.* Blockade of ketamine-induced psychosis with olanzapine. *Schizophr. Res.* **36**, 310-310 (1999).

58. Lahti, A.C., Koffel, B., Laporte, D. & Tamminga, C.A. Subanesthetic Doses of Ketamine Stimulate Psychosis in Schizophrenia. *Neuropsychopharmacology* **13**, 9-19 (1995).

59. Bressan, R.A*., et al.* Impact of schizophrenia and chronic antipsychotic treatment on [(123)I]CNS-1261 binding to N-methyl-D-aspartate receptors in vivo. *Biol. Psychiatry* **58**, 41-46 (2005).

60. Castner, S.A. & Williams, G.V. Tuning the engine of cognition: A focus on NMDA/D1 receptor interactions in prefrontal cortex. *Brain Cogn.* **63**, 94-122 (2007).

61. Snyder, M.A. & Gao, W.J. NMDA hypofunction as a convergence point for progression and symptoms of schizophrenia. *Front. Cell. Neurosci.* **7**(2013).

62. Sullivan, R*., et al.* The international society for developmental psychobiology annual meeting symposium: Impact of early life experiences on brain and behavioral development. *Dev. Psychobiol.* **48**, 583-602 (2006).

63. van den Buuse, M. Modeling the Positive Symptoms of Schizophrenia in Genetically Modified Mice: Pharmacology and Methodology Aspects. *Schizophr. Bull.* **36**, 246-270 (2010).

64. Li, N.X., Wu, X.H. & Li, L. Chronic administration of clozapine alleviates reversal-learning impairment in isolation-reared rats. *Behav. Pharmacol.* **18**, 135-145 (2007).

65. D'Hooge, R. & De Deyn, P.P. Applications of the Morris water maze in the study of learning and memory. *Brain Res Rev* **36**, 60-90 (2001).

66. Dix, S.L. & Aggleton, J.P. Extending the spontaneous preference test of recognition: evidence of object-location and object-context recognition. *Behav. Brain Res.* **99**, 191-200 (1999).

67. Antunes, M. & Biala, G. The novel object recognition memory: neurobiology, test procedure, and its modifications. *Cogn Process* **13**, 93-110 (2012).

68. Birrell, J.M. & Brown, V.J. Medial frontal cortex mediates perceptual attentional set shifting in the rat. *J. Neurosci.* **20**, 4320-4324 (2000).

69. Lodge, D.J. & Grace, A.A. Gestational methylazoxymethanol acetate administration: A developmental disruption model of schizophrenia. *Behav. Brain Res.* **204**, 306-312 (2009).

70. Fone, K.C.F. & Porkess, M.V. Behavioural and neurochemical effects of post-weaning social isolation in rodents - Relevance to developmental neuropsychiatric disorders. *Neurosci. Biobehav. Rev.* **32**, 1087-1102 (2008).

71. Kesby, J.P., Burne, T.H.J., McGrath, J.J. & Eyles, D.W. Developmental vitamin D deficiency alters MK 801-induced hyperlocomotion in the adult rat: An animal model of schizophrenia. *Biol. Psychiatry* **60**, 591-596 (2006).

72. Shi, L.M., Fatemi, H., Sidwell, R.W. & Patterson, P.H. Maternal influenza infection causes marked behavioral and pharmacological changes in the offspring. *J. Neurosci.* **23**, 297-302 (2003).

73. Zuckerman, L., Rehavi, M., Nachman, R. & Weiner, I. Immune activation during pregnancy in rats leads to a postpubertal emergence of disrupted latent inhibition, dopaminergic hyperfunction, and altered limbic morphology in the offspring: A novel neurodevelopmental model of schizophrenia. *Neuropsychopharmacology* **28**, 1778-1789 (2003).

74. Nestler, E.J. & Hyman, S.E. Animal models of neuropsychiatric disorders. *Nat. Neurosci.* **13**, 1161-1169 (2010).

75. Lipska, B.K., Jaskiw, G.E. & Weinberger, D.R. Postpubertal Emergence of Hyperresponsiveness to Stress and to Amphetamine after Neonatal Excitotoxic Hippocampal Damage - a Potential Animal-Model of Schizophrenia. *Neuropsychopharmacology* **9**, 67-75 (1993).

76. Varty, G.B. & Higgins, G.A. Examination of drug-induced and isolation-induced disruptions of prepulse Inhibition as models to screen antipsychotic drugs. *Psychopharmacology (Berl.)* **122**, 15-26 (1995).

77. Ellenbroek, B.A., van den Kroonenberg, P.T.J.M. & Cools, A.R. The effects of an early stressful life event on sensorimotor gating in adult rats. *Schizophr. Res.* **30**, 251-260 (1998).

78. Bakshi, V.P., Swerdlow, N.R., Braff, D.L. & Geyer, M.A. Reversal of isolation rearing-induced deficits in prepulse inhibition by seroquel and olanzapine. *Biol. Psychiatry* **43**, 436-445 (1998).

79. Suddath, R.L., Christison, G.W., Torrey, E.F., Casanova, M.F. & Weinberger, D.R. Anatomical Abnormalities in the Brains of Monozygotic Twins Discordant for Schizophrenia. *N. Engl. J. Med.* **322**, 789-794 (1990).

80. Carr, D.B. & Sesack, S.R. Hippocampal afferents to the rat prefrontal cortex: Synaptic targets and relation to dopamine terminals. *J. Comp. Neurol.* **369**, 1-15 (1996).

81. Lipska, B.K., Al-Amin, H.A. & Weinberger, D.R. Excitotoxic lesions of the rat medial prefrontal cortex - Effects on abnormal behaviors associated with neonatal hippocampal damage. *Neuropsychopharmacology* **19**, 451-464 (1998).

82. Richtand, N.M.*, et al.* Risperidone pretreatment prevents elevated locomotor activity following neonatal hippocampal lesions. *Neuropsychopharmacology* **31**, 77-89 (2006).

83. Bertolino, A.*, et al.* The relationship between dorsolateral prefrontal neuronal N-acetylaspartate and evoked release of striatal dopamine in schizophrenia. *Neuropsychopharmacology* **22**, 125-132 (2000).

84. O'Donnell, P. & Grace, A.A. Phencyclidine interferes with the hippocampal gating of nucleus accumbens neuronal activity in vivo. *Neuroscience* **87**, 823-830 (1998).

85. Mathe, J.M., Nomikos, G.G., Schilstrom, B. & Svensson, T.H. Non-NMDA excitatory amino acid receptors in the ventral tegmental area mediate systemic dizocilpine (MK-801) induced hyperlocomotion and dopamine release in the nucleus accumbens. *J. Neurosci. Res.* **51**, 583-592 (1998).

86. Patil, S.T.*, et al.* Activation of mGlu2/3 receptors as a new approach to treat schizophrenia: a randomized phase 2 clinical trial (vol 13, pg 1102, 2007). *Nat. Med.* **13**, 1264-1264 (2007).

87. Stauffer, V.L.*, et al.* Pomaglumetad methionil: No significant difference as an adjunctive treatment for patients with prominent negative symptoms of schizophrenia compared to placebo. *Schizophr. Res.* **150**, 434-441 (2013).

88. Pritchard, J.K. & Cox, N.J. The allelic architecture of human disease genes: common disease - common variant ... or not? *Hum. Mol. Genet.* **11**, 2417-2423 (2002).

89. Karayiorgou, P.*, et al.* Schizophrenia Susceptibility Associated with Interstitial Deletions of Chromosome 22q11. *Proc. Natl. Acad. Sci. U. S. A.* **92**, 7612-7616 (1995).

90. Ripke, S.*, et al.* Biological insights from 108 schizophrenia-associated genetic loci. *Nature* **511**, 421-+ (2014).

91. Wang, Y.*, et al.* Heterogeneity in the pyramidal network of the medial prefrontal cortex. *Nat. Neurosci.* **9**, 534-542 (2006).

92. GoldmanRakic, P.S. Architecture of the prefrontal cortex and the central executive. *Ann Ny Acad Sci* **769**, 71-83 (1995).

93. Elston, G.N. Cortex, cognition and the cell: New insights into the pyramidal neuron and prefrontal function. *Cereb. Cortex* **13**, 1124-1138 (2003).

94. Benda, J., Longtin, A. & Maler, L. Spike-frequency adaptation separates transient communication signals from background oscillations. *J. Neurosci.* **25**, 2312-2321 (2005).

95. Nyhus, E. & Curran, T. Functional role of gamma and theta oscillations in episodic memory. *Neurosci. Biobehav. Rev.* **34**, 1023-1035 (2010).

96. Raghavachari, S.*, et al.* Gating of human theta oscillations by a working memory task. *J. Neurosci.* **21**, 3175-3183 (2001).

97. Bracci, E., Vreugdenhil, M., Hack, S.P. & Jefferys, J.G.R. On the synchronizing mechanisms of tetanically induced hippocampal oscillations. *J. Neurosci.* **19**, 8104-8113 (1999).

98. Koychev, I., El-Deredy, W., Mukherjee, T., Haenschel, C. & Deakin, J.F.W. Core dysfunction in schizophrenia: electrophysiology trait biomarkers. *Acta Psychiatr. Scand.* **126**, 59-71 (2012).

99. Moran, L.V. & Hong, L.E. High vs Low Frequency Neural Oscillations in Schizophrenia. *Schizophr. Bull.* **37**, 659-663 (2011).

100. Stam, C.J. Use of magnetoencephalography (MEG) to study functional brain networks in neurodegenerative disorders. *J. Neurol. Sci.* **289**, 128-134 (2010).

101. Shrivastava, I.H., Tieleman, D.P., Biggin, P.C. & Sansom, M.S.P. K+ versus Na+ ions in a K channel selectivity filter: A simulation study. *Biophys. J.* **83**, 633-645 (2002).

102. Hellgren, M., Sandberg, L. & Edholm, O. A comparison between two prokaryotic potassium channels (KirBac1.1 and KcsA) in a molecular dynamics (MD) simulation study. *Biophys. Chem.* **120**, 1-9 (2006).

103. Alberts, B.*, et al.* Molecular Biology of the Cell, Sixth Edition. *Molecular Biology of the Cell, Sixth Edition*, 1-1342 (2015).

104. Ghatta, S., Nimmagadda, D., Xu, X.P. & O'Rourke, S.T. Large-conductance, calcium-activated potassium channels: Structural and functional implications. *Pharmacol. Ther.* **110**, 103-116 (2006).

105. Gribkoff, V.K., Starrett, J.E. & Dworetzky, S.I. Maxi-K potassium channels: Form, function, and modulation of a class of endogenous regulators of intracellular calcium. *Neuroscientist* **7**, 166-177 (2001).

106. Layne, J.J., Nausch, B., Olesen, S.P. & Nelson, M.T. BK channel activation by NS11021 decreases excitability and contractility of urinary bladder smooth muscle. *Am J Physiol-Reg I* **298**, R378-R384 (2010).

107. McLeod, J.F.*, et al.* GAL-021, a new intravenous BKCa-channel blocker, is well tolerated and stimulates ventilation in healthy volunteers. *Br. J. Anaesth.* **113**, 875-883 (2014).

108. Ledoux, J., Werner, M.E., Brayden, J.E. & Nelson, M.T. Calcium-activated potassium channels and the regulation of vascular tone. *Physiology* **21**, 69-78 (2006).

109. Ishii, T.M.*, et al.* A human intermediate conductance calcium-activated potassium channel. *Proc. Natl. Acad. Sci. U. S. A.* **94**, 11651-11656 (1997).

110. Adelman, J.P., Maylie, J. & Sah, P. Small-Conductance Ca2+-Activated K+ Channels: Form and Function. *Annual Review of Physiology, Vol 74* **74**, 245-269 (2012).

111. Goldstein, S.A.N.*, et al.* International Union of Pharmacology. LV. Nomenclature and molecular relationships of two-P potassium channels. *Pharmacol. Rev.* **57**, 527-540 (2005).

112. Hibino, H.*, et al.* Inwardly Rectifying Potassium Channels: Their Structure, Function, and Physiological Roles. *Physiol. Rev.* **90**, 291-366 (2010).

113. Lopatin, A.N., Makhina, E.N. & Nichols, C.G. Potassium Channel Block by Cytoplasmic Polyamines as the Mechanism of Intrinsic Rectification. *Nature* **372**, 366-369 (1994).

114. Matsuda, H. Open-State Substructure of Inwardly Rectifying Potassium Channels Revealed by Magnesium Block in Guinea-Pig Heart-Cells. *J Physiol-London* **397**, 237-258 (1988).

115. Hansen, S.B., Tao, X. & MacKinnon, R. Structural basis of PIP2 activation of the classical inward rectifier K+ channel Kir2.2. *Nature* **477**, 495-U152 (2011).

116. Gutman, G.A.*, et al.* International Union of Pharmacology. LIII. Nomenclature and molecular relationships of voltage-gated potassium channels. *Pharmacol. Rev.* **57**, 473-508 (2005).

117. Wulff, H., Castle, N.A. & Pardo, L.A. Voltage-gated Potassium Channels as Therapeutic Drug Targets. *Nature reviews. Drug discovery* **8**, 982-1001 (2009).

118. Neher, E. & Sakmann, B. Single-Channel Currents Recorded from Membrane of Denervated Frog Muscle-Fibers. *Nature* **260**, 799-802 (1976).

119. Sakmann, B. & Neher, E. Patch Clamp Techniques for Studying Ionic Channels in Excitable-Membranes. *Annu. Rev. Physiol.* **46**, 455-472 (1984).

120. Brueggemann, A.G., M.; Klau, M.; Beckler, M.; Steindl, M.; Behrends, J.C.; Fertig, N. Ion Channel Drug Discovery and Research: The Automated Nano-PatchClamp Technology. *Current Drug Discovery Technologies* **1**, 91-96 (2004).

121. Davis, M.J., Donovitz, J.A. & Hood, J.D. Stretch-Activated Single-Channel and Whole Cell Currents in Vascular Smooth-Muscle Cells. *Am. J. Physiol.* **262**, C1083-C1088 (1992).

122. Yu, S.P. & Kerchner, G.A. Endogenous voltage-gated potassium channels in human embryonic kidney (HEK293) cells. *J. Neurosci. Res.* **52**, 612-617 (1998).

123. Hu, L., Pennington, M., Jiang, Q., Whartenby, K.A. & Calabresi, P.A. Characterization of the functional properties of the voltage-gated potassium channel Kv1.3 in human CD4(+) T lymphocytes. *J. Immunol.* **179**, 4563-4570 (2007).

124. Beacham, D.W., Blackmer, T., O'Grady, M. & Hanson, G.T. Cell-Based Potassium Ion Channel Screening Using the FluxOR (TM) Assay. *J Biomol Screen* **15**, 441-446 (2010).

125. Titus, S.A*., et al.* A new homogeneous high-throughput screening assay for profiling compound activity on the human ether-a-go-go-related gene channel. *Anal. Biochem.* **394**, 30-38 (2009).

126. Tang, W.M*., et al.* Development and evaluation of high throughput functional assay methods for hERG potassium channel. *J Biomol Screen* **6**, 325-331 (2001).

127. Bruggemann, A.*, et al.* Automated Patch Clamping of 384 Cells at Once for Massively Parallel Ion Channel Screening. *Biophys. J.* **106**, 132a-132a (2014).

128. Vandenberg, J.I.*, et al.* hERG K(+) channels: structure, function, and clinical significance. *Physiol. Rev.* **92**, 1393-1478 (2012).

129. Aptula, A.O. & Cronin, M.T.D. Prediction of herg K+ blocking potency: Application of structural knowledge. *SAR QSAR Environ. Res.* **15**, 399-411 (2004).

130. Titus, S.A.*, et al.* A new homogeneous high-throughput screening assay for profiling compound activity on the human ether-a-go-go-related gene channel. *Anal. Biochem.* **394**, 30-38 (2009).

131. Kaplan, W.D.T., W. E. The Behavior of Four Neurological Mutants of Drosophila. *Genetics* **61**, 399-409 (1969).

132. Chiesa, N., Rosati, B., Arcangeli, A., Olivotto, M. & Wanke, E. A novel role for HERG K+ channels: Spike-frequency adaptation. *J Physiol-London* **501**, 313-318 (1997).

133. Sacco, T., Bruno, A., Wanke, E. & Tempia, F. Functional roles of an ERG current isolated in cerebellar Purkinje neurons. *J. Neurophysiol.* **90**, 1817-1828 (2003).

134. Sanguinetti, M.C. & Tristani-Firouzi, M. hERG potassium channels and cardiac arrhythmia. *Nature* **440**, 463-469 (2006).

135. Smith, P.L., Baukrowitz, T. & Yellen, G. The inward rectification mechanism of the HERG cardiac potassium channel. *Nature* **379**, 833-836 (1996).

136. Lu, Y.*, et al.* Effects of premature stimulation on HERG K+ channels. *J Physiol-London* **537**, 843-851 (2001).

137. Clark, R.B.*, et al.* A rapidly activating delayed rectifier K+ current regulates pacemaker activity in adult mouse sinoatrial node cells. *Am J Physiol-Heart C* **286**, H1757-H1766 (2004).

138. Kurata, Y., Hisatome, I., Imanishi, S. & Shibamoto, T. Roles of L-type Ca2+ and delayed-rectifier K+ currents in sinoatrial node pacemaking: insights from stability and bifurcation analyses of a mathematical model. *Am J Physiol-Heart C* **285**, H2804-H2819 (2003).

139. Warmke, J.W. & Ganetzky, B. A Family of Potassium Channel Genes Related to Eag in Drosophila and Mammals. *Proc. Natl. Acad. Sci. U. S. A.* **91**, 3438-3442 (1994).

140. Piper, D.R., Hinz, W.A., Tallurri, C.K., Sanguinetti, M.C. & Tristani-Firouzi, M. Regional specificity of human ether-a'-go-go-related gene channel activation and inactivation gating. *J. Biol. Chem.* **280**, 7206-7217 (2005).

141. Gravel, A.E., Arnold, A.A., Dufourc, E.J. & Marcotte, I. An NMR investigation of the structure, function and role of the hERG channel selectivity filter in the long QT syndrome. *Bba-Biomembranes* **1828**, 1494-1502 (2013).

142. Li, X.D., Xu, J. & Li, M. The human Delta 1261 mutation of the HERG potassium channel results in a truncated protein that contains a subunit interaction domain and decreases the channel expression. *J. Biol. Chem.* **272**, 705-708 (1997).

143. Gustina, A.S. & Trudeau, M.C. A recombinant N-terminal domain fully restores deactivation gating in N-truncated and long QT syndrome mutant hERG potassium channels. *Proc. Natl. Acad. Sci. U. S. A.* **106**, 13082-13087 (2009).

144. Ke, Y.*, et al.* Trafficking defects in PAS domain mutant Kv11.1 channels: roles of reduced domain stability and altered domain-domain interactions. *Biochem. J.* **454**, 69-77 (2013).

145. Ke, Y., Hunter, M.J., Ng, C.A., Perry, M.D. & Vandenberg, J.I. Role of the cytoplasmic N-terminal Cap and Per-Arnt-Sim (PAS) domain in trafficking and stabilization of Kv11.1 channels. *J. Biol. Chem.* **289**, 13782-13791 (2014).

146. Haitin, Y., Carlson, A.E. & Zagotta, W.N. The structural mechanism of KCNH-channel regulation by the eag domain. *Nature* **501**, 444-448 (2013).

147. Smith, J.L.*, et al.* Trafficking-deficient hERG K(+) channels linked to long QT syndrome are regulated by a microtubule-dependent quality control compartment in the ER. *Am. J. Physiol. Cell Physiol.* **301**, C75-85 (2011).

148. Li, Q.X.*, et al.* NMR solution structure of the N-terminal domain of hERG and its interaction with the S4-S5 linker. *Biochem. Biophys. Res. Commun.* **403**, 126-132 (2010).

149. Ng, C.A.*, et al.* The N-Terminal Tail of hERG Contains an Amphipathic alpha-Helix That Regulates Channel Deactivation. *PLoS One* **6**(2011).

150. Foo, B.W., B.; Young, J. C.; Lukacs, G.; Shrier, A. hERG quality control and the long QT syndrome. *The Journal of Physiology*, n/a-n/a (2016).

151. Baaklini, I.*, et al.* The DNAJA2 Substrate Release Mechanism Is Essential for Chaperone-mediated Folding. *J. Biol. Chem.* **287**, 41939-41954 (2012).

152. Walker, V.E.*, et al.* Hsp40 chaperones promote degradation of the HERG potassium channel. *J. Biol. Chem.* **285**, 3319-3329 (2010).

153. Walker, V.E., Atanasiu, R., Lam, H. & Shrier, A. Co-chaperone FKBP38 promotes HERG trafficking. *J. Biol. Chem.* **282**, 23509-23516 (2007).

154. Albesa, M., Grilo, L.S., Gavillet, B. & Abriel, H. Nedd4-2-dependent ubiquitylation and regulation of the cardiac potassium channel hERG1. *J. Mol. Cell. Cardiol.* **51**, 90-98 (2011).

155. Phartiyal, P., Sale, H., Jones, E.M. & Robertson, G.A. Endoplasmic reticulum retention and rescue by heteromeric assembly regulate human ERG 1a/1b surface channel composition. *J. Biol. Chem.* **283**, 3702-3707 (2008).

156. Petrecca, K., Atanasiu, R., Akhavan, A. & Shrier, A. N-linked glycosylation sites determine HERG channel surface membrane expression. *J Physiol-London* **515**, 41-48 (1999).

157. Chapman, H.*, et al.* Downregulation of the HERG (KCNH2) K+ channel by ceramide: evidence for ubiquitin-mediated lysosomal degradation. *J. Cell Sci.* **118**, 5325-5334 (2005).

158. London, B.*, et al.* Two isoforms of the mouse ether-a-go-go-related gene coassemble to form channels with properties similar to the rapidly activating component of the cardiac delayed rectifier K+ current. *Circ. Res.* **81**, 870-878 (1997).

159. Jones, E.M.C., Roti, E.C.R., Wang, J.L., Delfosse, S.A. & Robertson, G.A. Cardiac I-Kr channels minimally comprise hERG 1a and 1b subunits. *J. Biol. Chem.* **279**, 44690-44694 (2004).

160. Braga, R.C.*, et al.* Tuning hERG Out: Antitarget QSAR Models for Drug Development. *Curr. Top. Med. Chem.* **14**, 1399-1415 (2014).

161. Thomas, S.H.L.*, et al.* Concentration-Dependent Cardiotoxicity of Terodiline in Patients Treated for Urinary-Incontinence. *Br. Heart J.* **74**, 53-56 (1995).

162. Brown, A.M. Drugs, hERG and sudden death. *Cell Calcium* **35**, 543-547 (2004).

163. Fenichel, R.R.*, et al.* Drug-induced Torsades de Pointes and implications for drug development. *J. Cardiovasc. Electrophysiol.* **15**, 475-495 (2004).

164. Mitcheson, J.S., Chen, J., Lin, M., Culberson, C. & Sanguinetti, M.C. A structural basis for drug-induced long QT syndrome. *Proc. Natl. Acad. Sci. U. S. A.* **97**, 12329-12333 (2000).

165. Herzberg, I.M., Trudeau, M.C. & Robertson, G.A. Transfer of rapid inactivation and sensitivity to the class III antiarrhythmic drug E-4031 from HERG to M-eag channels. *J Physiol-London* **511**, 3-14 (1998).

166. Jamieson, C., Moir, E.M., Rankovic, Z. & Wishart, G. Medicinal chemistry of hERG optimizations: Highlights and hang-ups. *J. Med. Chem.* **49**, 5029-5046 (2006).

167. Shealy, R.T., Murphy, A.D., Ramarathnam, R., Jakobsson, E. & Subramaniam, S. Sequence-function analysis of the K(+)-Selective family of ion channels using a comprehensive alignment and the KcsA channel structure. *Biophys. J.* **84**, 2929-2942 (2003).

168. Ficker, E., Jarolimek, W. & Brown, A.M. Molecular determinants of inactivation and dofetilide block in ether a-go-go (EAG) channels and EAG-related K+ channels. *Mol. Pharmacol.* **60**, 1343-1348 (2001).

169. Hoshi, T. & Armstrong, C.M. C-type inactivation of voltage-gated K+ channels: Pore constriction or dilation? *J. Gen. Physiol.* **141**, 151-160 (2013).

170. Numaguchi, H.*, et al.* Probing the interaction between inactivation gating and D-sotalol block of HERG. *Circ. Res.* **87**, 1012-1018 (2000).

171. Perrin, M.J., Kuchel, P.W., Campbell, T.J. & Vandenberg, J.I. Drug Binding to the Inactivated State Is Necessary but Not Sufficient for High-Affinity Binding to Human Ether-a-go-go-Related Gene Channels. *Mol. Pharmacol.* **74**, 1443-1452 (2008).

172. Salvo, F.*, et al.* Sudden Cardiac and Sudden Unexpected Death Related to Antipsychotics: A Meta-analysis of Observational Studies. *Clin. Pharmacol. Ther.* **99**, 306-314 (2016).

173. Shepard, P.D., Canavier, C.C. & Levitan, E.S. Ether-a-go-go-Related gene potassium channels: What's all the buzz about? *Schizophr. Bull.* **33**, 1263-1269 (2007).

174. Ji, H.F.*, et al.* Functional characterization of ether-a-go-go-related gene potassium channels in midbrain dopamine neurons - implications for a role in depolarization block. *Eur. J. Neurosci.* **36**, 2906-2916 (2012).

175. Yu, N., Tucker, K.R., Levitan, E.S., Shepard, P.D. & Canavier, C.C. Implications of Cellular Models of Dopamine Neurons for Schizophrenia. *Prog Mol Biol Transl* **123**, 53-82 (2014).

176. Huffaker, S.J.*, et al.* A primate-specific, brain isoform of KCNH2 affects cortical physiology, cognition, neuronal repolarization and risk of schizophrenia. *Nat. Med.* **15**, 509-518 (2009).

177. Cannon, T.D.*, et al.* The inheritance of neuropsychological dysfunction in twins discordant for schizophrenia. *Am. J. Hum. Genet.* **67**, 369-382 (2000).

178. Bookheimer, S.Y.*, et al.* Patterns of brain activation in people at risk for Alzheimer's disease. *N. Engl. J. Med.* **343**, 450-456 (2000).

179. Callicott, J.H.*, et al.* Physiological dysfunction of the dorsolateral prefrontal cortex in schizophrenia revisited. *Cereb. Cortex* **10**, 1078-1092 (2000).

180. Egan, G.*, et al.* Neural correlates of the emergence of consciousness of thirst. *Proc. Natl. Acad. Sci. U. S. A.* **100**, 15241-15246 (2003).

181. Atalar, F.*, et al.* Two four-marker haplotypes on 7q36.1 region indicate that the potassium channel gene HERG1 (KCNH2, Kv11.1) is related to schizophrenia: a case control study. *Behav Brain Funct* **6**(2010).

182. Hashimoto, R.*, et al.* The KCNH2 gene is associated with neurocognition and the risk of schizophrenia. *World J. Biol. Psychiatry* **14**, 114-120 (2013).

183. Henningsson, S.Z., A.; Hovey, D.; Jonsson, L.; Svärd, J.; Cortes, D.; Sanchez,; Melke, J.; Ebner, N. C.; Laukka, P.; Fischer, H.; Westberg, L. Association between polymorphisms in NOS3 and KCNH2 and social memory. *Front. Neurosci.* **9**(2015).

184. Keefe, R.*, et al.* Baseline neurocognitive assessment of 1364 patients with schizophrenia in the clinical antipsychotic trials for intervention effectiveness (CATIE) project. *Biol. Psychiatry* **57**, 79s-79s (2005).

185. Swartz, M.S.*, et al.* Assessing clinical and functional outcomes in the Clinical Antipsychotic Trials of Intervention Effectiveness (CATIE) schizophrenia trial. *Schizophr. Bull.* **29**, 33-43 (2003).

186. Apud, J.A., Zhang, F.Y., Decot, H., Bigos, K.L. & Weinberger, D.R. Genetic Variation in KCNH2 Associated With Expression in the Brain of a Unique hERG Isoform Modulates Treatment Response in Patients With Schizophrenia. *Am. J. Psychiatry* **169**, 725-734 (2012).

187. Heide, J., Mann, S.A. & Vandenberg, J.I. The schizophrenia-associated Kv11.1-3.1 isoform results in reduced current accumulation during repetitive brief depolarizations. *PLoS One* **7**, e45624 (2012).

188. Heide, J., Vandenberg, J.I. & Weickert, C.S. Expression of KCNH2-3.1 mRNA is increased in small neurons in the dorsolateral prefrontal cortex in patients with schizophrenia. *Eur J Psychiat* **29**, 85-103 (2015).

189. Heide, J.*, et al.* Differential Response to Risperidone in Schizophrenia s Patients by KCNH2 Genotype and Drug Metabolizer Status. *Am. J. Psychiatry* **173**, 53-59 (2016).

190. Carr, G.*, et al.* KCNH2-3.1 expression impairs cognition and alters neuronal function in a model of molecular pathology associated with schizophrenia. *Mol. Psychiatry* (2016).

191. Johnson, J.N.*, et al.* Identification of a possible pathogenic link between congenital long QT syndrome and epilepsy. *Neurology* **72**, 224-231 (2009).

192. Farre, C. & Fertig, N. HTS techniques for patch clamp-based ion channel screening - advances and economy. *Expert Opin Drug Discov* **7**, 515-524 (2012).

193. Gianulis, E.C. & Trudeau, M.C. Rescue of aberrant gating by a genetically encoded PAS (Per-Arnt-Sim) domain in several long QT syndrome mutant human ether-a-go-go-related gene potassium channels. *J. Biol. Chem.* **286**, 22160-22169 (2011).

194. Anderson, C.L*., et al.* Large-scale mutational analysis of Kv11.1 reveals molecular insights into type 2 long QT syndrome. *Nat Commun* **5**(2014).

195. Gianulis, E.C., Liu, Q. & Trudeau, M.C. Direct interaction of eag domains and cyclic nucleotide-binding homology domains regulate deactivation gating in hERG channels. *J. Gen. Physiol.* **142**, 351-366 (2013).

196. Gustina, A.S. & Trudeau, M.C. The eag domain regulates hERG channel inactivation gating via a direct interaction. *J. Gen. Physiol.* **141**, 229-241 (2013).

197. Gong, Q.M., Anderson, C.L., January, C.T. & Zhou, Z.F. Pharmacological rescue of trafficking defective HERG channels formed by coassembly of wild type and long QT mutant N470D subunits. *Biophys. J.* **82**, 253a-254a (2002).

198. Mehta, A*., et al.* Re-trafficking of hERG reverses long QT syndrome 2 phenotype in human iPS-derived cardiomyocytes. *Cardiovasc. Res.* **102**, 497-506 (2014).

199. Smith, J.L*., et al.* Pharmacological correction of long QT-linked mutations in KCNH2 (hERG) increases the trafficking of Kv11.1 channels stored in the transitional endoplasmic reticulum. *Am. J. Physiol. Cell Physiol.* **305**, C919-930 (2013).

200. Zhang, K.P., Yang, B.F. & Li, B.X. Translational toxicology and rescue strategies of the hERG channel dysfunction: biochemical and molecular mechanistic aspects. *Acta Pharmacol. Sin.* **35**, 1473-1484 (2014).

201. Zhou, Z., Gong, Q. & January, C.T. Correction of defective protein trafficking of a mutant HERG potassium channel in human long QT syndrome. Pharmacological and temperature effects. *J. Biol. Chem.* **274**, 31123-31126 (1999).

202. Mihic, A., Chauhan, V.S., Gao, X., Oudit, G.Y. & Tsushima, R.G. Trafficking defect and proteasomal degradation contribute to the phenotype of a novel KCNH2 long QT syndrome mutation. *PLoS One* **6**, e18273 (2011).

203. Thomas, D., Kiehn, J., Katus, H.A. & Karle, C.A. Defective protein trafficking in hERG-associated hereditary long QT syndrome (LQT2): molecular mechanisms and restoration of intracellular protein processing. *Cardiovasc. Res.* **60**, 235-241 (2003).

204. Zhou, Z.F., Gong, Q.M. & January, C.T. Correction of defective protein trafficking of a mutant HERG potassium channel in human long QT syndrome - Pharmacological and temperature effects. *J. Biol. Chem.* **274**, 31123-31126 (1999).

205. Zhou, J.*, et al.* Novel potent human ether-a-go-go-related gene (hERG) potassium channel enhancers and their in vitro antiarrhythmic activity. *Mol. Pharmacol.* **68**, 876-884 (2005).

206. Wang, T.Z.*, et al.* Muscarinic Receptor Activation Increases hERG Channel Expression through Phosphorylation of Ubiquitin Ligase Nedd4-2. *Mol. Pharmacol.* **85**, 877-886 (2014).

207. Potet, F.*, et al.* Identification and Characterization of a Compound That Protects Cardiac Tissue from Human Ether-a-go-go-related Gene (hERG)-related Drug-induced Arrhythmias. *J. Biol. Chem.* **287**(2012).

208. Massey, A.J.*, et al.* A novel, small molecule inhibitor of Hsc70/Hsp70 potentiates Hsp90 inhibitor induced apoptosis in HCT116 colon carcinoma cells. *Cancer Chemother. Pharmacol.* **66**, 535-545 (2010).

209. Zhang, H.*, et al.* Modulation of hERG potassium channel gating normalizes action potential duration prolonged by dysfunctional KCNQ1 potassium channel. *Proc. Natl. Acad. Sci. U. S. A.* **109**, 11866-11871 (2012).

210. Wu, Z.Y., Chen, K., Haendler, B., McDonald, T.V. & Bian, J.S. Stimulation of N-terminal truncated isoform of androgen receptor stabilizes human ether-a-go-go-related gene-

encoded potassium channel protein via activation of extracellular signal regulated kinase 1/2. *Endocrinology* **149**, 5061-5069 (2008).

211. Kagan, A., Yu, Z.H., Fishman, G.I. & McDonald, T.V. The dominant negative LQT2 mutation A561V reduces wild-type HERG expression. *J. Biol. Chem.* **275**, 11241-11248 (2000).

212. Foghsgaard, L.*, et al.* Cathepsin B acts as a dominant execution protease in tumor cell apoptosis induced by tumor necrosis factor. *J. Cell Biol.* **153**, 999-1009 (2001).

213. Wang, K.K.W.*, et al.* An alpha-mercaptoacrylic acid derivative is a selective nonpeptide cell-permeable calpain inhibitor and is neuroprotective. *Proc. Natl. Acad. Sci. U. S. A.* **93**, 6687-6692 (1996).

214. Withana, N.P.*, et al.* Cathepsin B inhibition limits bone metastasis in breast cancer. *Cancer Res.* **72**, 1199-1209 (2012).

215. Myers, M.C., Shah, P.P., Diamond, S.L., Huryn, D.M. & Smith, A.B., 3rd. Identification and synthesis of a unique thiocarbazate cathepsin L inhibitor. *Bioorg. Med. Chem. Lett.* **18**, 210-214 (2008).

216. Richardson, P.G.*, et al.* A phase 2 study of bortezomib in relapsed, refractory myeloma. *N. Engl. J. Med.* **348**, 2609-2617 (2003).

217. Chapman, H.*, et al.* Downregulation of the HERG (KCNH2) K(+) channel by ceramide: evidence for ubiquitin-mediated lysosomal degradation. *J. Cell Sci.* **118**, 5325-5334 (2005).

218. Rubio, M.D., Wood, K., Haroutunian, V. & Meador-Woodruff, J.H. Dysfunction of the ubiquitin proteasome and ubiquitin-like systems in schizophrenia. *Neuropsychopharmacology* **38**, 1910-1920 (2013).

219. Bousman, C.A*., et al.* Preliminary Evidence of Ubiquitin Proteasome System Dysregulation in Schizophrenia and Bipolar Disorder: Convergent Pathway Analysis Findings from Two Independent Samples. *American Journal of Medical Genetics Part B-Neuropsychiatric Genetics* **153B**, 494-502 (2010).

220. Apud, J.A., Zhang, F., Decot, H., Bigos, K.L. & Weinberger, D.R. Genetic variation in KCNH2 associated with expression in the brain of a unique hERG isoform modulates treatment response in patients with schizophrenia. *Am. J. Psychiatry* **169**, 725-734 (2012).

221. Silvestre, J.S., O'Neill, M.F. & Prous, J.R. Evidence for a crucial modulating role of the sodium channel in the QTc prolongation related to antipsychotics. *J Psychopharmacol* **28**, 329-340 (2014).

222. Doran, A*., et al.* The impact of P-glycoprotein on the disposition of drugs targeted for indications of the central nervous system: Evaluation using the MDR1A/1B knockout mouse model. *Drug Metabolism and Disposition* **33**, 165-174 (2005).

223. Farre, C. & Fertig, N. HTS techniques for patch clamp-based ion channel screening - advances and economy. *Expert Opin Drug Dis* **7**, 515-524 (2012).

224. Zou, B.Y*., et al.* Profiling Diverse Compounds by Flux- and Electrophysiology-Based Primary Screens for Inhibition of Human Ether-a-go-go Related Gene Potassium Channels. *Assay Drug Dev Techn* **8**, 743-754 (2010).

225. Bridal, T.R., Margulis, M., Wang, X., Donio, M. & Sorota, S. Comparison of Human Ether-a-go-go Related Gene Screening Assays Based on IonWorks Quattro and Thallium Flux. *Assay Drug Dev Techn* **8**, 755-765 (2010).

226. Tie, H., Walker, B.D., Valenzuela, S.M., Breit, S.N. & Campbell, T.J. The heart of psychotropic drug therapy. *Lancet* **355**, 1825-1825 (2000).

227. Brown, P.C. 205422Orig1s000 New Drug Application, Pharmacology review. (Food and Drug Administration, 2014).

228. Caillier, B.*, et al.* QRS widening and QT prolongation under bupropion: a unique cardiac electrophysiological profile. *Fundam. Clin. Pharmacol.* **26**, 599-608 (2012).

229. Yoshida, K. & Niwa, T. Quantitative structure-activity relationship studies on inhibition of HERG potassium channels. *J. Chem. Inf. Model.* **46**, 1371-1378 (2006).

230. Vigneault, P., Pilote, S., Patoine, D., Simard, C. & Drolet, B. Iloperidone (Fanapt (R)), a novel atypical antipsychotic, is a potent HERG blocker and delays cardiac ventricular repolarization at clinically relevant concentration. *Pharmacol. Res.* **66**, 60-65 (2012).

231. Spyker, D.A., Voloshko, P., Heyman, E.R. & Cassella, J.V. Loxapine Delivered as a Thermally Generated Aerosol Does Not Prolong QTc in a Thorough QT/QTc Study in Healthy Subjects. *J. Clin. Pharmacol.* **54**, 665-674 (2014).

232. Brown, P.C. 200603 New Drug Application, Pharmacology review. (Food and Drug Administration, 2009).

233. Kongsamut, S., Kang, J.S., Chen, X.L., Roehr, J. & Rampe, D. A comparison of the receptor binding and HERG channel affinities for a series of antipsychotic drugs. *Eur. J. Pharmacol.* **450**, 37-41 (2002).

234. Dosa, P.I.*, et al.* Solubilized phenyl-pyrazole ureas as potent, selective 5-HT2A inverse-agonists and their application as antiplatelet agents. *Bioorg. Med. Chem. Lett.* **19**, 5486-5489 (2009).

235. McCarthy, A. The NIH Molecular Libraries Program: Identifying Chemical Probes for New Medicines. *Chem. Biol.* **17**, 549-550 (2010).

236. Muci, A.R. & Buchwald, S.L. Practical palladium catalysts for C-N and C-O bond formation. *Cross-Coupling Reactions* **219**, 131-209 (2002).

237. Nikolov, N.G., Dybdahl, M., Jonsdottir, S.O. & Wedebye, E.B. hERG blocking potential of acids and zwitterions characterized by three thresholds for acidity, size and reactivity. *Bioorgan Med Chem* **22**, 6004-6013 (2014).

238. Hartman, J.H., Knott, K. & Miller, G.P. CYP2E1 hydroxylation of aniline involves negative cooperativity. *Biochem. Pharmacol.* **87**, 523-533 (2014).

239. Wager, T.T., Hou, X.J., Verhoest, P.R. & Villalobos, A. Moving beyond Rules: The Development of a Central Nervous System Multiparameter Optimization (CNS MPO) Approach To Enable Alignment of Druglike Properties. *ACS Chem. Neurosci.* **1**, 435-449 (2010).

240. Yin, J.J. & Buchwald, S.L. Pd-catalyzed intermolecular amidation of aryl halides: The discovery that xantphos can be trans-chelating in a palladium complex. *J. Am. Chem. Soc.* **124**, 6043-6048 (2002).

241. Fors, B.P., Davis, N.R. & Buchwald, S.L. An Efficient Process for Pd-Catalyzed C-N Cross-Coupling Reactions of Aryl Iodides: Insight Into Controlling Factors. *J. Am. Chem. Soc.* **131**, 5766-5768 (2009).

242. Guth, B.D. Preclinical cardiovascular risk assessment in modern drug development. *Toxicol. Sci.* **97**, 4-20 (2007).

243. Lancaster, M.A. & Knoblich, J.A. Organogenesis in a dish: Modeling development and disease using organoid technologies. *Science* **345**(2014).

244. Scott, M.R., Rubio, M.D., Haroutunian, V. & Meador-Woodruff, J.H. Protein Expression of Proteasome Subunits in Elderly Patients with Schizophrenia. *Neuropsychopharmacology* **41**, 896-905 (2016).

Appendix

Primer and Plasmid Sequences

All sequences are in 5'-3' notation

KCNH2-HA cloning primers

Forward: CCGGAATTCATGCCGGTGCGGAGGGG

Reverse:

ATAGTTTAGCGGCCGCCTAAGCGTAATCTGGAACATCGTATGGGTAACTGCCCGGGT

KCNH2-3.1-HA cloning primers

Forward: AACGTGAATTCGACCATGTCCTCCCACTCTGCA

Reverse:

ATAGTTTAGCGGCCGCCTAAGCGTAATCTGGAACATCGTATGGGTAACTGCCCGGGT

QPCR Primers- KCNH2- both isoforms

Forward: CGCACCACCTACGTCAATGC

Reverse: GCCGAAGATGAGCAGGTCGA

QPCR Primers- GAPDH Control

Forward: CCTTTTGCAGACAGTCCA

Reverse: GCAGGGATGATGTTCTGGAGA

Curriculum Vitae for Nicholas E. Calcaterra

ncalcat1@gmail.com • (314) 620-4103 • 2024 E Lombard St. • Baltimore, MD 21231

Education and Training:

2011-2016 Ph.D. Pharmacology and Molecular Sciences **Johns Hopkins School of Medicine** – Expected May 2016

2008-2011 B.S. Biochemistry, Business Minor **University of Missouri-Columbia**
summa cum laude-Phi Beta Kappa

Research Experience:

2011-Present Lieber Institute for Brain Development- Drug Discovery Division
James C. Barrow Lab-Thesis
-Development and characterization of expression/trafficking deficient ion-channel cell lines for drug development.
-Establish high throughput fluorescent and electrophysiological assays
-Screen antipsychotic libraries on novel ion channel target
-Synthesis and assay of high throughput screen hit analogs
-Development of inositol hexakisphosphate kinase assay

2012 Johns Hopkins School of Medicine
Samuel Denmeade Lab-Rotation
-Effects of androgens and proteasome inhibition on androgen therapy resistant prostate cancer model cell lines.

2011 Johns Hopkins School of Medicine
Caren Meyers Lab-Roation
-Synthesis of rationally designed bisphosphonate substrate inhibitors of DXP synthase

2009-2011 University of Missouri-Columbia

Stephan Sarafianos-Undergraduate research

-High throughput screening of SARS-CoV nsp12/13 inhibitors

Publications

1. **Calcaterra NE**, Hoeppner DJ, Wei H, Jaffe AE, Maher BJ, Barrow JC. Schizophrenia-Associated hERG channel Kv11.1-3.1 Exhibits a Unique Trafficking Deficit that is Rescued Through Proteasome Inhibition for High Throughput Screening. Scientific Reports, **2016** 16 Feb.
2. Maynard, KR, Hill, JL, **Calcaterra NE**, Palko ME, Kardian A, Paredes D, Sukumar M, Adler BD, Jimenez DV, Schloesser RJ, Tessarollo L, Lu B, Martinowich K. Functional Role of BDNF Production from Unique Promoters in Aggression and Serotonin Signaling. Neuropsychopharmacology, **2015** 16 Nov.
3. **Calcaterra NE**, Barrow JC. *Classics in Chemical Neuroscience: Diazepam (Valium).* ACS Chemical Neuroscience, **2014** 19 Feb.
4. Adedeji AO, Singh K, **Calcaterra NE**, DeDiego ML, Enjuanes L, Weiss S, Sarafianos SG. Severe Acute Respiratory Syndrome Coronavirus Replication Inhibitor That Interferes with the Nucleic Acid Unwinding of the Viral Helicase. Antimicrobial Agents and Chemotherapy, **2012** 25 Jun.

Posters:

Calcaterra NE, Hoeppner DJ, Wei H, Maher BJ, Barrow JC. Rescue of the Trafficking Deficient Schizophrenia-Associated KCNH2 Splice Variant Kv11.1-3.1 for the Purpose of Drug Discovery. Society for Neuroscience Meeting, Washington D.C. 2014